Development of Multicomponent Force Sensory Systems and Palpation Methods for Enhancing Tumor Localization in Laparoscopic Surgery

(腹腔鏡下手術における腫瘍の位置同定を強化するための多成分力覚システムと触診法の開発)

2022

Ly Hoang Hiep

The work presented in this thesis has been supported by Japan Society for the Promotion of Science with Grant-in-Aid for JSPS Research Fellow and Grant-in-Aid for Scientific Research(A) (Grant numbers: JP19J23169 and JP17H01252).

Development of Multicomponent Force Sensory Systems and Palpation Methods for Enhancing Tumor Localization in Laparoscopic Surgery

by

Ly Hoang Hiep

A dissertation
submitted to the Department of Electrical and Mechanical Engineering,
Graduate School of Engineering, Nagoya Institute of Technology
in partial fulfillment of the requirements for
the degree of Doctor of Engineering

Abstract

Cancer is one of the most dangerous diseases in the world. The survival rates can increase when the cancer is diagnosed and treated early. For most types of cancer, surgery to remove the cancerous tumor is the most effective treatment. The effectiveness of this treatment depends mainly on the assessment of the primary tumor characteristics, such as its location, size, and depth. This information allows surgeons to remove the entire tumor with minimum margins while preserving the function of the remaining organ, thereby enhancing cancer's curability and the patient's postoperative quality of life. In general, the tissue characteristics could be determined using preoperative imaging techniques, such as Magnetic Resonance Imaging (MRI) and Computed Tomography (CT). However, the obtained information from these techniques is not completely reliable during surgery because intraoperative soft tissues and tumors often move and deform. In the case of open surgery, surgeons can determine the tumor by palpating the target tissue with their fingers. In minimally invasive surgery (MIS), such as laparoscopic surgery (LS) or robot-assisted minimally invasive surgery (RMIS), in which surgeons no longer contact the tissues directly, they could rely on sensory feedback from laparoscopic feedback devices, such as ultrasonic or haptic devices, to examine abnormal tissues. This thesis focuses on haptic devices for laparoscopic palpation.

A haptic system in laparoscopic tissue palpation often consists of a sensing device and a display device. Various haptic devices, such as tactile array sensors and pin–array tactile displays, were introduced to assist surgeons in their palpation procedure. However, these devices are often complex in structure, unsuitable for clinical applications, or require high–precision haptic data that may only be achieved in RMIS. Thus, haptic devices that have simple structures and high clinical applicability, such as single–point tactile sensors using optical or acoustic principles and wearable tactile displays using pneumatic power, tend to be preferred for tumor localization in LS. However, the haptic information from these devices is often affected by the deformation of the tissue during palpation, the surgeon's manipulation of the surgical probe, or the display method of the haptic information to the surgeon. These degrade the

performance and confidence of the surgeon in tumor determination. Furthermore, the assessment of tumor size and depth using these devices still be arguable.

This thesis aims to develop tissue palpation systems for surgeons to determine tumors intraoperatively, especially in LS. The systems consist of biocompatible elements that could ensure the safety requirements in a clinical environment, such as sterilizability and disposability. Moreover, the simplicity of the devices' structure is required in the development of the palpation systems. Since sensing lumps or tumors by palpation is a complex process (even for human sensation), haptic devices for tissue palpation are required to have multiple sensing or display functions to enrich the surgeon's perception of tumors. However, too many sensing (or display) elements might cause the complex structure and bulk size of the tactile devices, leading to disadvantages in MIS application. For example, a large sensing device cannot insert into the patient's body through a trocar (diameter of 12 mm), and a complex display device could impede the surgeon's intraoperative movements. Thus, this thesis focuses on the balance between the devices' functions and the simplicity in their structure. In manual tissue palpation, a combination of perpendicular (related to normal force) and lateral (related to shear force) motions is more effective in exploring hard nodules (or tumors). Therefore, we focused on developing devices capable of two force sensing (or display) components, including normal and shear force components, to achieve the balancing purpose. In addition, if the obtained information is stable and largely unaffected by the tissue deformation, the surgeon's motions, or the method of the target tissue information transmission to the surgeons, it will be helpful for the surgeon's decision–making in their tumor detection. Furthermore, the system proposed in this thesis also aims to enable surgeons to identify the characteristics of tumors, such as depth and size.

Firstly, a forceps–type tactile sensor was developed for intraoperative tumor detection in LS for early–stage tumor resection such as gastric cancer. The tactile sensor based on the acoustic reflection principle provides real–time visual information of the two contact force components, including normal and shear force information. Since the tactile sensor has no electrical components inserted into the patient's body, it offers great advantages in MIS, such as disposable, sterilizable, and electrical safety. Surgeons can use the tactile sensor to palpate the stomach's surface to detect the tumor. However, the bending of the gastric tissue due to the force applied by surgeons often reduces

the sensitivity of tumor detection. The results of a tissue palpation experiment with a phantom of the stomach wall having an embedded tumor showed that the normal force information fluctuated significantly during the tissue palpation procedures, leading to the difficulty in tumor localization. On the other hand, the shear force information obtained from the tactile sensor was relatively stable. It changed significantly at the tumor location, regardless of the bending of the tissue and the sensor's movements by the user. This could potentially improve the performance and confidence of the surgeon in localizing tumors intraoperatively. In summary, this finding showed that the shear force information from a tactile sensor significantly contributes to laparoscopic tumor localization.

Visual feedback used in the first part of this thesis is a common feedback modality to represent the contact force component information to surgeons. However, since surgeons need to focus on laparoscopic images during surgery, this feedback modality may cause overloads of the visual channel. Tactile feedback is a promising alternative to provide the contact force information to surgeons in MIS. Since tactile feedback is independent of the visual channel, it can prevent sensory overload during intraoperative tissue palpation. The second part of this thesis aims to develop a ring–type tactile display, called SuP–Ring, that can provide normal and shear force feedback to assist surgeons in laparoscopic tumor localization. Normal indentation, a substitutional feedback modality, was employed to represent the force feedback. The intensity of contact force components was interpreted on three tactile elements of the SuP–Ring, including the middle one representing normal force feedback and the others representing positive and negative shear force feedback. Tactile display using this tactile feedback modality could provide reliable contact force information because with the feedback modality, the shear force feedback is rendered regardless of friction between the human skin and tactile display's moving element, compared to the other tactile feedback modalities such as lateral skin stretch. In addition, since the SuP–Ring used pneumatic power to drive the normal indentation of the tactile elements, it is simple structure, low–cost fabrication, sterilizable and disposable. The fundamental investigations of the tactile display showed that the tactile feedback rendered by the tactile element was relatively consistent, and users could perceive the change of the shear force feedback regardless of the differences in the normal force feedback. The effectiveness of the SuP–Ring for

tumor localization was also determined through a simulated tissue palpation with an artificial phantom tissue having an embedded tumor. The experimental results showed that the shear force feedback of the tactile display could improve the performance and confidence of users in localizing the tumor, and the normal force feedback could contribute to ensuring the safety requirements in MIS. Thus, a tactile display that can represent normal and shear force could be useful for intraoperative tumor localization.

Detecting the tumor location is only the first step of the tumor localization procedure in MIS. Surgeons should determine the tumor characteristics, such as tumor depth and size, to perform a maximum tumor resection procedure to prevent damage to the remaining tissue. In the final part of the thesis, we proposed a palpation strategy using tactile feedback to assist the surgeon in determining the tumor feature information. In this palpation strategy, the depth of tumor can be determined by recognizing the presence of the tumor at the given depth position (indentation depth) of the sensor, while the tumor size may be obtained by localizing the edges of the tumor. Fundamental experiments were conducted to investigate the use of contact force component information in determining tumor features using the proposed strategy. The results indicated that the normal force is more useful in estimating the indentation depth, and the shear force is highly effective in detecting the regions and edges of the tumor. Users' ability to characterize the tumor using tactile feedback from the SuP–Ring was demonstrated through tissue palpation tasks. Participants (without medical background) who received both normal force and shear force feedback could identify the depth and size of the embedded tumor with 66 % and 65 % accuracy, respectively. These results suggest that the tactile displays that provide normal and shear force feedback can be successfully used for tumor characterization.

In summary, the results and findings in this thesis demonstrate the essence of using tactile devices having multicomponent force feedback function in intraoperative tumor localization. The tactile sensor with shear force measurement function could provide stable and effective visual information of contact force response in tumor area for surgeons, regardless of the effect of tissue bending or sensor movement by the surgeons. This could contribute to improving the surgeons' decision–making in intraoperative tumor localization. In addition, the tactile display with normal and shear force feedback displays could prevent the surgeons' visual channel from overloading

and enhance the surgeons' performance and confidence in detecting the tumor. Moreover, the tactile display enabled surgeons to determine the depth and size of the tumor during the intraoperative tissue palpation. This contributes to minimizing the tissue resection margin to preserve the patient's organ function after surgery. However, several improvements to these devices need to be carried out to apply the devices in actual surgery. For example, the developed tactile sensor and tactile display have not been used as a complete system for tumor characterization. The structure of the sensor and the tactile display could be improved to achieve a 3–axis force sensor and a 3–DoF force feedback tactile display. In that case, surgeons could use the sensor and the display together to palpate tissue from more directions to gain more information about the tissue, enabling more accurate tumor detection in actual surgery. Furthermore, the proposed sensing (and display) device and principle are considered using in a wide range of fields, such as virtual reality or robot teleoperation, in addition to MIS.

Acknowledgements

I am grateful to all those who supported me through the various stages of my study journey.

Foremost, I would like to express my sincere gratitude to my advisor Professor Yoshihiro Tanaka for his guidance, support, encouragement, and patience during my research since I was a master's student. He provided me with an excellent research environment and development opportunities to embark on my doctoral studies. Thanks to the insightful discussions with Professor Tanaka, I learned a lot from him, ranging from priceless scientific thinking and academic writing to budget management skills that will be highly useful in my future career. I would not complete my five years of study in Japan without his instructions and support.

I would like to extend my gratitude to Professor Akihito Sano, my supervisor during my master's program. He gave me excellent opportunities and valuable advice for my research. Professor Sano always encouraged me to find novelty in my research. He is also an internal examiner of my doctoral dissertation committee. The thesis has become more transparent and robust, thanks to his constructive comments.

I would like to thank the other examiners of the dissertation committee for their time and effort. I am grateful to Professor Manabu Yamada for his helpful comments and discussions. I would also like to thank Professor Jumpei Arata from Kyushu University for his excellent comments and suggestions from the perspective of medical device development and evaluation. The thesis is greatly improved thanks to them.

I am grateful to Professor Michitaka Fujiwara from Nagoya University for his collaboration in my doctoral research. He always provided me with valuable comments on my research from a clinical perspective to strengthen this research. My articles might be more challenging to be accepted without his significant support.

I would like to thank Dr. Pham Quang Trung and Dr. Tomohiro Fukuda for their support, discussion, and encouragement of my research. Dr. Trung is the one who introduces me to the haptic field. Through discussions with him, I was able to get many great ideas. I am always impressed by his broad knowledge. Dr. Fukuda

was my mentor when I was a master's student. I learned many from him, including technical skills and academic writing. My doctoral research was much inspired by his research. He also gave me great advice on my doctoral research. I wish Dr. Trung and Dr. Fukuda all the best in their careers.

I am grateful to the laboratory's staff, including Ms. Aiko Ito, Ms. Junko Kawakami, Ms. Kaori Iwasaki, and Ms. Aya Matsui, for their kind support during my doctoral studies. Especially, I would like to thank Ms. Reiko Nishimura for her great support in my budget management.

I am also grateful to all the members of the Robotics laboratory for their excellent support, valuable suggestions, and discussions during the five years of my research. I am delighted to be a part of this laboratory.

I am thankful to Pham Duy Tung, Tran Vu Trung, Quang Huu Hieu, Nguyen Thanh Tuan, Nguyen Manh Tien, Ninh Thanh Tung, Nguyen Canh Son, Nguyen Thanh Giang, Bui Duy Do, Nguyen Kim Chung, and many other friends for their enthusiastic support and the time spent together. Thanks to them, my life outside of research has been more accessible and enjoyable.

Finally, no words can express my deepest gratitude to my family, including my parent, Ly Sy Chuc and Vu Thi Hien, and my younger sister, Ly Ha Trang, for their love, understanding, and encouragement during my study abroad. They are always there for me when times are hard. I am happy to get a doctoral degree, but it is just the beginning of my research journey. I hope that my future research could greatly contribute to the body of knowledge.

Contents

List of Figures

List of Tables

Chapter 1

Introduction

1.1 Background

1.1.1 Tissue palpation

In current decades, cancer is becoming one of the most dangerous diseases threatening many people's lives around the world. Most deaths caused by cancer result from the late detection of the disease when the cancer is almost in its final stage. If a patients' cancer is diagnosed and treated at an early stage, the survival rates will improve [1]. Surgery is the most effective treatment for most types of cancer [2]. Identifying the cancer stage often relies on the evaluations of the characteristics of the patients' primary tumor (where the cancers started), including the location, size, or depth of the tumor.

According to the American Joint Committee on Cancer and the Union for International Cancer Control, tumor size could describe four cancer stages [1]: T1 stage (tumor size less than 20 mm); T2 stage (tumor size greater than 20 mm and but less than 50 mm), T3 stage (tumor size more than 50 mm across), T4 stage (tumors of any size with direct extension to the skin). Discovering the tumor at T1 stage significantly increases the survival rate [1]. Tumor depth is also a useful factor in determining the stage of cancers [3, 4]. Subcutaneous tumors are more likely to be detected early, while deeper tumors tend to go unrecognized until they are larger in size (often at a later stage). Alkureishi et al. [3] and William et al. [4] showed that the tumors in the head, neck or oral cavity that are more than 4 mm deep are at higher risk for cancer upstaging.

Generally, advanced imaging techniques, such as Magnetic Resonance Imaging (MRI), Computed Tomography (CT) or Ultrasound (US) imaging, can be used to characterize tumors preoperatively [5]. These techniques can provide an accurate image of

the tumor location and its mechanical properties such as depth, size, and chemical structure [6]. Such preoperative imaging approaches are effective for rigid structures, such as skulls or bones, but are challenging for soft tissue. Intraoperative deformation of organs, soft tissue, and tumor shift during a surgical procedure can complicate the accurate registration of the tumor, and preoperative information is not completely reliable [5, 7]. The palpation technique is a promising approach to obtain tumor characteristics during surgery.

In the palpation procedure, surgeons/practitioners use their hands or surgical probe to examine the patient's tissue or organ. The tactile information obtained can be used to evaluate the mechanical properties of the target tissue. In open surgery, surgeons rely on the tactile sensation of their fingers to palpate and explore the tumors [8]. Since the tumor is generally stiffer than the surrounding tissue, surgeons can easily detect the tumor location and depth and determine its size and margin [9,10]. This allows the surgeon to remove the entire tumor with a minimum resection to protect the function of surrounding tissue and remaining organs [11, 12]. This improves the patient's postoperative quality of life and reduces the likelihood of cancer recurrence. However, since the traditional open surgery involves a large incision, most patients experience postoperative pain. Furthermore, postoperative recovery takes several weeks, which increases costs and hospital stays. Therefore, patients tend to prefer other surgical methods, such as Minimally Invasive Surgery, which can address these issues.

1.1.2 Minimally invasive surgery

Minimally Invasive Surgery (MIS), also known as laparoscopic surgery (LS) or keyhole surgery, has become an increasingly popular standard surgical procedure for removing tumors in addition to the traditional open surgery. In MIS, surgeons use long–shaft surgical tools such as scissors, graspers to operate through small incisions on the patient's abdomen. Due to smaller incisions, MIS offers numerous benefits in terms of patient outcomes, including less postoperative pain, shorter recovery time, and better cosmetic healing [13]. However, this surgical procedure has some limitations. Surgeons have to cope with constrained motion when they manipulate the long surgical tools within the small holes in the abdomen. Moreover, restricted visual and haptic information during surgery is another limitation of MIS. These problems might lead to an

increase in the surgeon's physical and cognitive loads, resulting in the possibility of surgical errors [14, 15].

In MIS, visual information of the operation site is obtained by an endoscope and displayed on a monitor. Narrow field of view and poor depth perception are common issues in performing surgery. The use of high–definition and high–magnification endoscopes can overcome the limited vision of the surgical environment [16]. The endoscopes provide high–resolution images that could not be obtained by human vision. The effect of reduced depth cues in MIS can be compensated by using 3D video systems that restore stereoscopic vision [17].

Regarding motion constraints in MIS, surgical robots have been developed to assist surgeons during their operations. A robot–assisted MIS system (RMIS) adopts a master–slave configuration in which the surgeon and patient are completely separated and manipulate surgical tools on the slave side by controlling a console on the master side. One of the best known commercially available RMIS is the da Vinci system (Intuitive Surgical, Inc.), which is equipped with surgical instruments with 7 degrees–of–freedom (7–DoF). RMIS can increase intraoperative accuracy and dexterity when performing complex surgeries such as mitral valve repair or coronary artery revascularization [18, 19]. However, the lack of haptic sensation provided to surgeons is still a major limitation of RMIS, even for the da Vinci system [20].

Several studies reported that the lack of haptic information in MIS causes excessive contact force, leading to an increase in tissue trauma [23, 24]; impairing performance; and resulting in increased mistakes, such as slippage or loosening of knots during surgery [25]. The provision of haptic information enables safer and more accurate MIS surgery. Regarding tissue palpation, since surgeons no–longer directly contact the target tissue, it is difficult to determine the tumor characteristics in MIS. However, the surgeon's haptic sensation could be compensated by haptic technology using haptic devices [26].

1.1.3 Challenges in laparoscopic tissue palpation

In manual palpation technique, global examination and local examination were two main strategies for evaluating the tumor [21, 22]. The global examination is that surgeons/practitioners using their fingers quickly scan the entire tissue surface to explore

abnormalities such as the tumor location. Then, the local movements are applied within a selected region to enable the surgeons/practitioners to confirm the location of abnormal tissue and understand its shape, size, and depth. In laparoscopic tissue palpation, surgeons can also conduct global and local movements using haptic systems to examine the target tissue. The goal of haptic technology in MIS is to provide "transparency" that allows surgeons/practitioners to feel as their own hands contact the patient's tissue [20]. However, the human haptic sensation is very complicated. It combines force, distributed pressure, vibration, texture, and temperature sensations, which are often difficult to quantify or model. Thus, it is still a major challenge to fully compensate for the natural tactile sensation of the human hand with haptic technology.

A haptic system consists of a haptic sensing device (or haptic sensor) that acquires haptic information on the patient's side and a display that conveys the information to surgeons. The surgeons rely on the haptic information (mainly force information) from the haptic system to determine the tumor because the haptic response at the tumor area is often different from the response in the surrounding tissue. However, palpated tissues and organs are often deformed or shifted during palpation. This might obscure the haptic response between tumor and normal tissue portions, leading to difficulty localizing the tumor. Moreover, in LS, surgeons manually manipulate the surgical probe (haptic sensing device) to examine the patient's tissue. Even palpation experts find it difficult to scan tissues as stably as in RMIS. Abnormal force information obtained during palpation may be due to excessive force applied by the surgeon rather than the effect of the tumor. This will reduce the accuracy of tumor localization. Furthermore, Doctors must rely on a lot of information during surgery to conduct an appropriate treatment for patients. This causes a potential sensory overload, leading to a decrease in the surgeons' performance in the surgery. Thus, providing the tactile information effectively to prevent the surgeons from the sensory overload is another challenge in MIS.

In order to determine the size and depth of the tumor, highly accurate and sensitive haptic devices are often required. However, such haptic devices are complex in structure and heavy in weight [27]. During surgery, the surgeon has to perform complex actions for long periods of time. Heavy and complex devices impede the surgeon's movements and cause discomfort to the surgeon. In addition, complex structures in-

crease the fabrication cost of the devices. Thus, devices with lightweight, low–cost, and simple structure tend to be preferred in surgery. Nevertheless, it is challenging to develop a simple device that is available for intraoperative tumor characterization.

Finally, the feasibility of haptic devices in MIS must be considered. For example, the sensing device must be small, less than 12 mm in diameter, since it will be used as a surgical tool inserted into the patient's body via a trocar. It is also necessary to consider how to display tactile information from the sensing device that does not interfere with the surgeon's perception and movement during surgery and effectively supports the surgeon's performance. Furthermore, the devices for tissue palpation must be safe for patients. Thus, they should be sterilizable and free of harmful elements. These requirements are challenges in the development of palpation devices for MIS.

1.2 Focuses of this thesis

This thesis aimed to propose a simple haptic system to assist surgeons in both global and local examinations in LS to determine basic tumor characteristics such as location, depth, and size. The development of the proposed haptic system focuses on overcoming the challenges in intraoperative tissue palpation.

The first component of the haptic system is a haptic sensor to acquire tactile information during tissue palpation. The tactile sensor must provide clear and stable tactile information that is largely unaffected by tissue deformation or surgeon manipulation in order to increase the surgeon's confidence and performance in tumor positioning. A tactile sensor with multiple sensing functions might be useful to characterize the tumor. However, too many sensing functions may complicate the structure and increase the size of the device, leading to an inability to use the sensor in MIS. In this thesis, we aimed to balance the simplicity of the sensor's structure and the number of sensing functions. In manual tissue palpation technique, Konstantinova et al. reported that a combination of lateral (mainly related to shear force component of the contact force) and perpendicular (mainly related to normal force component of the contact force) motions is more helpful in examining the target tissue, such as localizing tumors [22]. Thus, to achieve the balancing goal, we focused on proposing a small sensor capable of two force sensing components, including normal and shear forces.

A sensory display modality, such as tactile modality, that could effectively convey the tactile information to surgeons (enables surgeons to avoid the potential sensory overload) during tissue palpation procedure, would be selected. Based on the sensory display modality, a display device will be developed. The display device could have multiple feedback features to enrich the tactile information given to the surgeons. However, to achieved the balancing purpose as the development of tactile sensors, it is essential to create a simple display device in structure and lightweight so as not to impede the surgeon's perception and workflow during surgery. Thus, we also focused on developing a small display device having two force feedback functions, including normal and shear force feedback.

Furthermore, it might be difficult to recognize the characteristics of the tumor straightforwardly using the haptic system. In typical tissue examination by hand, surgeons have to use local palpation strategies to identify the tumor. Thus, a tissue palpation strategy using the haptic system will be introduced to surgeons to assist them in determining the depth and size of the tumor in this thesis.

Finally, considering the feasibility of the device in MIS, this thesis focuses on developing a haptic system based on sensing and display principles that ensure the requirements of the device in a clinical environment.

1.3 Organization of the thesis

This thesis is organized as follows:

In Chapter 2, current tactile sensing and sensory display technologies based on force sensation for intraoperative tissue palpation are summarized. The tactile sensing technologies are summarized based on the structure of sensing devices. Display technologies are classified based on sensory modalities. The pros and cons of the technologies for tissue palpation are discussed. Furthermore, the technologies for developing the tactile system in this thesis will be presented.

In Chapter 3, a forceps–type tactile sensor for intraoperative detection of gastric tumor is proposed. This sensor has dimensions suitable for use in MIS. It was developed based on the acoustic reflection principle, a sensing technology that ensures safety requirements in a clinical environment. The sensor can acquire normal and

shear force components during tissue palpation, and the force information is presented by visual sensory feedback. The effectiveness of the sensor for locating tumors was evaluated using an artificial stomach phantom with an embedded tumor. The effects of tissue deformation and users' contact behaviors on the sensor output were shown in the experimental results. The findings in this chapter indicate which contact force components surgeons should rely on for tumor localization.

In Chapter 4, a pneumatic ring–type tactile display having two force feedback functions, including normal and shear force feedback, was proposed to assist surgeons in their laparoscopic tissue palpation. The use of tactile feedback prevents surgeons from potentially overloading visual channels as the current feedback of the forceps–type tactile sensor. The tactile display employed normal indentation, a substitutional sensory modality, that is largely unaffected by skin friction, to provide force feedback to the surgeon. Moreover, since the tactile display's elements were pneumatically driven, it is structurally simple, low cost, disposable, and resistant to sterilization, making it highly clinically applicable. The fundamental performance of the tactile display is investigated. A simulated tissue palpation with an artificial phantom tissue was established to evaluate the effectiveness of tactile display in tumor localization. The experimental results show the role of each force feedback component of the tactile display in localizing the embedded tumors.

Previous chapters have focused on the detection of tumor position using multi-component force sensing and display devices. In Chapter 5, the user's ability to use multiple contact force components for determining tumor characteristics, such as tumor depth and size, was investigated. A palpation strategy using tactile feedback to characterize the tumor was proposed. Fundamental experiments using artificial phantom tissue models with different tumor sizes and depths were performed to investigate the response of the contact force component for tissue palpation. The experimental results indicated which force component is useful in determining the depth or size of the tumors based on the proposed palpation strategy. Next, psychophysical experiments were conducted to investigate the user's ability to identify the tumor characteristics using the tactile feedback from the tactile display proposed in Chapter 4. In the experiments, participants wore the ring–type tactile display and palpated the prepared phantom tissue models, and were required to quickly respond to the depth and size

of the embedded tumor based on the tactile feedback represented on their skin. The experimental results showed the effectiveness of tactile display with multicomponent force feedback function for tumor characterization.

Chapter 6 summarizes the results and findings in this thesis and discusses the future works that may extend from these studies.

Chapter 2

Related works

This chapter summaries the state–of–the–art tactile sensing technologies and display technologies for intraoperative tissue palpation. Tactile sensing technologies are categorized based on the structure of the sensing devices. Meanwhile, display technologies are summarized based on the human sensory modalities for representing the tactile data and artificial sensory algorithms for obtaining tissue characteristics from the tactile data. Furthermore, the technologies selected to develop the haptic system in this thesis are described in detail.

2.1 Introduction

In open surgery, surgeons/practitioners manipulate and palpate tissue using their hands. In this case, the perception of the characteristics of the abnormal structure, such as tumor, was based on their haptic sensation. Since MIS eliminates the natural sense of touch, it is difficult for surgeons to manipulate surgical instruments and palpate tissue in surgery. However, haptic technology can compensate for the lack of haptic sense and enable surgeons to perceive the intraoperative tissue and determine the tumor characteristics in MIS [20, 26].

Numerous haptic systems have been proposed to assist surgeons in tissue palpation during laparoscopy. The systems consist of sensing devices or tactile sensors for acquiring the haptic data and display devices for conveying the acquired data to surgeons. This chapter summarizes the current sensing and display technologies for tissue palpation and discusses the capabilities of the technologies for intraoperative tumor characterization.

2.2 Sensing technologies

Tactile sensors are used to collect tactile data of the contact area between surgical tools and the target tissue. The tactile data could be contact force information, tissue temperature, or vibration during the scan of the surgical probe on the tissue surface. Force data is literally the primary form of tactile data, and tactile sensors tend to be composed of one or multiple force–sensing components. In general, force–based tactile sensors in MIS can be categorized into array–type tactile sensors and single–point tactile sensors [27].

2.2.1 Array–type tactile sensors

A tactile array sensor consists of multiple (discrete) force–sensing elements arranged in arrays. The force–sensing elements of the tactile array sensor were developed based on piezoresistive [28] ,piezoelectric [29–33], magnetic [34] or capacitive [35–39] principles. For tissue palpation, a tactile sensor is pressed vertically against the target tissue. The location and size of the embedded tumor were reflected in spatial (distribution) information from the sensors. The tumor depth might be obtained by estimating the indentation displacements of the tactile sensors in RMIS, but it is difficult to achieve in LS. Moreover, high contact stresses at the edges of the sensor array may degrade the spatial information obtained, leading to tissue assessment difficult [5]. Furthermore, there may be potential risks since the sensors consist of electrical elements in the body. Electrical activity, such as leakage currents generated during tissue palpation, may adversely affect the patient. Tactile array sensors based on optical principles can protect the patient's tissue from the risk of electrical activity because there is no electrical element in the sensing area [40, 41]. However, the general problem with the above array–type sensors is that they combine multiple sensing elements, which results in a complex structure and large size, making them unsuitable tactile sensors for actual MIS [42].

2.2.2 Single–point tactile sensors

A single–point tactile/force sensor used only one sensing element to collect the applied force data at the contact area. Single–point tactile sensors using strain gauge [43], piezoelectric transducers [44–47], magnetic field [48] or capacitive transducers [49] often have simple structures, and low–cost fabrications, and appropriate dimensions for laparoscopic tissue palpation, compared to array–type tactile sensors. For tissue palpation procedures, the single–point tactile sensor was used to acquire contact force data by applying discrete point uniaxial indentations [50,51], continuous indentations [52,53] or sweeping motions [54] on the tissue surface. Based on the spatial information obtained by the sensor during palpating tissue, surgeons can localize the tumor and determine its size. The tumor depth was also determined based on the indentation depth of the sensors. However, since the indentation depth of the sensors is required to maintain at a constant level during palpation, the sensor might be only available for tissue palpation in RMIS. In addition, it takes time to create a tissue stiffness map, so the information obtained cannot be completely reliable if the tissue shifts.

Other studies relied on instantaneous tactile data from single–point sensors to evaluate the target tissue [49, 56, 57]. Thus, surgeons could use the sensor to quickly determine the embedded tumor in LS. Single–point sensors based on acoustic reflection principles [58, 59] have an advantage in terms of electrical safety because they do not insert electrical elements into the patient's body. Moreover, the type of tactile sensor is sterilizable and disposable. However, the obtained information of the sensor can be largely affected by sensing conditions; the surgeon is required to operate the sensor steadily and dexterously during palpation.

2.3 Display technologies

Force/tactile information from force/tactile sensing devices can be provided to surgeons in various methods. Surgeons could perceive the information by their natural sensory system to evaluate the palpated tissue. On the other hand, the information could be analyzed using artificial sensory algorithm to identify the tissue characteristics. Thus, the display technologies are categorized based on human sensory display and artificial

sensory algorithms.

2.3.1 Display technologies based on human sensory display

Visual, auditory, and haptic feedback are three common human sensory display modalities used to convey haptic information in tissue palpation. The technologies using these three display modalities are summarized.

Visual feedback

In MIS, surgeons observe visual information of intraoperative tissue and organ on monitors. Visual feedback is a popular feedback modality that displays the haptic information on the surgeon's visual channel. The visual information for tissue palpation could be color map images [28–30, 34, 35, 50, 52, 60–63] or time–series signal images [45, 47, 58, 59].

For color map images, tactile information from array–type tactile sensors or single–point sensors are used to establish mappings of the distribution of force and stiffness in the soft tissue examined. The distribution image can be presented by overlaying the color images on monitors in LS. Since the color of tumor area often differs from the color of surrounding tissue, surgeons could determine the tumor location or size. However, the overlay image degrades the surgical image, leading to difficulty for the surgeon to observe the surgical site. Moreover, since the color image's acquisition tends to be time–consuming, the tumor location information is not completely reliable when the tumor is shifted.

For time–series signal images, surgeons observe the instantaneous dynamic reaction signal of contact force during tissue palpation. By detecting this abnormal signal, the location of the tumor can be determined. Although surgeons can quickly locate the tumor position using the visual feedback method, the determination of tumor depth and size using the method is arguable. Since visual information is the dynamic signal, it could be impaired by tissue deformation or palpation movement, causing reductions in the surgeon's performance in tumor detection. In addition, simultaneous observation of tactile signal and intraoperative image might overload the visual channel of surgeons [64].

Auditory feedback

Another approach to convey tactile/force information is auditory feedback. Cutler et al. represented force feedback by producing an auditory signal using a conventional speaker to users [65,66]. The graded sound was proportional to the force level. In this case, because surgeons did not wear any device on their hand, the feedback did not induce movement in the surgeon's hand during the procedure. In addition, the use of other sensory modalities for providing haptic information could prevent the surgeon from the visual sensory overload. However, continuous sound during long operations is noisy and distractive to surgeons' communication [67,68].

Haptic feedback

Haptic feedback is a promising alternative for providing haptic information to surgeons during intraoperative tissue palpation. This feedback modality is independent of the visual channel and rarely impedes the surgeon's operation.

Kinesthetic feedback is a haptic sensory modality that allows surgeons to be aware the position, movement, and contact force of surgical tools during operation [69–75]. In LS, due to surgeons manipulate the surgical tools by hand, they directly receive the kinesthetic feedback. However, the haptic information provided by kinesthesis feedback is reduced because of friction between the trocar and the surgical tool. Thus, although kinesthesis feedback is a straightforward approach to obtain the contact force information, it only contributes to the manipulation of surgical instruments and cannot be used to palpate tissue. In RMIS, the kinesthetic feedback is provided to surgeons via a master console, and the fidelity of the feedback relies on the performance of the RMIS system. However, the kinesthetic feedback in RMIS can compromise the manipulation of the sensing device or the stability of the teleoperation's control loop [76].

Tactile feedback is another haptic feedback modality commonly used in laparoscopic tissue palpation. A tactile display is a device used to provide tactile feedback to a user's skin. Tactile displays could be categorized based on the tactile sensing group mentioned in the previous section. For example, pin–array displays are often utilized to deliver the force information from array–type tactile sensor to the user's skin by moving the pins of the tactile display [20]. Based on the spatially distributed

pressure generated by the device, the surgeon could evaluate the contact tissue to localize the tumor and determine the tumor size. Such pins can be actuated using shape memory alloy wires [77,78], multiple servomotors [79], and pneumatic systems [80–82]. Although pin–array type displays can provide haptic cues with high fidelity, they tend to have complex structures with high fabrication costs and require a bulky drive unit for their actuation [83]. Thus, these types of devices are unaffordable for widespread application and are only appropriate for the RMIS system.

Tactile displays that represent force information acquired from single–point tactile sensors are often developed for temporal information–based palpation. Based on the instantaneous sensory feedback provided by the displays, the surgeon could detect the intraoperative tumor or abnormal tissue. The tactile feedback of such tactile display was generated by vibration [84], and pneumatic power [85]. The advantages of the tactile display are simple structure and lightweight, causing hardly interfering with the surgeon's motions in operation. Moreover, the tactile display based on pneumatic power meets the requirements of clinical applications such as disposable and sterilizable. However, since the tactile feedback from the tactile display is too simple, it might not be sufficient to determine the tumor depth or size using the tactile display.

2.3.2 Display technologies based on artificial sensory algorithms

The use of human sensory modalities for obtaining tactile information is a straightforward way for tissue palpation. However, the performance of tumor characterization based on the natural sensory feedback is greatly dependent on the surgeon's experience and perceptual abilities. Other research has focused on analyzing force data using haptic perception algorithms (or artificial sensory algorithms) to obtain tissue characteristics.

Computational models established using artificial neural networks (ANN) [7,86] and deep neural networks (DNN) [87] have been used to identify the location, size, and depth of abnormal tissue. Other researchers have proposed models for estimating the characteristics of tumors using a finite–element–based method [88] or a dynamic position sensing method [89]. These computational models can determine the size and

depth of the tumor with high accuracy, regardless of the surgeon's perception ability and experience. However, the performance of these methods is highly dependent on the data collected, complicating their application to various tissue.

2.4 Haptic technology used in this thesis

In this thesis, we aimed to propose a haptic system to assist surgeons in characterizing the location, depth, and size of tumors in LS. The system includes a tactile sensor for collecting the tactile information during tissue palpation and a tactile display for representing the tactile information to surgeons.

In this study, we developed a single–point tactile sensor that has the advantages of simple structure, lightweight, and low cost. If the sensor could measure only normal force component of contact force [58, 59], the effect of tissue deformation or surgeon's motions on the sensor output will not be eliminated. This can be addressed by making the sensor have a new contact force component, such as shear force, in addition to the normal direction force, since the response of shear force tends to be affected only by contact friction. In this way, a multiple degree–of–freedom (DoF) tactile sensor can be developed. However, too high DoF might cause complicate the structure of the device. Therefore, a 2–DoF tactile sensor will be introduced into LS to minimize the size and simplify the tactile sensor. Moreover, the proposed sensor will be developed based on the acoustic reflection principle. This allows the sensor to have significant advantages in MIS, such as disposability, sterilizability, and electrical safety for the patient's body.

Regarding the display method in tissue palpation, tactile feedback from a tactile display is used to provide tactile information to surgeons. The use of tactile feedback prevents the possibility of the surgeon overloading the visual channel. Moreover, human sensory modality such as tactile feedback has the advantage of being applicable to a wider range of tissues and MIS procedures than artificial sensory algorithms. In addition, the tactile display will be developed using pneumatic power to ensure the requirements of surgical devices in a clinical environment. Furthermore, in order to simplify the structure of the display, only 2–DoF feedback functions are included. Surgeons rely on tactile feedback from tactile devices to evaluate the tumor and determine the tumor characteristics.

2.5 Summary

This chapter summaries current tactile sensing and display technologies for intraoperative tissue palpation. Sensing devices for acquiring tactile data were summarized in two groups: array–type tactile sensors group and single–point sensor group. The tactile data from tactile sensors could deliver to surgeons based on human sensory or artificial sensory algorithms. Visual, auditory, and tactile feedback is three common human sensory modalities that can be used to develop display devices. ANN and DNN are two common artificial sensory algorithms that can be used to provide the characteristics of the tumor during tissue palpation to surgeons. In this thesis, single–point tactile sensor based on acoustic reflection principle and pneumatic–based tactile display will be developed because of their advantages for intraoperative tissue palpation.

Chapter 3

A tactile sensor using acoustic reflection principle for assessing contact force components in tumor localization

In Chapter 3, a forceps–type tactile sensor for intraoperative detection of gastric tumor is proposed. The tactile sensor has two contact force component measurement functions and is developed based on acoustic reflection principle. The advantages of the tactile sensor for clinical application are discussed. The effectiveness of the force component information from the sensors for localizing tumor regarding to the effect of tissue deformation and user's behaviors are assessed through a tissue palpation experiment with an artificial stomach phantom.

3.1 Introduction

In many domains of surgical operation, the evaluation of the anatomical structures of the patient's body is an important procedure. Surgeons can detect lumps or tumors, leading to enhanced surgical quality, such as dissecting such tumors with a minimum margin. However, structures such as gastric tumors are often beneath the tissue surface and may not be seen intraoperatively. Although preoperative imaging techniques, such as CT and MRI, can be used to detect the location of the tumor, the preoperative information is not completely reliable since the tumors often shifts during surgery, especial in MIS. Intraoperative ultrasound is a technique that could be applied to confirm the location of the gastric tumors in MIS [90]. Nonetheless, the technique has high computational expenses [91], often provides relatively poor quality images [92] and might not be effective in detecting tumors less than 10 mm in size [93]. Moreover, the lack of contact force information during MIS causes the surgeon's difficulties in

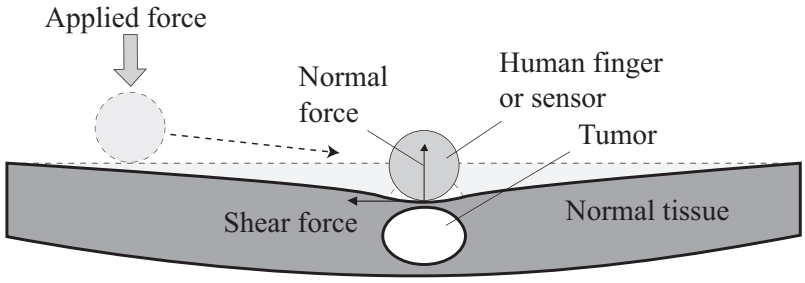

Fig. 3.1: Illustration of contact force components when a human finger or a sensor palpate tissue with a tumor

manipulating the ultrasonic sensor, leading to impairing performance or increasing potential tissue trauma [23, 24]. In open surgery, surgeons tend to rely on their tactile sensation to explore the anatomical structures. In MIS, the use of haptic devices, such as tactile sensor, is a promising method to compensate for the elimination of haptic sensation and support surgeons in their tumor detection.

For laparoscopic palpation, a tactile sensor using an optical tactile array [41], a sensor employing an optical fiber sensing scheme [53], a fiber bragg grating–based force sensor [94], a tactile sensor using the piezoelectric vibrator principle [95], and a palpation probe employing capacitive transducers [96] were proposed. Because tactile devices are designed as forceps–type sensors, surgeons can easily use them as general surgical instruments. However, these sensors have some issues in terms of practical application in MIS, such as complex structure, high fabrication cost, risks of leak current and unsterilizable. A tactile sensor based on acoustic reflection principle could be deal with the mentioned problem in MIS [58]. This sensor was proven to be feasible for surgical application because of its suitable dimensions, electrical safety for human tissue, simple structure and strong robustness to sterilization. The position of a lump can be detected by observing the contact force responses when the sensor slides over a tissue surface. However, the tissue deformation and user's actions during palpating tissue often reduce the performance of the tactile sensors in tumor localization.

In previous studies on tissue palpation, experiments were conducted under the condition that the tissue was stably fixed on rigid base plates [22, 53, 96]. However,

owing to the anatomical structure, the surface of the human organ such as stomach does not have a rigid base [58]. Bending of the tissue due to the applied force tends to occur during actual tissue palpation may affect the sensitivity of lump detection, as shown in Fig. 3.1. The current force information obtained from the current acoustic–based tactile sensor might be insufficient to localize a tumor, as it corresponds to the normal force [58]. When a human finger or sensor slides along the surface of a tissue with a tumor, the normal force is significantly affected by the force applied by the user. Meanwhile, the shear force response might be influenced by contact friction. Humans tend to apply lateral force (related to shear force) to improve the perceived tactile information [22]. Furthermore, Kim et al. reported that the angular difference between the normal force and surface normal directions during tissue palpation could be used to detect the lump region [56]. The angular values are correlated with the shear force response. Thus, we hypothesize that the shear force might be more sensitive to tumor position and might not be strongly impacted by the bending of the contacted tissue.

In this chapter, we aimed to develop a tactile sensor with multiple force measurement functions using the acoustic reflection principle for intraoperative tumor detection in LS for early–stage gastric tumor resection. The sensor has two acoustic cavities, and it is capable of measuring the normal and shear components of the contact force. The sensor offers the advantages of acoustic-based tactile sensor, such as the absence of electrical elements at its sensor tip, a simple structure without complex wiring, and sterilizability. Additionally, the fabrication of a sensor prototype is presented. Fundamental tests were conducted to validate the performance of the tactile sensor prototype. Finally, a tissue palpation test using the tactile sensor and an artificial phantom with an embedded tumor was performed to evaluate the use of the contact force components of the sensor in intraoperative tumor detection.

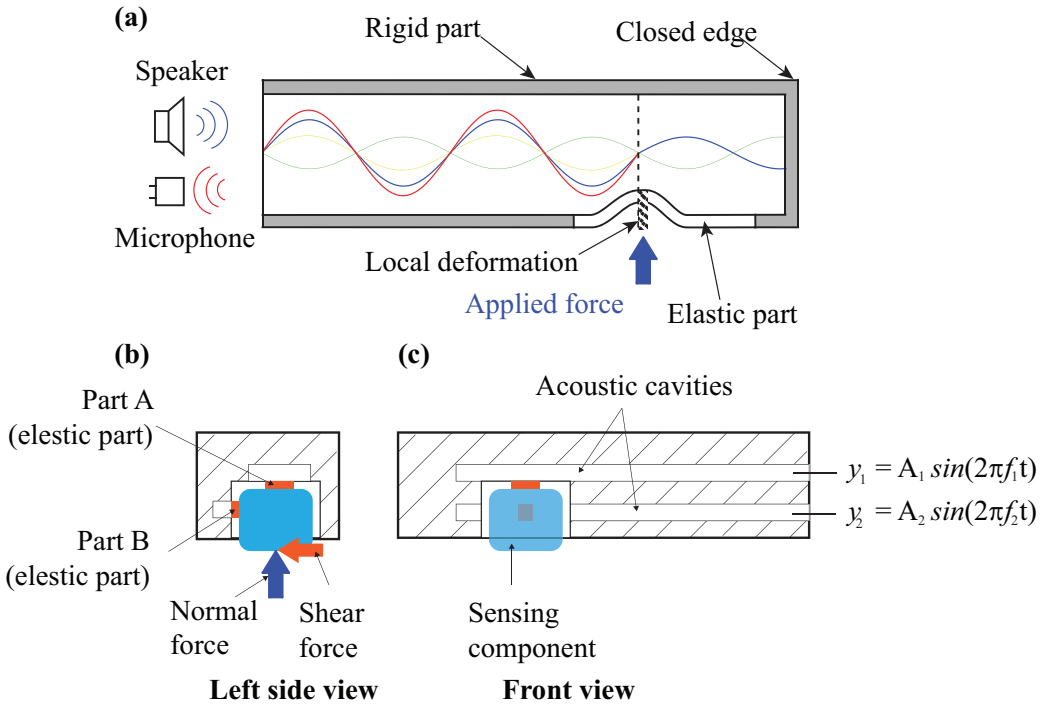

Fig. 3.2: Acoustic reflection principle concept (a) Acoustic reflection principle for a single cavity (b) Left–side view of the proposed concept of a sensor with two acoustic cavities using the acoustic principle (c) Front view of the proposed concept of the sensor.

3.2 Tactile sensor

3.2.1 Two–axis force sensing with the acoustic reflection principle

In the previous tactile sensor using the acoustic reflection principle, an acoustic wave with a single frequency is transmitted into a cavity as shown in Fig. 3.2 (a) [58]. The cavity consists of a rigid part and an elastic part. When a loading force is applied to the elastic part, a deformation appears that changes the acoustic wave. The applied force can be estimated by measuring the amplitude change of the acoustic wave. In general, a sensor using the acoustic principle with one cavity can measure only one

component of the applied force. To measure multiple components of the applied force using the acoustic principle, we propose a novel sensor design with multiple acoustic cavities. Each cavity corresponds to each component of the applied force.

Fig. 3.2 (b) and Fig. 3.2 (c) illustrate the concept of a 2–axis tactile sensor for normal force and shear force measurement purposes. It is composed of a body part with two acoustic cavities and a sensing component (blue part). Each acoustic cavity consists of a rigid part and a deformable part as a general cavity of the acoustic reflection principle. The acoustic cavities are defined as the normal cavity and shear cavity based on their respective measurement function. The sensing component is in contact with deformable part A of the normal cavity and part B of the shear cavity, as shown in Fig. 3.2 (b). Therefore, the sensor has the capability to measure the normal force and shear force in one direction. As surgeons tend to scan tissue using a tactile sensor in one direction, the sensor's measurement ability is sufficient to obtain the necessary contact force during tissue palpation. Two corresponding sinusoidal acoustic waves y_1 (with frequency f_1) and y_2 (with frequency f_2), are transmitted into the normal cavity and the shear cavity to estimate the contact force applied to the sensing component.

3.2.2 Tactile sensor prototype

Based on the proposed concept, we developed a forceps–type sensor prototype with two force measurement functions. The prototype consists of a sensor tip, two brass tubes, an outer tube, and two acoustic cases with speakers (Kingstate, KDMG1000) and microphones (ICC/Intervox, MEU–65PD–02–704), as shown in Fig. 3.3 (b) and Fig. 3.3 (c). The sensor tip is composed of a rigid body with two acoustic cavities, and two silicone pads as the deformation components of the cavities cover the open parts of the acoustic cavities, as shown in Fig. 3.3 (a). The sensing component, which is attached to the sensor tip body, is always in contact with both silicone pads. The brass tubes are connected to the acoustic cases and the sensor tips through the couplings for disposal purposes.

The fully assembled sensor prototype is presented in Fig. 3.4. The entire length of the sensor is approximately 460 mm, and the composed cavity lengths are approximately 460 mm. The sensing component (4 mm $\times$ 8 mm $\times$ 8 mm) with a round corner

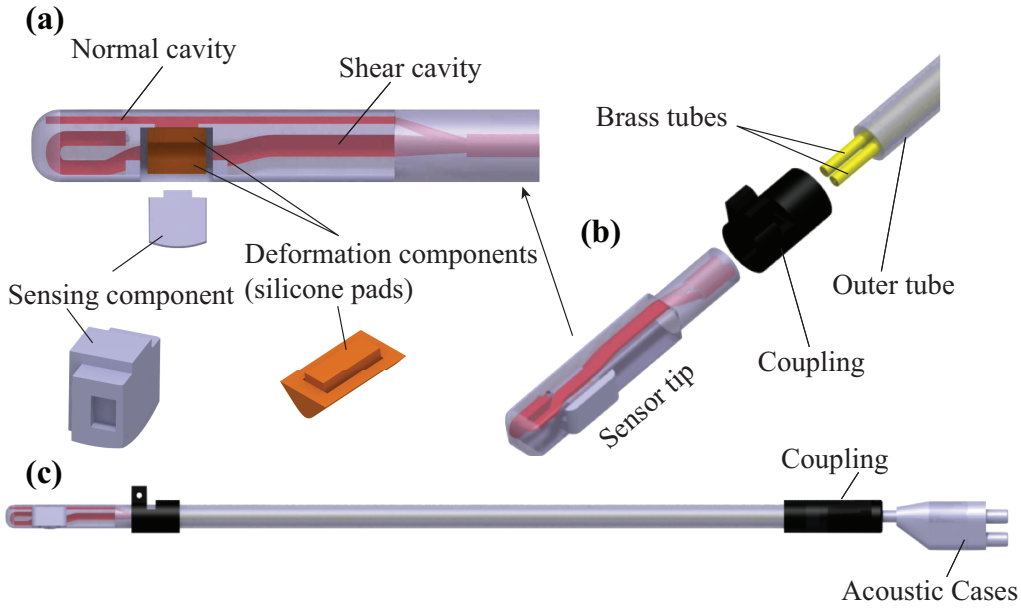

Fig. 3.3: Design of the tactile sensor (a) Sensor tip components. (b) Tactile sensor components. (c) Fully assembled sensor

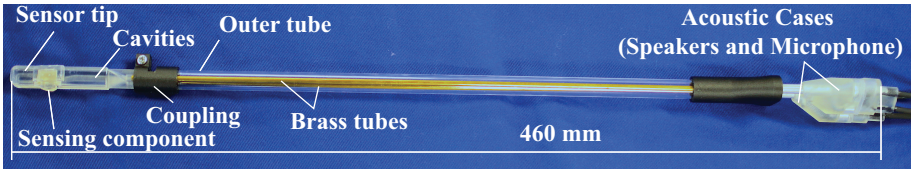

Fig. 3.4: Tactile sensor prototype

radius of 10 mm was attached to the sensor tip body (10 mm × 10 mm × 30 mm). The embedded cavities have a rectangular cross–section (1 mm × 2 mm). The prototype employs brass tubes having an external and internal diameter of 3 mm and 2 mm, respectively. The external diameters of the outer tube and the coupling at the sensor tip are 10 mm and 14 mm, respectively. The bodies of the sensor tip and the sensing component were constructed from photopolymer resin using a 3–D printer (Formlab Inc., Form2). The silicone pads were made from pourable silicone (Young's modulus: 22 kPa) using a 3–D printed mold.

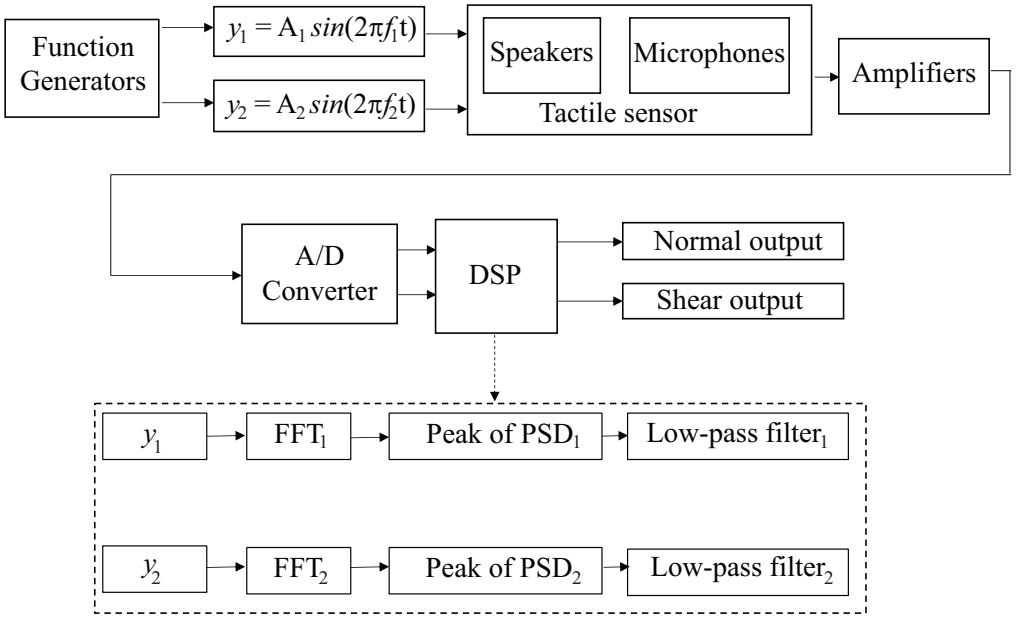

Fig. 3.5: Measurement system

3.2.3 Measurement system

The measurement system for the tactile sensor is depicted in Fig. 3.5. Two sinusoidal acoustic waves with frequencies of 2980 Hz (f_1) and 3210 Hz (f_2) were chosen as input signals. They were generated by function generators and speakers. The signals obtained from the microphones were amplified using microphone amplifiers before being sent to the A/D converter (National Instruments, 16–bit resolution, 30 kHz sampling frequency) for analysis. The fast Fourier transform (FFT) with $n = 2048$ data points of the signals was calculated. The power spectral density values of the generated wave frequencies were selected as the sensor output. The outputs obtained from the normal and shear cavities were defined as the normal and shear outputs, respectively. The outputs were updated approximately every 7 ms and smoothed using a low–pass filter with a cutoff frequency of 5 Hz. The sensor outputs were calibrated using a 6–axis commercial force sensor (ATI, Inc. Gamma Si–32–2.5), whose output was also collected by the same A/D converter.

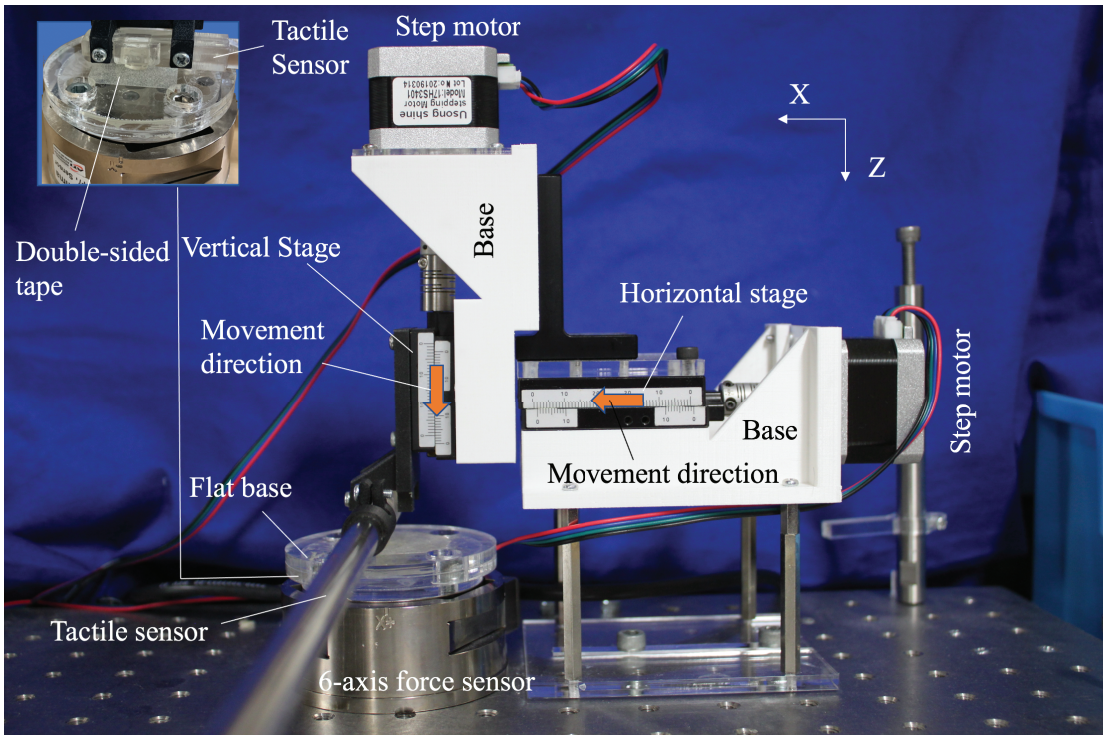

Fig. 3.6: Experimental setup

3.3 Experiments and Results

3.3.1 Calibration test

An experimental setup was established to collect the sensor output response to an applied force for calibration.

Setup and procedure

The experimental apparatus is depicted in Fig. 3.6. In the setup, the sensor tip of the tactile sensor was fixed on a vertical stage, which was mounted on a horizontal stage. The displacement of each stage was controlled by two stepper motors to adjust the applied normal force and shear force. A flat base as a contact area was attached over the 6–axis force sensor for protection. A piece of double–sided tape (30 mm $\times$ 30 mm)

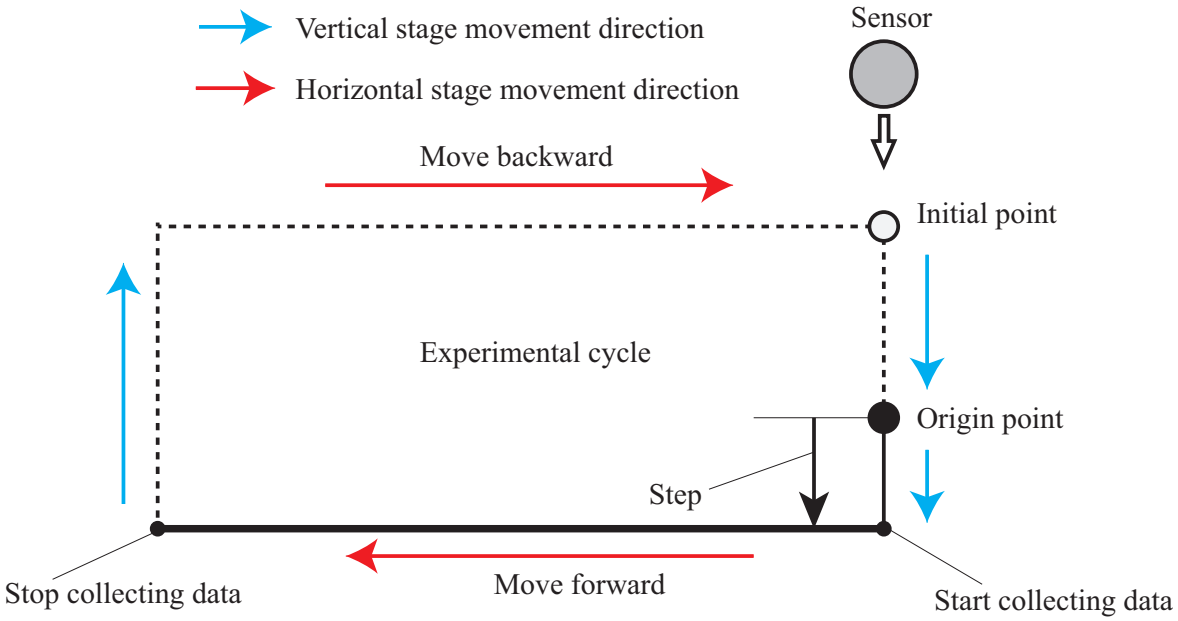

Fig. 3.7: Explanation of the experimental cycle

was applied on the flat base to improve the friction of the contact area as shown in the left inset of Fig. 3.6. With the tape, the sensor tip almost sticks to the flat base, thereby preventing slippage during the calibration test. To automate the calibration test, some essential points were defined. First, the stages were adjusted to the position where the sensing component was in contact with the flat base, while the applied force was still zero. This point was defined as the origin point, with $X = 0$ mm and $Z = 0$ mm. Then, the vertical stage was moved backward by 2 mm. This position was defined as the initial point, with $X = 0$ mm and $Z = -2$ mm. The two points are shown in Fig. 3.7.

For the calibration test, at the beginning, the vertical stage started at the initial point and then quickly moved to the origin point. Next, the horizontal stage was slowly adjusted by displacing from 0 to 1.75 mm in increments of 0.25 mm to increase the applied shear force. The difference between the initial and the instantaneous sensor outputs with wave y_1 ($\Delta V_N = V_N - V_{N0}$) and wave y_2 ($\Delta V_S = V_S - V_{S0}$) was computed at every increment of the force. V_{N0} and V_{S0} are the initial values of the normal and shear outputs at the origin point, respectively. V_N and V_S are the instantaneous values

of the corresponding normal and shear outputs, respectively. The ratios of ΔV_{N} to V_{N0} and ΔV_{S} to V_{S0} were collected as normalized normal output (U_{N}) and normalized shear output (U_{S}), respectively. At the final point, the collected data were saved. Then, the vertical stage was returned to the initial point to complete the experimental cycle. In the next cycle, after moving to the origin point, the vertical stage was moved forward by 0.25 mm, and then, the described cycle was repeated. For a better understanding, the experimental cycle is depicted in Fig. 3.7. The vertical stage was adjusted from 0 to 1.75 mm in increments of 0.25 mm, corresponding to an increase in the applied normal force. At every vertical stage increment, the cycle was repeated.

3.3.2 Means of feedback of the sensor output

Calibration method

The sensor output responses during the calibration test are presented in Fig. 3.8. The normal output almost corresponds to the applied normal force and is slightly affected by the applied shear force. In contrast, the tendency of the shear output changes at different increments of the vertical force. Thus, the normal force (F_{N}) estimated from the sensor can be computed using only the normal output, whereas the shear force (F_{S}) estimated from the sensor should be computed using both the normal and shear outputs. This characteristic of the sensor can be represented by the following equations:

$$F_{\mathrm{N}} = a \times {U_{\mathrm{N}}}^2 + b \times U_{\mathrm{N}}, \tag{3.1}$$

$$F_{\mathrm{S}} = k \times U_{\mathrm{N}} + m \times U_{\mathrm{S}}, \tag{3.2}$$

where $U_{\mathrm{N}} = \Delta V_{\mathrm{N}}/V_{\mathrm{N0}}$, $U_{\mathrm{S}} = \Delta V_{\mathrm{S}}/V_{\mathrm{S0}}$, and a, b, k and m are calibration coefficients, which are calculated from the calibration test results. The polynomial fitting method of degree $n = 2$ was employed to compute the a and b coefficients. Similarly, the k and m coefficients were determined using the linear regression method for both the normal and shear output data. The coefficients were calculated as $[a, b, k, m]^{\mathrm{T}}$ $= [89.4907, 15.2447, 1.53149, 7.9215]^{\mathrm{T}}$.

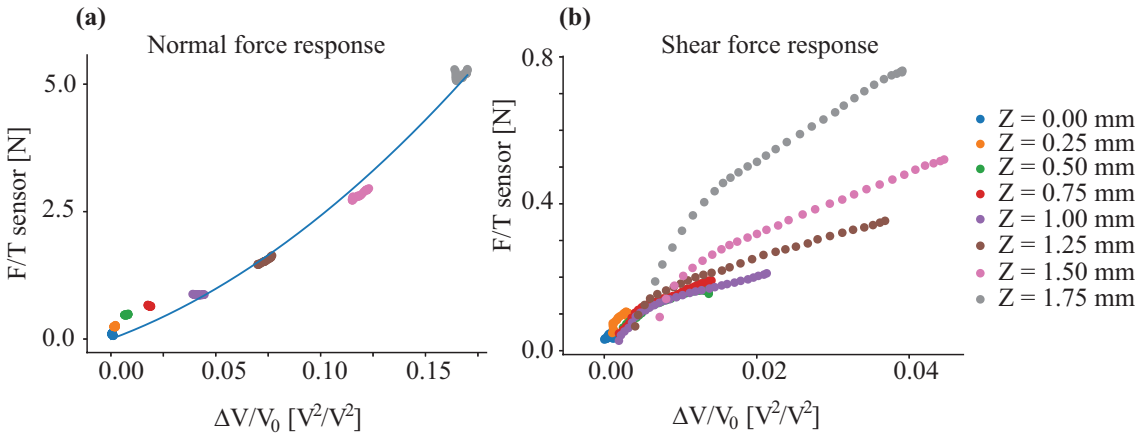

Fig. 3.8: Experimental results of the calibration test (a) Normal output of the sensor compared to the actual normal loading force (b) Shear output of the sensor compared to the actual shear loading force.

3.3.3 Verification tests

To evaluate the performance of the prototype sensor, verification tests were conducted using the 6–axis force sensor. This experimental setup was similar to that used in the calibration test. To determine the hysteresis of the normal force, the vertical stage was slowly moved forward from 0 to 1.75 mm and backward to zero, while the horizontal stage was kept unchanged. Similarly, in the verification of the shear force hysteresis, the horizontal stage was slowly adjusted from 0 to 1.75 mm while the vertical stage was kept unchanged at position $Z = 1.5$ mm. The repeatability of the sensor performance was obtained by computing the standard deviation of each estimated force when the same loading forces were applied at least three times. The calculations of the hysteresis and repeatability of the sensor can be found in [97]. The sensor resolution was obtained by estimating the peak–to–peak noise of the sensor.

To examine the accuracy of the sensor, the acoustic sensor was manually pushed against the 6–axis force sensor to arbitrarily produce an applied force. The experimental results of the accuracy test are shown in Fig. 3.9. The root mean square errors (RMSEs) of the accuracy test and the specifications of the sensor are summarized in Table 3.1.

	Normal force	Shear force
Force Range	0–5N	0–0.75 N
Resolution	23 mN	20 mN
RMSE	206 mN (4.12 % FSO)	54 mN (7.2 % FSO)
Repeatability	0.92 % FSO	1.90 % FSO
Hysteresis	19.54 % FSO	19.6 % FSO

Tab. 3.1: Specifications of the proposed sensor

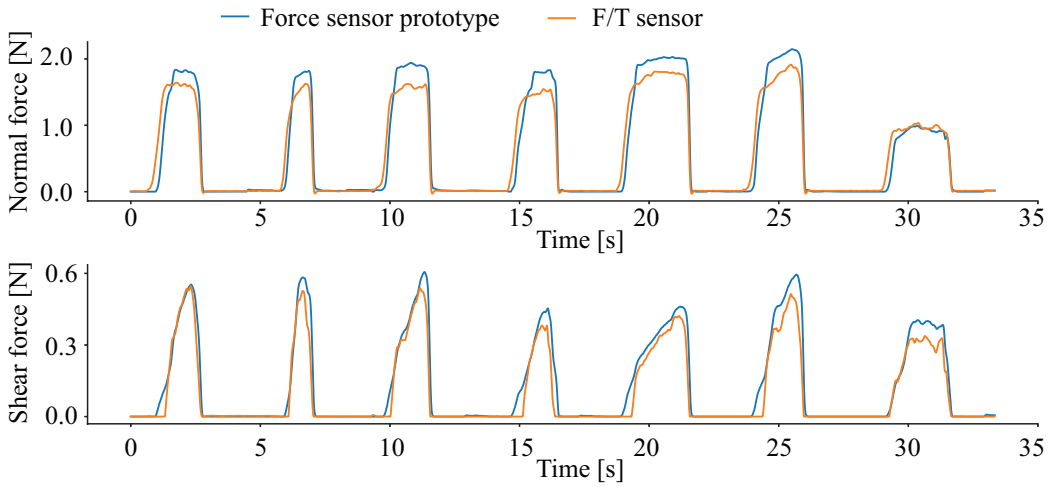

Fig. 3.9: Responses of the sensor prototype and the standard 6-axis force sensor for normal and shear forces over 33 s.

3.3.4 Experiments using a phantom of the stomach wall

To evaluate the feasibility of using the proposed sensor for gastric tumor detection in laparoscopic palpation, the sensor prototype was applied to a phantom of the stomach wall.

Setup and procedure

In this experiment, we aimed to localize a 0–IIc (superficial ulcerative) type of early–stage gastric tumor [98]. Such gastric tumors tend to have a toroidal shape and are located on the mucosa of the stomach. An artificial phantom of the stomach wall with a tumor was fabricated based on the actual properties of the stomach as well as the tumor as indicated in [59, 85]. The phantom has dimensions of 180 mm × 160 mm × 9 mm, as shown in Fig. 3.10 (a). The phantom sample consists of two layers with different stiffness values. The harder layer with a thickness of 2 mm imitates the serosa of the stomach wall, and the softer layer with a thickness of 7 mm imitates the mucosa. These layers were made of polyurethane gels (Hapla Pudding Gel, Plysis Cp., Ltd) with different hardness values. The tumor was located in the harder layer and made of the same gel as the harder layer. The outer diameter, inner diameter, and height of the tumor were 20 mm, 13 mm, and 8 mm, respectively. The mean stiffness of the phantom (measured using an Asker Durometer Type FP, Kobunshi Keiki Co., Ltd) was Asker FP 63 for the normal region and Asker FP 81 for the tumor. The phantom was placed on a sponge plate with a thickness of 10 mm, as shown in Fig. 3.9 (b). The two ends of the phantom and the sponge plate were supported by rigid semicircular bases and fixed by semi–cylindrical plates. No rigid plate was placed beneath the sponge plate to mimic the space inside an actual stomach.

The sensor was palpated on the smooth side of the phantom (serosa) to investigate the tumor. This procedure is similar to a surgeon localizing the tumor from outside the actual stomach during clinical operation. During the palpation test, the acoustic sensor was pushed against the phantom (loading zone) and then scanned over its surface (slip zone) before being released from the phantom (unloading zone). The procedure was repeated to detect the tumor position on the phantom.

Tissue palpation results

The responses of the tactile sensor prototype during tissue palpation are shown in Fig. 3.11. Fig. 3.11 (a) and Fig. 3.11 (b) show the response of the tactile sensor when scanned over the phantom region with and without a tumor four times, respectively. The gray areas shown in Fig. 3.11 (a) illustrate the phases when the sensor traversed

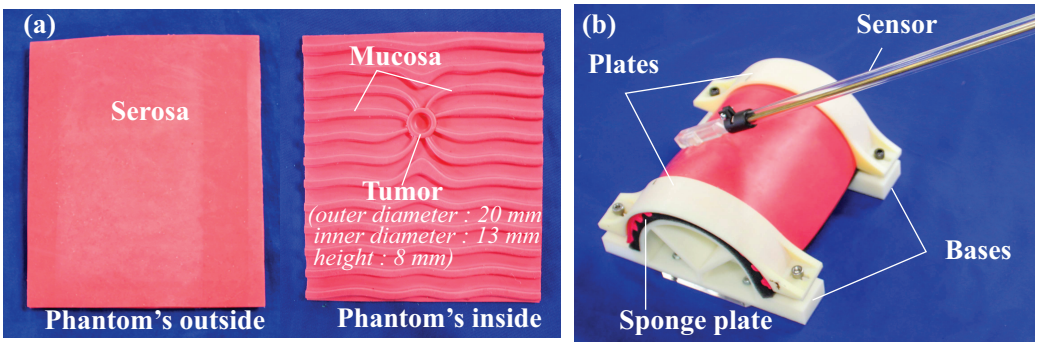

Fig. 3.10: Tissue palpation using a phantom of the stomach wall (a) Phantom of the stomach wall with an embedded tumor (b) Tissue palpation using the phantom and the proposed sensor prototype.

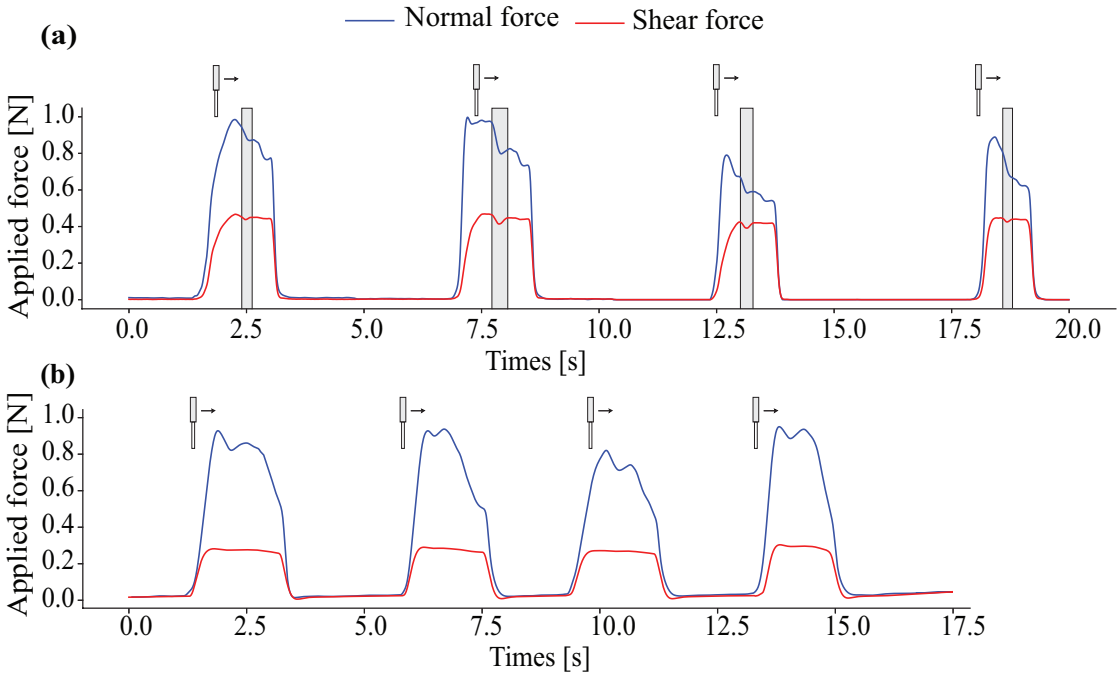

Fig. 3.11: Response of the proposed sensor prototype during the tissue palpation (a) Response of the sensor in the phantom region having the embedded tumor (b) Response of the sensor in the phantom region without tumor.

the tumor area. Fig. 3.12 (a) and Fig. 3.12 (b) highlight the sensor response during the third palpation shown in Fig. 3.11 (a). To localize the tumor, only the contact force responses in the slip zone were evaluated. The normal force response in the slip zone gradually decreased during scanning. Abnormal convex curves of the normal force response occurred in the slip zone as shown in Fig. 3.11 (a). However, it is difficult to identify the convex curve corresponding to the tumor of the phantom by observing the normal force response. In contrast, the shear force output was relatively stable, and hence the tumor can be easily localized by evaluating the shear force output. The convex curve of the shear force response in the slip zone corresponded well to the tumor position as shown in Fig. 3.11 (a). Regarding the sensor output for the phantom region without a tumor, as shown in Fig. 3.11 (b), the shear force output in the slip zone was almost stable, whereas a part of the convex curve of the normal force output appeared in the slip zone. Thus, it might be difficult to confirm the appearance of the tumor if only the normal force output was evaluated.

To quantitatively evaluate the impact of the normal and shear forces on tumor localization during tissue palpation, the responses of these force components for the tissue areas within and surrounding the tumor were selected. By observing both the change in the sensor output and movement of the sensor on the phantom's surface, we defined t as the period during which the sensor palpated the tumor area. Then, the responses of the sensor in three phases (3t), in front of the tumor area (IFOTA), within the tumor area (TA), and behind the tumor area (BTA), were investigated. The three phases shown in Fig. 3.12 (a) and Fig. 3.12 (b) were located in the slip zone. The first and last points of each phase were utilized to establish the evaluation lines. The evaluation lines were considered as the response of the sensor for the phantom region without a tumor. These lines were also considered as the sensor output when the user could control the sensor well during the tissue palpation. The lines do not include the variance of the sensor output due to the variance of the manual operation of the sensor probe. The RMSEs between the sensor force response and the evaluation lines of each phase were calculated. The differential ratio between the RMSEs of each phase and the average RMSEs within the tumor area (TA) of all collected data was used as an evaluation metric. The differential ratios were computed for eight tissue palpation cycles, and the mean differential ratios and their standard deviations for each area are

presented in Fig. 3.12 (c). The evaluation results show that the shear force response within the tumor area was higher than that within the surrounding areas compared with the normal force information.

3.4 Discussion

The experimental results indicated that the applied normal force could be obtained from only the normal output of the tactile sensor prototype, whereas the shear output shows effects of both the applied normal and shear forces. Therefore, the applied shear force should be estimated from both the normal and shear outputs of the sensor. One possible reason for this phenomenon may be the tilting of the sensing component due to the lateral motion. This caused a small change in the contact area between the sensing component and the deformation component of the shear cavity (part B, as shown in Fig. 3.2 (b)), leading to distortion of the shear output.

For general MIS procedures, the normal force range of the sensor (0–5 N) is adequate for common tissue manipulation [55]. In tissue palpation, McCreepy et al. reported that a force range of 0–2 N was sufficient for lung tumor detection [99]. Moreover, in conventional tissue scanning, the wet state of the human tissue results in slipping of the tactile sensor on the tissue surface, which leads to the obtained shear force values tending to be small. Thus, the measured shear force of our tactile sensor (ranging from 0 to 0.75 N) exhibits the potential to achieve an appropriate measurement range of the force required in tissue palpation. The use of a high–performance A/D converter (NI–DAQ) and low–pass filter of 5 Hz led to the high resolution of the sensor of 23 mN for normal force and 20 mN for shear force. The hysteresis of the normal force (20.9 % of the full–scale output – FSO) and shear force (19.6 % of the FSO) is quite high. This might be reduced by choosing an appropriate stiffness for the deformable component and reducing its thickness. The RMSEs of the force evaluation were computed as 206 mN (4.12 % of the FSO) and 54 mN (7.2 % of the FSO) for the corresponding normal and shear forces. The accuracy of the sensor could be improved by reducing the hysteresis of the sensor or by choosing an optimal calibration method. The sensor has good repeatability in terms of force measurement in MIS with 0.84 % of the FSO for normal force and 1.9 % of the FSO for shear force.

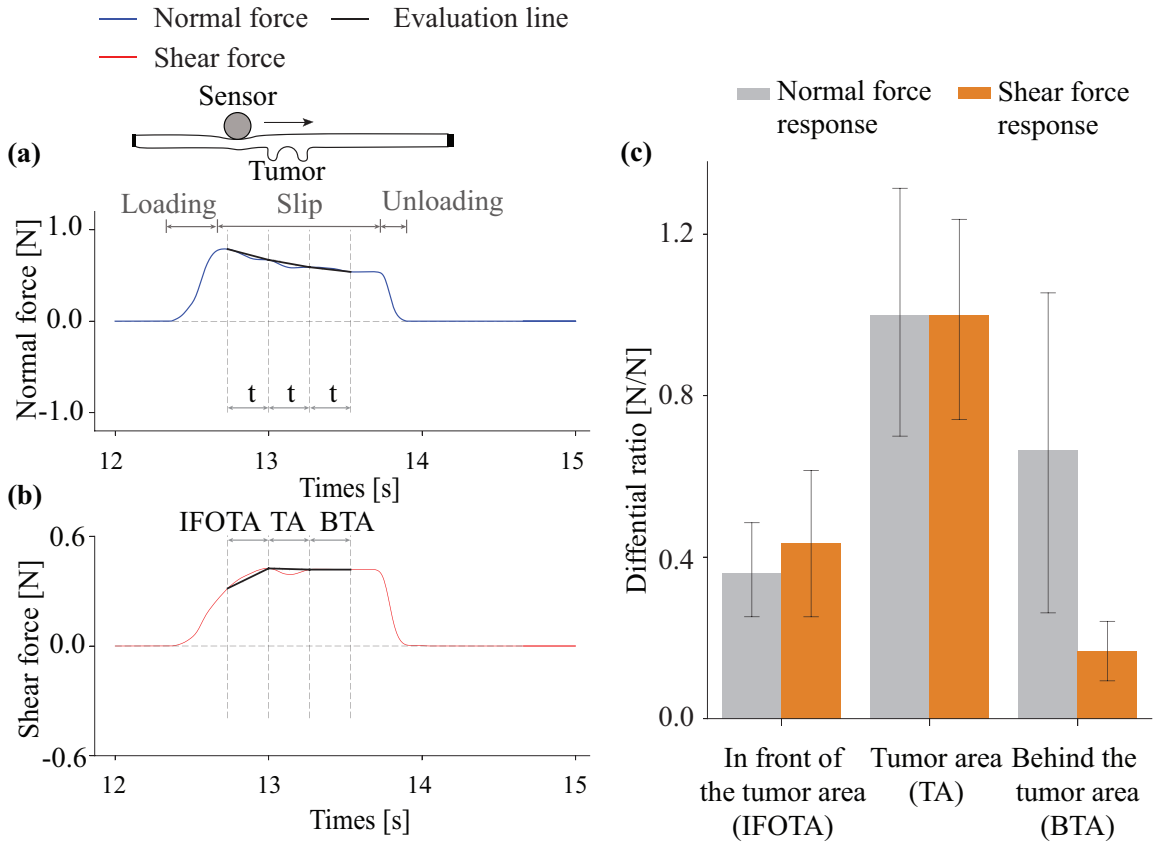

Fig. 3.12: Sensor force responses around the tumor area, and evaluation of the responses (a) Normal force response in the tumor area and the surrounding tissue areas (b) Shear force response in the tumor area and the surrounding tissue areas (c) Mean of the differential ratios in the tumor area (TA) and the surrounding tissue areas for eight tissue palpation cycles.

The developed sensor prototype was manually tested using an artificial gastric phantom with an embedded tumor. In each experimental cycle, while only one convex curve occurred in the slip zone for the shear force, several local convex curves were found for the normal force response in the slip zone. Thus, it is easier to localize the tumor by observing the response of the shear force in comparison with that of the normal force. These results support the hypothesis regarding the effectiveness of the shear force. Because the surface of the experimental tissue was lubricated, the

sensor could be moved smoothly over the surface. Thus, the shear force response was relatively stable during tissue palpation. However, the normal force response was relatively unsteady, and it gradually decreased in the slip zone. This stems from the bending of the experimental phantom, which causes difficulty in manually controlling the applied force during tissue palpation.

The results of the quantitative evaluation of the effects of the normal force and shear force in tumor localization, indicate the shear force response in the TA was considerably higher than that in the surrounding tissue areas, as shown in Fig. 3.12 (c). However, although the evaluated ratio of the shear force in the IFOTA was lower than that in the TA, it was still high. The slight increase in the shear force in the IFOTA, as shown in Fig. 3.12 (b), might yield a high value. During the sensor scanning, the increase in the shear force in the IFOTA results from overcoming the static friction to initiate slipping of the sensor over the tissue surface. Meanwhile, the response of the shear force in the BTA was much lower than that in the TA. This stems from the TA and BTA being completely in the full slip region, where the shear force was only affected by the dynamic friction. Thus, a wider space of tissue palpation could improve the detection sensitivity for the tumor.

The experimental results indicated that the shear force is more informative than the normal force in laparoscopic tumor detection. Thus, a tactile sensor with only a shear force measurement function might be sufficient for localizing a tumor. However, the combination of multiple components of the applied force information still has some advantages in tissue palpation. Firstly, the normal force information from the tactile sensor could allow surgeons to control the applied force during their palpation procedure. The information can enable them to easily scan the tissue surface and prevent the target tissue from the possible damage due to excessive applied force, compared to the other sensing devices such as ultrasonic sensors. Secondly, tissue information, such as tumor dimensions and tumor depth, is necessary for precisely and entirely dissecting the tumor. Humans could explore the contact environment more efficiently when they combine lateral and normal motions [22]. In future work, we plan to explore the characteristics of the detected tumor that can be estimated using both the normal and shear forces distributions during tissue palpation. Moreover, we intend to use a motion capture system to precisely observe the tumor area as well as monitor the movement

of the sensor. The motion capture system will be used as a reference system for estimating the sensor output response to the tissue structure such as tumor size or tumor depth. This could improve the quality of the sensor's performance in tissue palpation. Furthermore, regarding practical applications, the miniaturization of the sensor and the influence of environmental conditions such as temperature on the sensor [100] will be considered to improve the sensor performance in further studies.

3.5 Summary

In this chapter, we aimed to develop a forceps–type tactile sensor with two force measurement functions using the acoustic reflection principle for gastric tumor localization in MIS. Owing to the bending caused by the boundary condition without a supporting rigid base of the stomach during practical tissue palpation, the effect of the obtained normal force in the tumor localization might be reduced. The shear force, which might be almost affected by the contact friction, was presumed to be more informative than the normal force in terms of tumor detection. A tactile sensor that has the capability to measure normal and shear forces could assess the force components in laparoscopic tumor localization. A tactile sensor prototype was fabricated based on the acoustic reflection principle. The sensor offers great advantages in MIS, such as low manufacturing and computational costs, disposability, sterilizability and electrical safety for the patient's body. The experimental results showed that the proposed sensor is capable of measuring the normal and shear forces. The sensor was also tested with a phantom of the stomach wall with an embedded tumor to simulate the tumor localization procedure in gastrointestinal laparoscopic surgery. The experimental results showed that the developed sensor is suitable for tumor detection, indicating that the shear force information contributes greatly to tumor detection in LS.

Chapter 4

SuP–Ring: A tactile display using substitutional representation of contact force components for tumor localization

This chapter proposes a pneumatic ring–type tactile display having two force feedback functions to assist surgeons during their laparoscopic tissue palpation. The tactile display has a simple structure and is lightweight, which could be worn on the surgeon's fingers and does not impede the surgeon's motions. The tactile display used normal indentation, a substitutional sensory modality, to provide stable and reliable force feedback to the surgeon in the palpation. The tactile display performance and its effectiveness on tumor localization were investigated by fundamental and psychophysical experiments with an artificial phantom tissue model. The advantages and disadvantages of the tactile display in terms of practical application are discussed.

4.1 Introduction

Sense of touch plays a crucial role in daily life, enabling humans to explore and manipulate various objects. In scenarios such as virtual worlds or teleoperations, users are unable to physically interact with objects; hence the natural haptic sensation is eliminated [101]. Haptic devices can provide essential haptic information to enhance perception levels and user performance in such situations [83].

In laparoscopic tissue palpation, visual feedback is common methods to convey the tactile information such as the contact force data (from the force/tactile sensors) in the form of an image to surgeon [26], as the developed tactile sensor proposed in previous chapter. The visual feedback might be displayed by overlaying the contact force data on the laparoscopic monitor [50]. However, this method will degrade the

surgical image. Moreover, the overload of the visual channel is a possible problem for surgeons because they are required to focus on laparoscopic imaging during their operation [64]. In this case, tactile feedback using tactile displays often shows better performance than visual feedback [59].

The concept of laparoscopic tissue palpation using a single–point force sensor is illustrated in Fig. 4.1. A reaction force occurs when the sensor is pressed against the tissue surface. If the sensor contacts the normal tissue without tumors, the reaction force will be its normal force components, as shown in Fig. 4.1 (a). Kim et al. reported that the reaction force direction changes in the contact tissue with tumors [56]. In this case, the reaction force includes the normal and shear force components, as shown in Fig. 4.1 (b). Shear force was proven to be more effective than normal force in laparoscopic tumor localization, as reported in previous chapter. Thus, we assumed that a tactile display capable of rendering shear force might be feasible for intraoperative tissue palpation.

Lateral skin stretch is a popular feedback modality in which a shear force is applied to the user's skin. To display the shear cues using the feedback modality, the end effector of the device was pressed to ensure sufficient friction and then moved laterally to the skin to deform it in shear [102–105]. Additionally, Minamizawa et al. [106] proposed a method of providing shear cues (also using lateral skin stretch) for the weight rendering of virtual objects by moving a belt on the user's fingertip. In the haptic feedback method, the user simultaneously received the force intensity and direction based on the skin stretch actions. Although the representing shear force method might provide high sensitivity [107], the control of rendering consistent shear force is complicated. The display of the shear force directly depends on the generated normal force and skin friction. The human skin can be approximated as an elastic polymer under dry conditions, but it becomes dissipative and plastic in a wet state [108]. This results in an increased skin friction coefficient, which affects the user's perception. A display modality without lateral skin stretch, unaffected by skin friction, like sensory substitution, may be a better method for providing shear force information.

Sensory substitution is an alternative method of conveying interaction forces to users, in which the force feedback can be replaced by another sensory modality, such as vibration or audition [68]. The feedback from the substitutional modalities can be

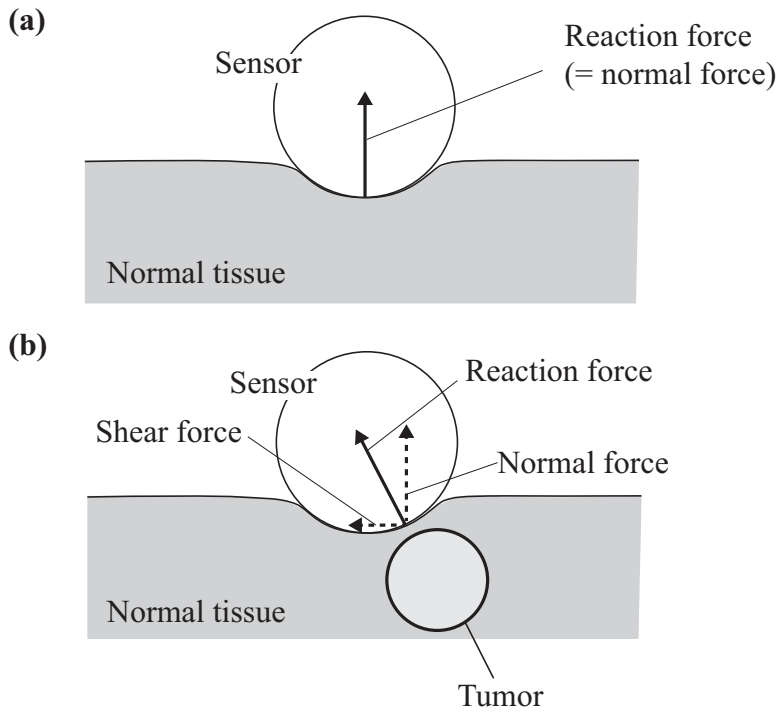

Fig. 4.1: Illustration of tissue palpation with a single–point force sensor. (a) reaction forces (including only normal force component) in tissue area without tumour. (b) reaction force (including both normal and shear force components) in tissue area with the tumour

designed to stably provide tactile information regardless of stimulus position or environmental conditions. Schoonmaker et al. utilized vibrotactile feedback to determine the magnitude of the contact force during operation [109]. Although the proposed method allows subjects to perform better, such as by reducing the maximum force applied, the extended use of tactile feedback can make the users uncomfortable, reducing their sensitivity to the vibration stimuli [66]. Another substitutional approach for force feedback is auditory modality. Cutler et al. represented force feedback by producing an auditory signal to users [65]. The graded sound was proportional to the force level. In this case, because surgeons did not wear any device on their hand, the feedback did not induce movement in the surgeon's hand during the procedure. However, continuous sound during long operations is noisy and distractive to surgeons' communication [67].

Normal indentation is a promising method employed to generate a normal force stimulus [83]. The tactile display using a normal indentation modality can have a simple structure, small size, and be used for long periods of time. Moreover, the normal force feedback generated by normal indentation is easy to control with high fidelity. Thus, the normal indentation can be a potential method for providing shear force feedback. The intensity and direction of shear force information were considered to present using the substitutional method.

In this chapter, we aim to develop a ring–type tactile display using normal indentation, a substitutional modality driven by pneumatic power, called SuP–Ring (Substitutional, Pneumatic Ring), for laparoscopic tissue palpation. Normal indentations were created by moving the three tactile elements of the device to produce both normal and shear feedback without using lateral skin stretch. Such a tactile display has a ring–type shape designed to be worn on the user's finger. The type of tactile display rarely impedes the motion of surgeons during their operation. The use of pneumatic power to develop the tactile display makes the device lightweight, cost–effective, and appropriate for the clinical environment [85]. Some participants were required to conduct psychophysical experiments to evaluate tactile display. First, just noticeable difference (JND) measurements were employed to quantitatively evaluate the presented pressure of tactile devices perceived by the users. Subsequently, a simulated laparoscopic setup was established to investigate the effectiveness of the tactile display for tumor localization. Participants without a medical background conducted the experiment in three situations with regard to the actions of the tactile display: displaying only normal feedback, only shear feedback, and both normal and shear feedback. The localization performance was evaluated by the experimental results.

4.2 Materials and methods

4.2.1 Tactile display

Design concept

Fig. 4.2 depicts a simple concept of a tactile feedback system with our proposed tactile display. The tactile display comprises two main components: one is its body and the

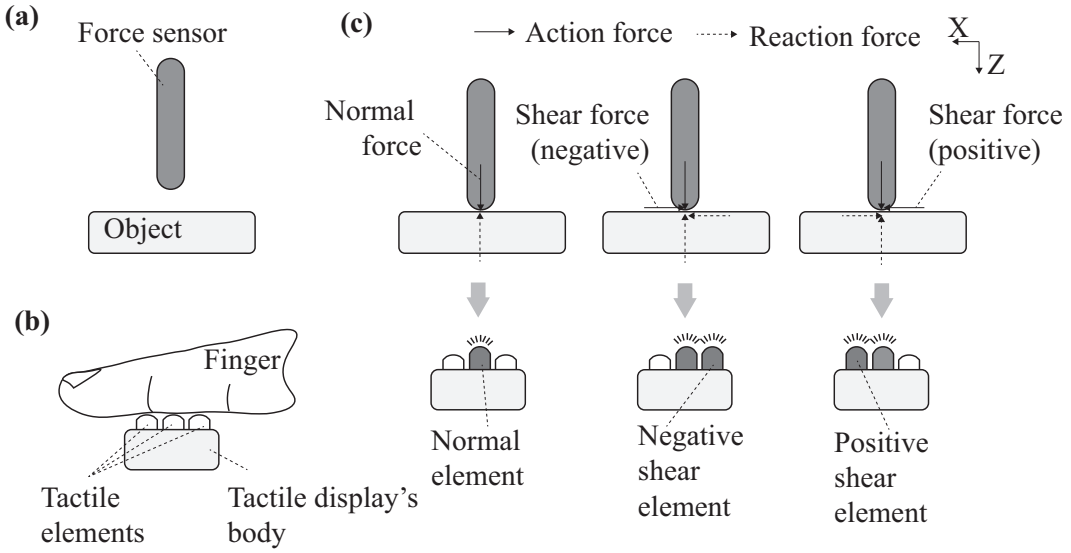

Fig. 4.2: Concept of a tactile system including a force sensor and our proposed tactile display. (a) Illustration of contact between a force sensor and an object. (b) Tactile display concept. (c) Mechanism of operation of the tactile system.

other is a combination of tactile elements that directly contact the user's finger as shown in Fig. 4.2 (b). In this design concept, the three tactile elements could render two contact force components obtained from the force sensor, as shown in Fig. 4.2 (a). Fig. 4.2 (c) illustrates the tactile display operation mechanism in the tactile feedback system. When the sensor exerts normal forces on the object, the middle tactile element is activated as the reaction force from the object pushes back the sensor. The normal indentation of the middle tactile element (called a normal element) interacts with the user's finger based on the measured normal force from the force sensor. The shear force information from the sensor can be represented by the normal indentations generated by the two remaining tactile elements of the tactile display. The tactile element's activation relies on the direction of the measured shear force as well as the intensity. When the shear force is exerted in the left direction (negative shear), a reaction force from the tissue occurs against the action force. In this case, the right tactile element (called the negative shear element) is activated to simulate the reaction force, as shown in Fig. 4.2 (c). Similarly, when the opposite direction of shear force (positive shear)

is exerted, the left tactile element (called the positive shear element) is activated. Only one shear element is activated at a time. When the negative shear element was activated, the positive shear element was deactivated, and vice versa.

SuP–Ring design and fabrication

Based on the proposed design concept, we developed a wearable tactile display with a ring shape. Fig. 4.3 describes the details of the SuP–Ring design. The device's body has a small size (22 mm × 24.5 mm × 11 mm) with a 3 mm thickness, as shown in Fig. 4.2 (a) and Fig. 4.3 (b). The device includes three air cavities that contain air pressure. The open portions of the air cavities with outer diameters of 3 mm were covered with three silicone rubber membranes (20 mm × 6 mm × 0.5 mm), as shown in Fig. 4.3 (c). The air pressure from a pneumatic control module is supplied through silicone tubes with a length of approximately 1 m and internal and external diameters of 1 mm and 2 mm, respectively. When the cavities are inflated/deflated, the membranes expand/contract, leading to an increase/decrease in the interaction force.

A tactile display prototype was developed based on the concept proposed, as shown in Fig. 4.4. The body of the SuP–Ring was fabricated from a photopolymer resin using a 3–D printer (Formlab Inc., Form2). The silicone rubber membranes were made from pourable silicone rubber (Young's modulus: 28 kPa) using a 3–D printed mold. A strap band shown in Fig. 4.3 (a) was employed to strap the device to the user's finger. The SuP–Ring was designed to be worn on any position of the user's finger. With this design, the device is easy to adjust, put on, or remove. The total mass of the tactile device is approximately 4 g (very lightweight), with an estimated fabrication cost of approximately $ 5 (low cost).

Tactile feedback system with the proposed tactile display

A tactile feedback system using a SuP–Ring is shown in Fig. 4.5. The system consists of a measurement system and a tactile display system. In general, the measured force information from the force sensor is rendered by the SuP–Ring. The measurement system consisted of a force sensor, a data acquisition device (NI–DAQ 6218, National Instrument, Inc., 16–bit resolution, 30 kHz sampling frequency), and a personal com-

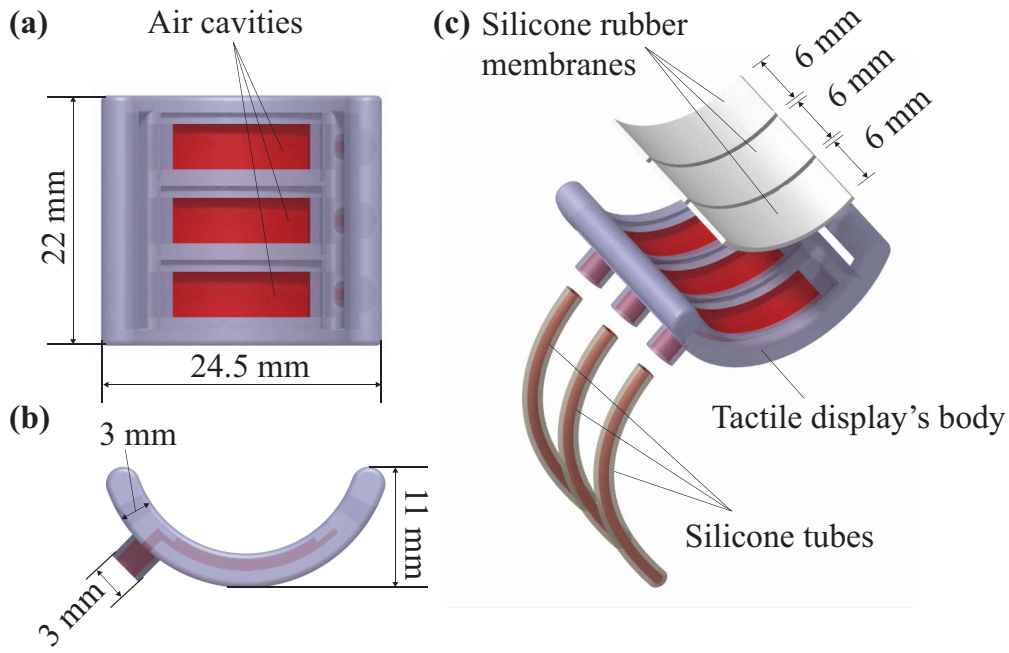

Fig. 4.3: Design of the SuP-Ring. (a) Top view of the SuP–Ring. (b) Side view of the SuP–Ring. (c) Components of the device.

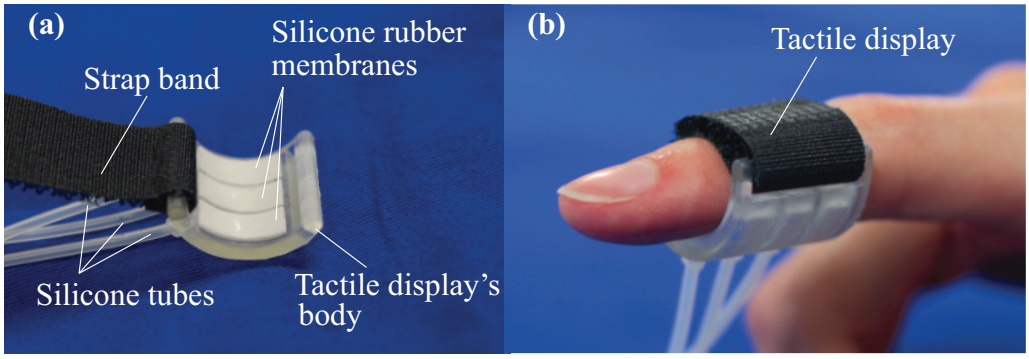

Fig. 4.4: Tactile display's prototype. (a) Prototype's components. (b) Use of the tactile display.

puter. The collected contact force data from the force sensor were processed using a data acquisition device and a computer. The data were smoothed using a low–pass filter with a cutoff frequency of 5 Hz. The normal and shear force components of the

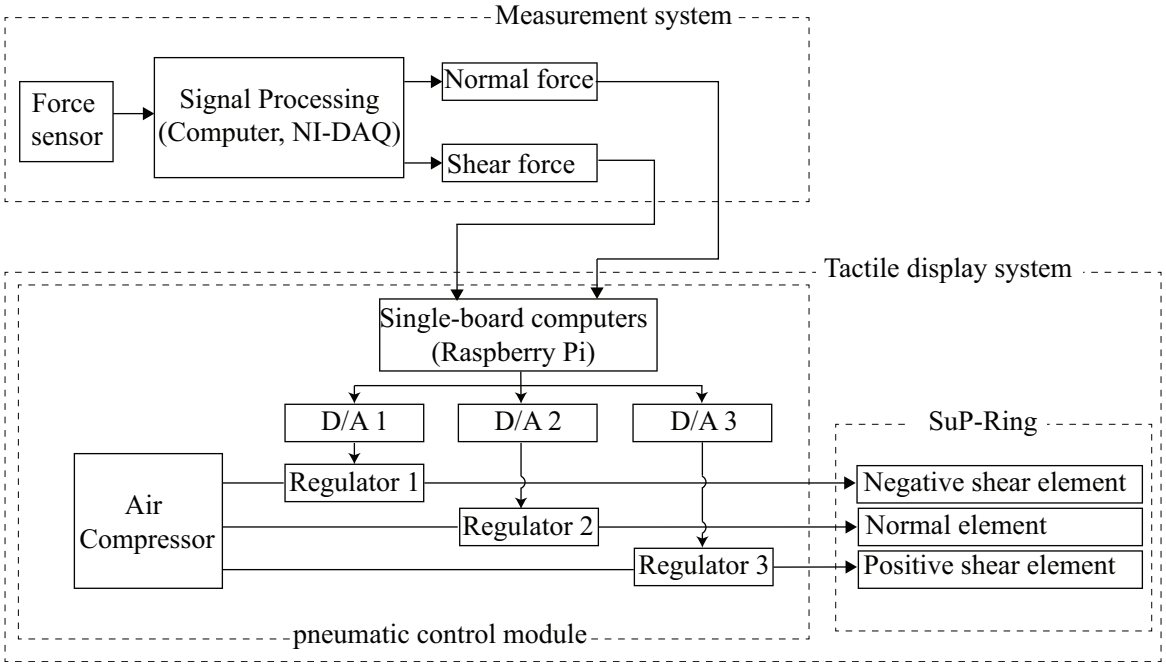

Fig. 4.5: Tactile feedback system with the SuP–Ring including a measurement system and a tactile display system.

contact force were utilized as inputs for the tactile display system. The tactile display system consists of a tactile device (SuP–Ring) and a pneumatic control module. The tactile feedback from the SuP–Ring was driven by the control module. The control module includes an air compressor (Fujiwara Sangyo Co., Ltd, SR–045), a single–board computer (Raspberry Pi 4 model B), digital/analog (D/A) converters (12–bit), and electropneumatic regulators (SMC Corp., ITV1030–212BL5–X88). An air pressure of 0.5 MPa is supplied to the regulators from the air compressor. Each regulator adjusts the inner pressure of each tactile display's tactile element. The inner pressure generated by the regulators was controlled by D/A converters and a single–board computer. The data from the measurement system are transmitted to the tactile feedback system via a user datagram protocol (UDP) with an Ethernet cable. A single–board computer provides appropriate control signals to the regulator based on the collected force from the measurement system. Regarding the shear feedback, the activation of negative and positive shear elements depends on the direction of the collected shear

force, as mentioned in Section 4.2.1.

4.2.2 Characterization of the tactile display system

In this section, we describe our proposed tactile display system. Fundamental experiments were conducted to estimate the static and dynamic pressure responses of the system.

To investigate the pressure at the silicone rubber membranes of the SuP–Ring, a pressure sensor (Ap–13A, KEYENCE Corp.) was directly connected to a regulator of the pneumatic control module via a silicone rubber tube instead of the tactile element of the SuP–Ring. The pressure data were collected at a sampling frequency of 10 kHz.

A series of input signals (0.164, 0.325, 0.486, 0.647, 0.808, and 0.969 V) were provided by the D/A converter and a single–board computer to control the regulator. For each input signal, the pressure was kept constant for a few seconds; then the pressure value was recorded. The inner pressure was measured for the six input signals to estimate the static response of the control module. The dynamic performance of the pneumatic control module was assessed by evaluating its step and frequency responses with the same series of input signals for the static response. For the step response, the input signals were turned on for 3 s. The inner pressure during the steps was collected for six different step pressures. To obtain the frequency response of the control module, we measured the inner pressure for input square wave frequencies of 0.1, 0.2, 0.5, 1, 2, 3, 4, 5, 6, 7, and 10 Hz. The magnitudes of the input square waves were obtained from a series of input signals. In this study, the gain value was estimated using the following equation:

$$Gain = 20 \times \log_{10}\left(\frac{P}{P_{static}}\right)[dB] \tag{4.1}$$

where P is the magnitude of the measured inner pressure, which corresponds to one input square wave frequency. P_{static} is the inner pressure value for a static input value with the same magnitude. The gain value indicated a reduction in the dynamic response compared to the static response. The experiments were repeated five times for each input signal in both investigations of the static and dynamic responses.

4.3 Psychophysical experiments

To evaluate the SuP–Ring performance, we conducted psychophysical experiments. First, the JND test, a classical psychophysical test, was performed to assess the differential threshold of normal and shear cues generated by the tactile device. Second, a tissue palpation task was conducted to investigate the effectiveness of the tactile display system for laparoscopic tumor localization.

4.3.1 JND test

The JND test aims to evaluate how users perceive the change in the SuP–Ring rendering pressure. The experiment involved 12 participants (2 females and 10 males, age 23±1), all of which were right–hand dominant except one. The participants consented to perform the task with an experimental protocol according to the ethical standards of the Helsinki Declaration and approved by the Ethical Committee of the Nagoya Institute of Technology.

The participants sit on an adjustable height chair with their back straight and kept their feet flat on the floor. They were required to put their forearms on the chair's armrest as forearm support for the JND test. The sitting posture was adjusted to ensure all participants conducted the test with almost the same posture in a comfortable position. The participants wore the SuP–Ring on their dominant hand's index finger, as shown in Fig. 4.4 (b). The participants could choose any position range from their distal to medial phalanx where they felt comfortable wearing the device. During the experiment, to avoid other cues that might affect experimental performance, the participants were required to close their eyes and wear noise–canceling headphones.

As mentioned in the design concept section, the SuP–Ring has three activation states: one is only the normal element activated for rendering the normal stimuli, the others were the normal and shear elements activated to render both normal and shear stimuli. The participant conducted three consecutive tasks for three reference stimuli of 31.1, 54.7, and 78.2 kPa, which were selected based on the pressure range of the tactile display system.

In the first task, normal feedback only (activating only the normal element) was

evaluated for the mentioned reference stimuli. In the beginning, the reference pressure was exerted on the participant's finger for a few seconds, and then the pressure was increased/decreased from the reference pressure value. The participant was required to detect a pressure change; then, the presented pressure value was recorded. Each increasing/decreasing pressure series was alternately conducted five times for each reference pressure. In the next two tasks, we evaluated the JND measurement of the shear stimulus in the case of a normal stimulus. At the beginning of the second task, we provided a constant pressure (the pressure value among the three reference pressures) to the normal element, and then a reference pressure from the three reference pressures was represented by the positive shear element. Afterward, the pressure adjustment of the negative shear element was conducted (similar to the first task) to collect the JND data. In this task, nine combinations of the pressure for the normal and negative shear elements were performed to estimate the JND measurement. Finally, the third task was conducted (similar to the second task) to estimate the JND measurement of the positive shear element instead of the negative shear element. In the three tasks of the JND test, the order of reference pressure was shuffled to partially counterbalance differences across each participant.

4.3.2 Tumor localization experiment

Tissue phantom with embedded tumor

To evaluate the effectiveness of SuP–Ring for tumor detection, we prepared an artificial phantom tissue as a sample for the experiment. The 150 mm × 50 mm × 11 mm phantom tissue consists of two tissue layers, as shown in Fig. 4.6. The bottom layer tissue with a thickness of 10 mm (as normal tissue), consisting of pourable urethane rubber (Young's modulus: 6 kPa), was made using a 3–D printer mold. The normal tissue stiffness is similar to that of the human liver (4–6.5 kPa) [110]. An embedded synthetic semispherical tumor with a 7.5 mm radius is located inside the phantom, as shown in Fig. 4.6 (b). The position of the embedded tumor is shown in Fig. 4.6 (a). The embedded tumor was made of silicone rubber (Young's modulus: 28 kPa). The artificial tumor stiffness is in the range of the hepatocellular carcinoma's stiffness (20.4–75 kPa), as reported by Masuzaki et al. [111]. The distance from the apex of the

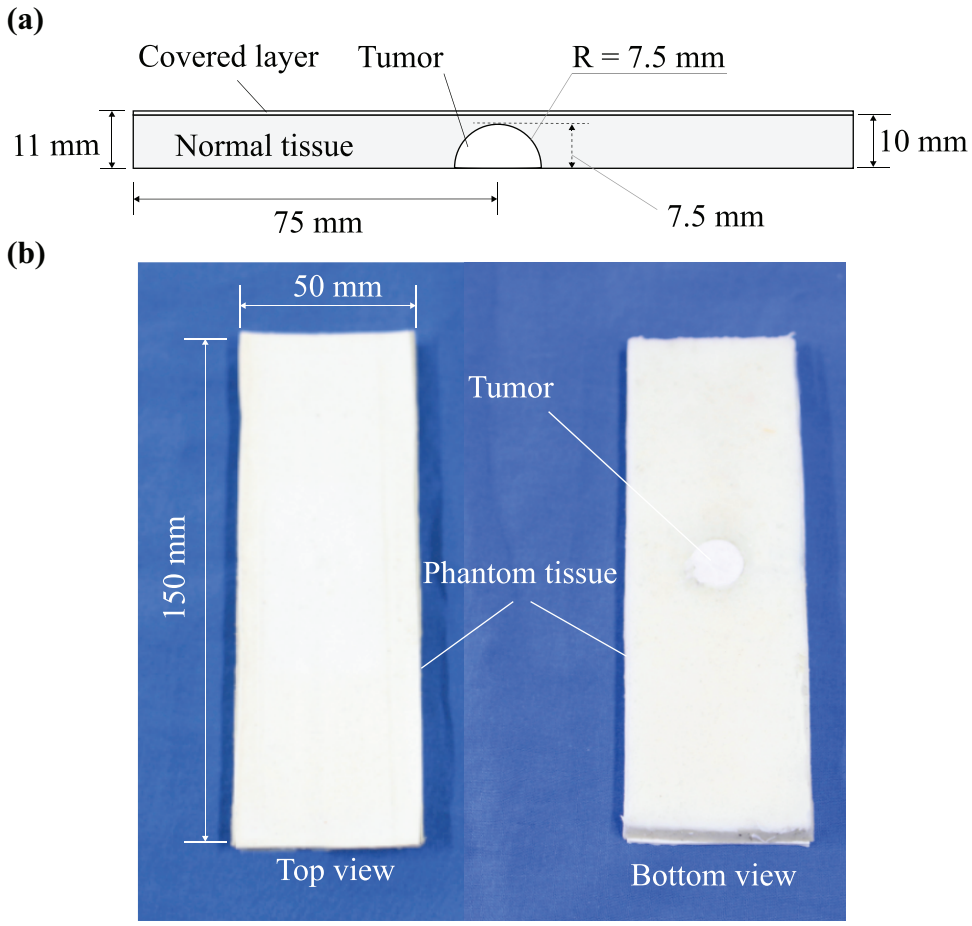

Fig. 4.6: Phantom tissue with embedded tumor. (a) Structure of the phantom tissue. (b) Top view and bottom view of the fabricated phantom tissue.

semispherical tumor to the normal tissue surface was small, making the tumor visible from the outside. A top layer made of silicone rubber (1 mm thickness) was used to cover the normal tissue and simulate the serous coat (serosa) of the liver. The rubber glue was used to stick the top layer on the surface of the bottom layer (normal tissue). Because of the thin top layer, there is no significant effect on the phantom tissue stiffness. Moreover, the bottom layer's structure cannot be seen from the outside along with the top layer. The silicone layer could also help to reduce the friction between the phantom tissue and the sensing probes during tissue palpation.

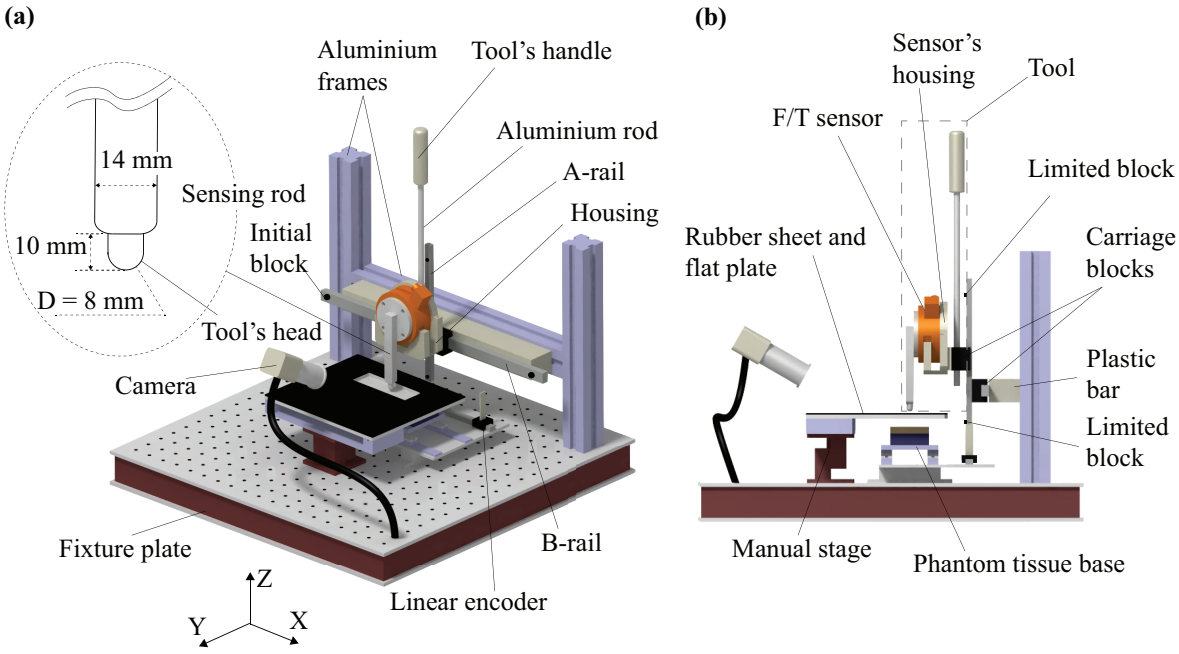

Fig. 4.7: Simulated laparoscopic setup. (a) Isometric view of the setup. (b) Side view of the setup.

Simulated laparoscopic setup

A simulated laparoscopic experiment was designed to evaluate the effectiveness of the SuP–Ring for tissue palpation. Because the tactile display can render 2–degree of freedom (2–DoF) force feedback, including normal and one–dimension shear feedback, the experiment will be set up to provide the 2–axis force information only. A simulated laparoscopic setup was established on a fixture plate to perform the tissue palpation task, as shown in Fig. 4.7. A tool using a six–axis force/torque (F/T) sensor (ATI, Inc. Gamma Si–32–2.5) and a custom apparatus was used to measure the contact force. The force sensor was fixed to the tool's housing, as shown in Fig. 4.7. A sensing rod was mounted on the sensor as the tool's sensing component. The sensing rod with a half–ball–shaped tip (diameter of 8 mm) was made of acrylonitrile styrene acrylate (ASA) white materials (Stratasys 3D printer), as shown in the left inset of Fig. 4.7 (a). The tool was mounted on a carriage block, as shown in Fig. 4.7 (b). The tool could smoothly slide on a linear guide rail (A–rail) along the z–axis. The A–rail was

mounted on another carriage block, which could move along the x–axis on another linear guide rail (B–rail). The user could control the tool's head position by moving the tool's handle connected with the housing through an aluminum rod, as shown in Fig. 4.7 (a). The z–axis and x–axis forces measured by the force sensor were collected as the normal and shear force components of the contact force, respectively. Limited blocks were placed on the distal and proximal ends of the guide rails to prevent the tool from falling out of the rails. The B–rail was fixed on a stand assembled from aluminum frames and a plastic bar. The phantom tissue was placed on a base under an acrylic flat plate (thickness of 5 mm) with a rectangular hole (size of 100 mm mm), as shown in Fig. 4.7 (b). A black rubber sheet (thickness of 2 mm) was attached to the flat plate top surface. With this setup, users could not see anything under the flat plate, except for the phantom tissue portion in the hole area. The flat plate was mounted on a manual stage, as shown in Fig. 4.7 (a) and Fig. 4.7 (b). The flat plate pitch was adjusted according to the manual stage for holding the phantom tissue in position.

The phantom tissue setup details are presented in Fig. 4.8. The phantom was placed on a 20 mm thick sponge plate to mimic the surrounding organs and tissues of the human liver. The sponge plate was attached to a support plate, as shown in Fig. 4.8 (b). The support plate was mounted on two carriage blocks that could be moved along two linear guide rails (mounted on a couple of support bars). A cylindrical neodymium magnet was placed on the side of the support plate. Three other cylinder magnets were embedded in the support bar, and their positions are shown in Fig. 4.8 (a). For the setup, when the support plate was moved, its position was only in one of the three bottom magnet positions. Letting the position of the centered magnet (among the three bottom magnets) be the origin position (0 mm), we prepared three different positions of the tumor (–20, 0, +20 mm) for the palpation task, as shown in Fig. 4.8 (c). A linear encoder was placed on the same base as the phantom tissue to measure the experimental position (as shown in Fig. 4.7 (a). The monitor mounted on a table displays the experimental images captured by the setup camera, as shown in Fig. 4.9. A wooden sheet was placed above the experimental setup through a pair of steel rods to simulate the abdominal wall. Because of the wooden sheet, the participants only obtained visual information via the monitor.

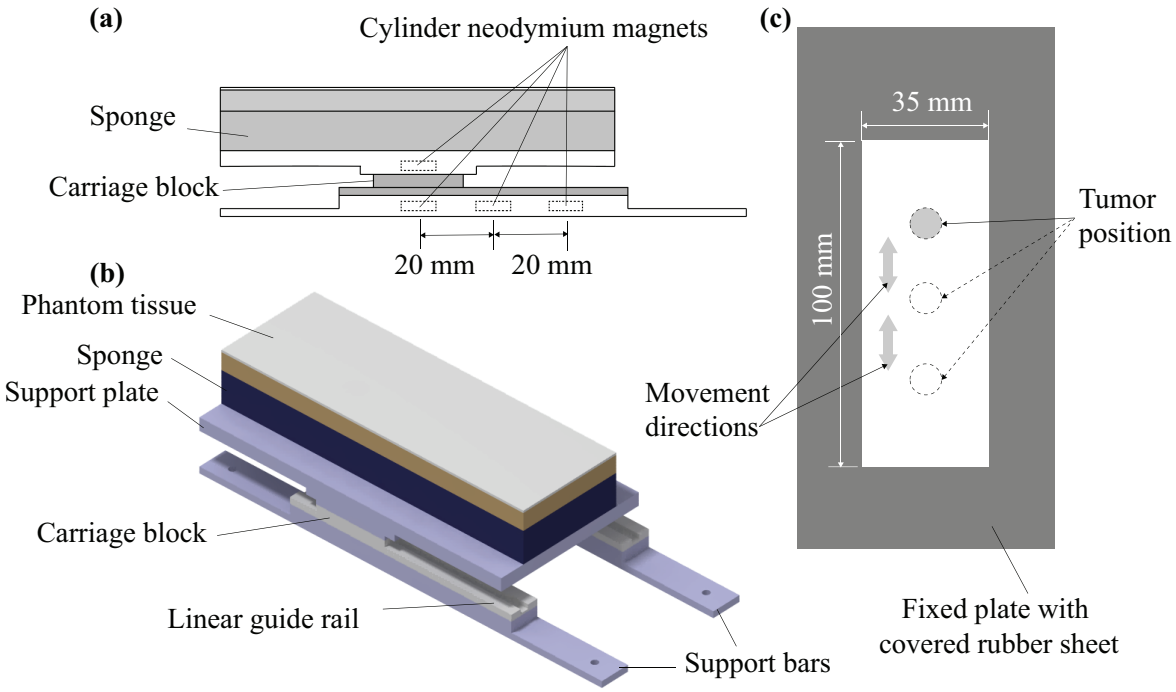

Fig. 4.8: Phantom tissue setup. (a) Front view of the setup. (b) Isometric view of the setup. (c) Top view of phantom tissue in the simulated laparoscopic setup.

Experimental procedure

For the palpation task, we aimed to evaluate the effectiveness of the SuP–Ring in a fair manner. Experts (professional surgeons) tend to have a large variation in their experience and surgical skills [85]. Thus, the novices (participants) were employed to reduce the influence of the variation in the task. Twelve participants (2 females and 10 males, age 23±1) without a medical background participated in the palpation task. Five of them did the JND test with the SuP–Ring, while the others did not take part in the test. All of the participants in the experiment were right–hand dominant. The SuP–Ring operation and the experimental procedure were explained beforehand to the participants. They conducted several task trials until they fully understood the experimental procedure. The participants consented to perform the task with an experimental protocol according to the ethical standards of the Helsinki Declaration

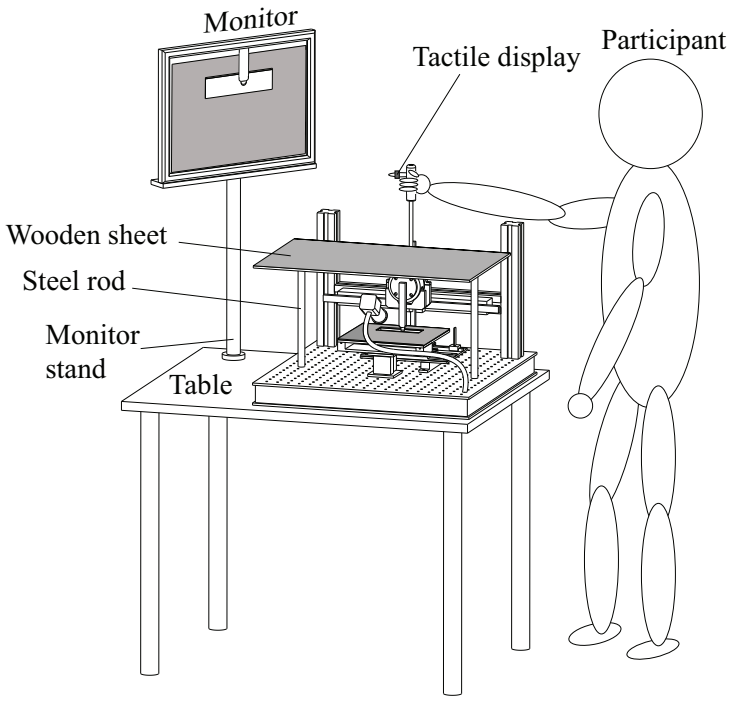

Fig. 4.9: Full setup for the palpation task.

and approved by the Ethical Committee of the Nagoya Institute of Technology.

The experimental procedure is illustrated in Fig. 4.10. First, the flat plate with the rubber sheet was lifted up using the manual stage, and the position of the tumor (–20, 0, +20 mm) was randomly selected by moving the support plate of the phantom tissue. Next, the flat plate was lifted off to maintain the position of the phantom tissue. The participants were required to wear the SuP–Ring on their right–hand index finger. After that, they held the tool's handle with their right–hand and then moved the tool to palpate the phantom tissue. The participants started moving the tool along the x–axis from the initial block (called the initial position) to the phantom tissue area, as shown in Fig. 4.10 (a). The movement of the sensing rod was observed via a monitor. Regarding tissue palpation, at each x–axis position, the participants pushed/pulled

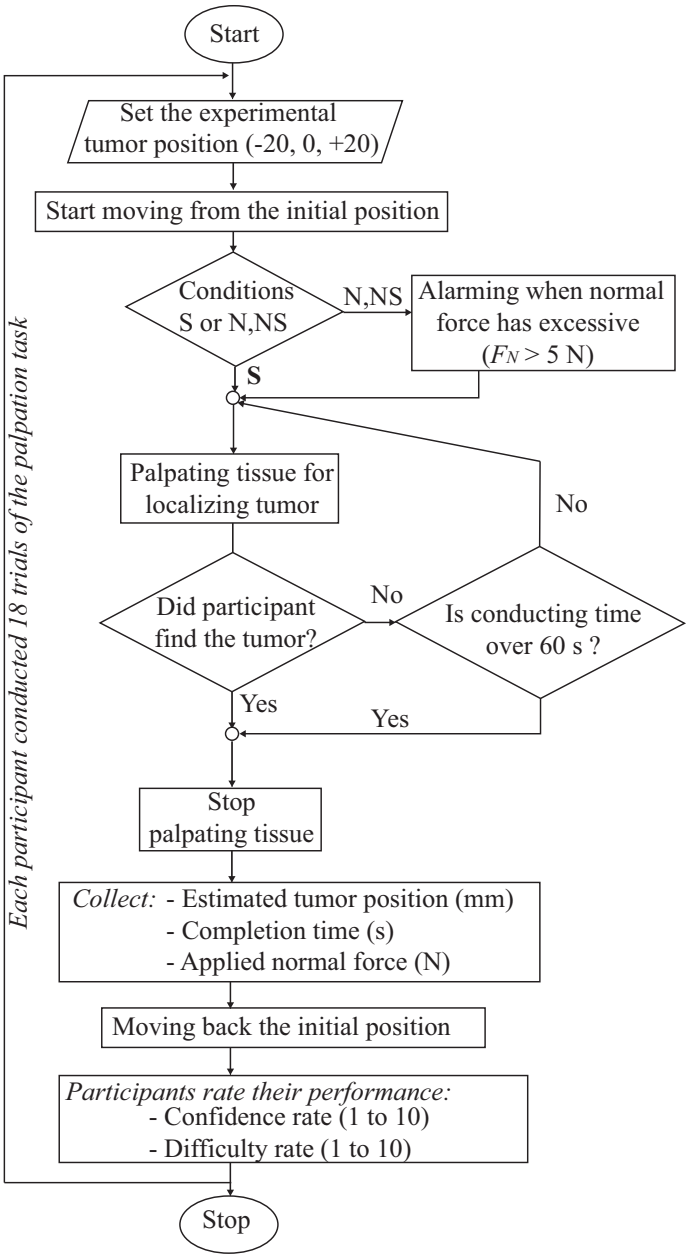

Fig. 4.10: Experimental procedure for the palpation task.

the tool against/out of the phantom tissue along the z–axis. The force outputs were smoothed using a 5 Hz low–pass filter. The SuP–Ring represents the relative pressure

based on the measured contact force, as follows:

$$P_{\mathrm{N}} = \begin{cases} P_{\mathrm{N0}} + G_{\mathrm{N}} \times F_{\mathrm{N}} & \text{if } P_{\mathrm{N0}} + G_{\mathrm{N}} \times F_{\mathrm{N}} \ \leq P_{\mathrm{threshold}} \\ P_{\mathrm{threshold}} & \text{otherwise} \end{cases} \tag{4.2}$$

$$P_{\mathrm{SP}} = \begin{cases} P_{\mathrm{S0}} + G_{\mathrm{S}} \times F_{\mathrm{S}} & \text{if } F_{\mathrm{S}} > 0 \text{ and } P_{\mathrm{S0}} + \ G_{\mathrm{S}} \times F_{\mathrm{S}} < P_{\mathrm{threshold}} \\ P_{\mathrm{threshold}}, & \text{if } F_{\mathrm{S}} > 0 \text{ and } P_{\mathrm{S0}} + \ G_{\mathrm{S}} \times F_{\mathrm{S}} \geq P_{\mathrm{threshold}} \\ P_{\mathrm{S0}} & \text{otherwise} \end{cases} \tag{4.3}$$

$$P_{\mathrm{SN}} = \begin{cases} P_{\mathrm{S0}} + G_{\mathrm{S}} \times (-F_{\mathrm{S}}) & \text{if } F_{\mathrm{S}} < 0 \text{ and } P_{\mathrm{S0}} + \ G_{\mathrm{S}} \times (-F_{\mathrm{S}}) < P_{\mathrm{threshold}} \\ P_{\mathrm{threshold}} & \text{if } F_{\mathrm{S}} < 0 \text{ and } P_{\mathrm{S0}} + G_{\mathrm{S}} \times (-F_{\mathrm{S}}) \geq P_{\mathrm{threshold}} \\ P_{\mathrm{S0}} & \text{otherwise} \end{cases} \tag{4.4}$$

where P_{N}, P_{SP}, and P_{SN} are the inner pressure values of the normal, positive shear, and negative shear elements, respectively. P_{N0}, P_{S0}, and G_{N} and G_{S} are the offset pressures and gain values of the corresponding normal and shear elements, respectively. F_{N} and F_{S} are the measured normal and shear forces from the sensor, respectively. $P_{\mathrm{threshold}}$ is the maximum pressure value of the SuP–Ring tactile elements. This value was set to prevent the risk of silicone membrane rupture. These parameter were set as $[P_{\mathrm{N0}}, P_{\mathrm{S0}}]^{\mathrm{T}}$ = [23.38 kPa, 31.1 kPa] , $[G_{\mathrm{N}}, G_{\mathrm{S}}]^{\mathrm{T}}$ = [7.39 kPa/N, 11.38 kPa/N] and $P_{\mathrm{threshold}}$ = 103.35 kPa.

The participants wore the SuP–Ring and stood in front of the table, as shown in Fig. 4.9. They looked at the monitor and determined the embedded tumor location based on the tactile feedback generated by the tactile display. When the participants found the tumors, they were required to place the tool's head on the apex of their estimated tumor position. The estimated positions were measured using a linear encoder. The position errors were computed as the absolute values of the difference between the actual and estimated tumor positions. The palpation task was performed within 60 s. The participant attempted to finish the task as soon as possible. Completion time was recorded using a stopwatch. If 60 s passed, the participant would be asked to stop

their palpation and estimate a tumor position with which they felt the most confident. Subsequently, the participant moved the tool back to its initial position. The normal force values applied within the performance of the participants were recorded. The average of the peaks of the applied normal force is computed. The average values of every trial were selected as the evaluation parameters for the palpation task.

Each participant conducted 18 trials of the palpation task, with six repetitions for each of the following three feedback conditions: only normal feedback (condition N), only shear feedback (condition S), and both normal and shear feedbacks (condition NS). In condition N, only the normal stimulus was displayed by the normal element. Under condition S, the two shear elements rendered the shear stimuli. The activation of the negative and positive shear elements relied on the direction of the measured shear force as well as the magnitude. Under condition NS, three tactile elements of the SuP–Ring were activated to render both the normal and shear force components of the contact force. In MIS, the applied normal force should be small for safety purposes [112]. Thus, during the palpation performance, the participants were required to reduce the applied force when they heard an auditory alarm (beep sound) from a headphone. The sound was sent to participants when the measured normal force in conditions N and NS reached 5 N. In condition S, because the normal force was not used, the participants did not hear any alarm sounds during their performance.

After finishing each trial, the participants were asked to provide a "confidence rating" and "difficulty rating." Regarding the confidence rating, the participants rated from 1 to 10 for the question "how confident are you in localizing the tumor position?" Similarly, regarding difficulty rating, they also rated from 1 to 10 for the question "how difficult was it to find the tumor position?" A score of 0 meant "not confident at all" and "very easy," and score of 10 meant "strongly confident" and "really difficult", respectively. The position of the embedded tumor was randomized across trials. Thus, three positions (–20, 0, +20) were tested twice in the six repetitions for each feedback condition. The order of the conditions was randomized to evaluate the six possible combinations twice. In this palpation task, each participant made several trials for three conditions to clearly understand the experimental procedure.

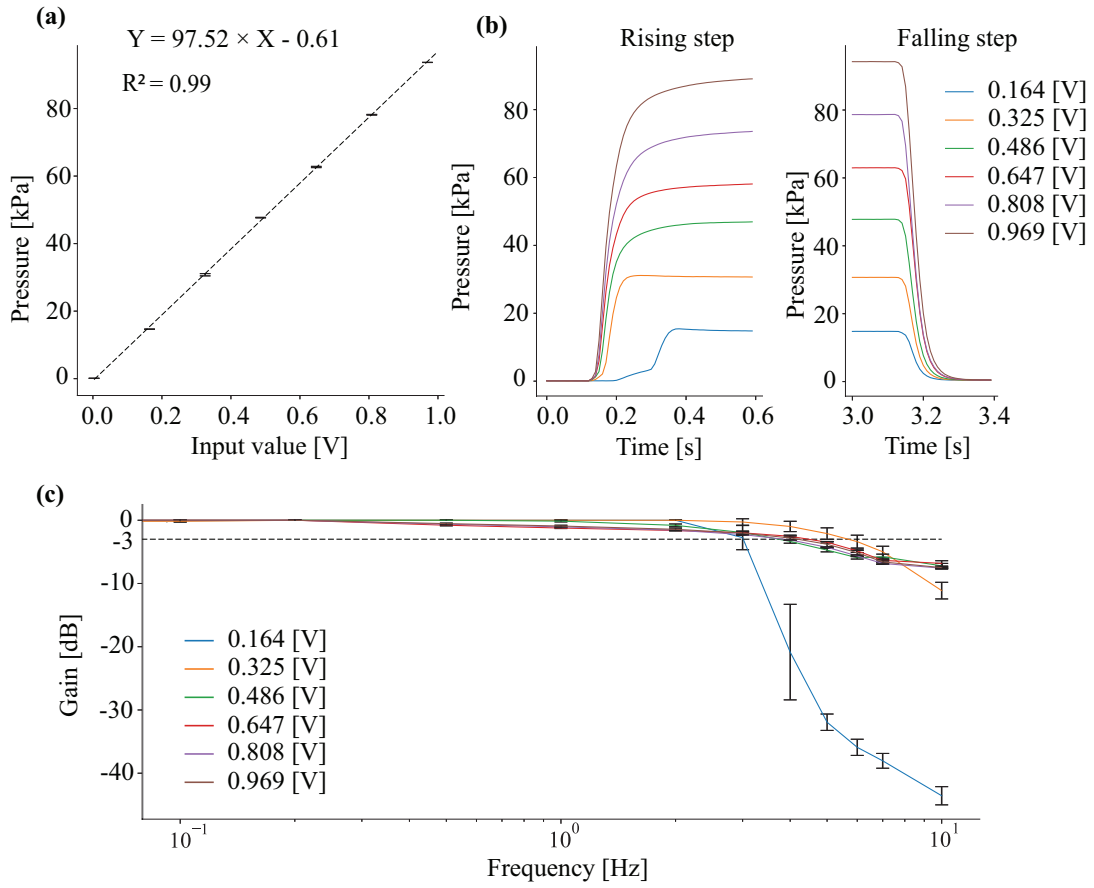

Fig. 4.11: Characterization of the tactile display system. (a) Static relationship between the inner pressure and the input voltage value. (b) Step response of the inner pressure for different target inputs. c) Frequency response of the inner pressure for different target inputs.

4.4 Results

4.4.1 Characterization of the tactile display system

Fig. 4.11 (a) shows the relationship between the input signal and the static inner pressure of the control module. The standard deviations of the six measurements are indicated by error bars. The linear relation between the input and the inner pressure

yields the following equation:

$$Y = a \times X - b \tag{4.5}$$

where Y is the inner pressure value and X is the input voltage. The coefficients were found to be $[a, b]^{\mathrm{T}} = [97.52, 0.61]$. The coefficient of determination was computed to be $R^2 = 0.99$. Regarding the step response shown in Fig. 4.11 (b), the rising time is longer than the falling time. The step decrease responses of the control module have a delay of approximately 0.15 s for all inputs. For a target pressure of 15.38 kPa (input signals of 0.164 V), the pressure reaches the target value with a rising time of 0.25 s, whereas the system quickly increases to the near value of the target pressure and then gradually reaches the exact target pressure. Fig. 4.9 (c) shows the frequency response for the considered pressure. The gain values decreased when the frequencies of the inputs were increased. The pressure bandwidth of the control module was computed at a gain value below –3 dB for every target pressure. The pressure bandwidth was above 4.5 Hz for values close to the target pressure, except for the target pressure of 15.38 kPa (bandwidth of 2 Hz).

4.4.2 Psychophysical experiments

JND test

Fig. 4.12 shows the outcomes of the JND test. The circles, error bars, and dashed lines indicate the means, standard deviations, and fitting lines of the JND values, respectively. Regarding the results of the first tasks for the normal element, as shown in Fig. 12a, the mean JND values are linearly related to the reference pressures. Fig. 4.12 (b) and Fig. 4.12 (c) show the JND values of the second and third tasks for the shear elements. The JND results for shear elements with different normal element stimuli are indicated by different colors. The red, blue, and black (circle, error bars, and dashed lines) illustrate the normal stimuli of 31.1, 57.4, and 78.2 kPa, respectively. In general, the JND values monotonically increased with the stimuli, consistent with Weber's law [113]. The Weber fractions were calculated for each reference pressure in

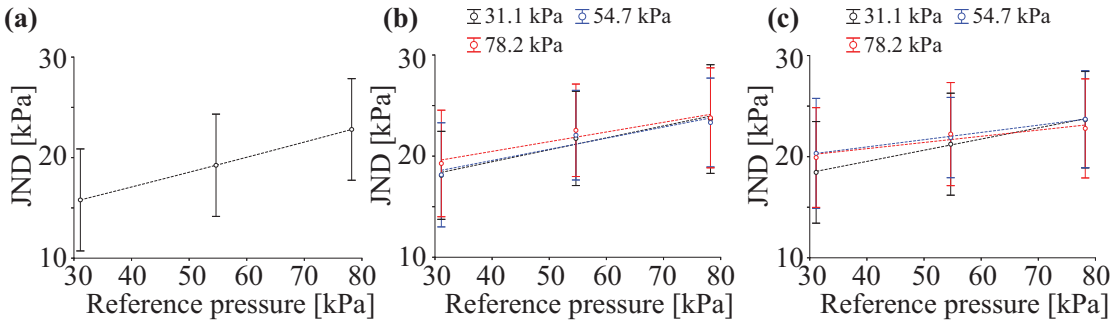

Fig. 4.12: Results of JND test. Open circles, error bars, and dashed lines indicated the means, standard deviations, and fitting lines of the test's data. (a) JND of normal element only. (b) JND of negative shear element for different normal element stimuli. c) JND of positive shear element for different normal element stimuli. Red, blue, and black color indicate the JND data for the normal stimuli of 31.1, 57.4, and 78.2 kPa, respectively.

the three experimental conditions as follows:

$$k = \frac{\Delta I}{I} \tag{4.6}$$

where k, ΔI, and I represent the Weber fraction (WF), JND, and reference values, respectively.

In Fig. 4.13, the dashed curves indicate the WF trend for each stimulus condition. The WF decreased with an increase in the reference pressure in the three tasks. Regarding the results of the first task shown in Fig. 4.13 (a), a one–way repeated measures ANOVA (with a significance value of 0.05) was used to evaluate the effect of the reference pressure of the normal element on the WF. The collected data were approximately normally distributed according to the Shapiro–Wilk normality test. The data passed Mauchly's test of sphericity. The ANOVA revealed that there was a significant effect of reference pressure of normal stimulus on the WF of the normal element ($F(2, 22) = 36.815$ and $p < 0.001$). Regarding the results of the second and third tasks, a two–way repeated measures ANOVA (with a significance value of 0.05) was conducted to examine the effect of the inner pressures of the normal and shear elements on the WF. The collected data were approximately normally distributed according to

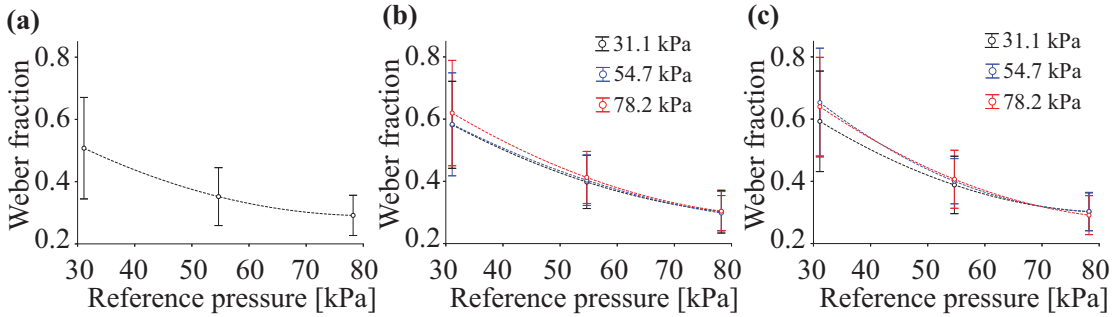

Fig. 4.13: Weber fractions. Open circles, error bars, and dashed curves indicated the means, standard deviations, and fitting curves of the test's data. (a) WF of normal element only. (b) WF of negative shear element for different normal element stimuli. (c) WF of positive shear element for different normal element stimuli. Red, blue, and black color indicate the WF for the normal stimuli of 31.1, 57.4, and 78.2 kPa, respectively.

the Shapiro–Wilk normality test. The data passed Mauchly's test of sphericity. The ANOVA showed that there was no significant effect of the normal stimulus on the WF of either shear element ($F(2, 22) = 1.147$ and $p = 0.336$ for the second task and $F(2, 22) = 3.255$ and $p = 0.058$ for the third task). Whereas, the reference pressure of shear stimulus was a significant effect on the WF of either shear element ($F(2, 22) = 87.424$ and $p < 0.001$ for the second task and $F(2, 22) = 130.805$ and $p < 0.001$ for the third task). There was a non–significant interaction between the normal stimulus and the reference pressure of shear stimulus, on the WF of either shear element ($F(4, 44) = 0.985$ and $p = 0.424$ for the second task and $F(4, 44) = 2.372$ and $p = 0.057$ for the third task).

Tumor localization experiment

To investigate the effect of the feedback conditions on the participant's performance, position errors in the tumor localization, task completion time, and averages of applied normal force during the performance, confidence and difficulty ratings were evaluated. The results of the 12 participants in the palpation task are shown in Fig. 4.14. Most of the raw data of the evaluated parameters did not pass the Shapiro–Wilk test, except

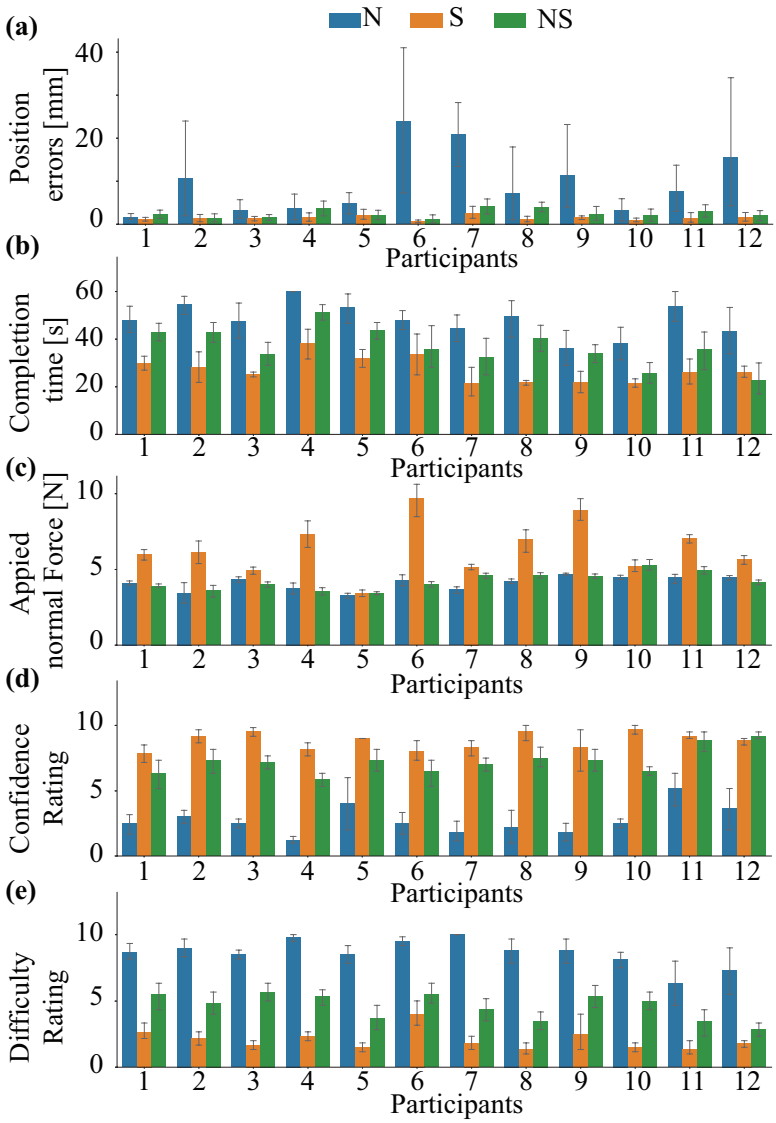

Fig. 4.14: Results of localization performance in individual participants. Blue, orange, and green bars indicate the experimental results for condition N,S, and NS, respectively. (a) Tumor position errors. (b) Completion time. (c) Average applied normal force. (d) Confidence ratings. (e) Difficulty rating.

for the completion time data and the applied normal force data for condition NS. Thus, a Friedman test (a nonparametric test) with a significance value of 0.05 was

employed to compare the collected parameters in the three feedback conditions. If the test results showed a statistically significant difference between the median of the three experimental conditions, three–pair Wilcoxon signed rank tests (post hoc tests) with Bonferroni correction were conducted.

Fig. 4.15 (a) shows the position errors for the experimental conditions. The Friedman test showed a significant difference between the three feedback conditions ($\chi^2(2) = 31.58$, $p < 0.001$). The Wilcoxon signed rank tests showed significant differences between conditions N and S ($W(12) = 226$, $p < 0.001$), between N and NS ($W(12) = 522$, $p < 0.001$), and between S and NS ($W(12) = 736$, $p = 0.0035$). This result shows that the tumor detection in conditions with shear feedback was more accurate than that in conditions with only normal feedback.

Fig. 4.15 (b) shows the completion time for each condition. The Friedman test showed a significant difference between the three feedback conditions ($\chi^2(2) = 93.66$, $p < 0.001$). The Wilcoxon signed rank test showed significant differences between conditions N and S ($W(12) = 1$, $p < 0.001$), between N and NS ($W(12) = 274$, $p < 0.001$), and between S and NS ($W(12) = 305$, $p < 0.001$). This result shows that the task performance in conditions with shear feedback took less time than those in other conditions with normal feedback.

Fig. 4.15 (c) shows the applied normal force during the palpation task. The Friedman test showed a significant difference between the three feedback conditions ($\chi^2(2) = 80.42$, $p < 0.001$). The Wilcoxon signed rank test showed significant differences between conditions N and S ($W(12) = 27$, $p < 0.001$), between N and NS ($W(12) = 1053.5$, $p = 0.595$), and between S and NS ($W(12) = 71$, $p < 0.001$). This result shows that the applied normal force in condition S was significantly higher than that in the other conditions. There was an insignificant difference between conditions N and NS.

Fig. 4.15 (d) shows the confidence rating results. The Friedman test showed a significant difference between the three feedback conditions ($\chi^2(2) = 125.95$, $p < 0.001$). The Wilcoxon signed rank test showed significant differences between conditions N and S ($W(12) = 0$, $p < 0.001$), between N and NS ($W(12) = 1.5$, $p < 0.001$), and between S and NS ($W(12) = 65.5$, $p < 0.001$). This result shows that the confidence ratings in the conditions with shear feedback were statistically higher than those in the condition with only normal feedback.

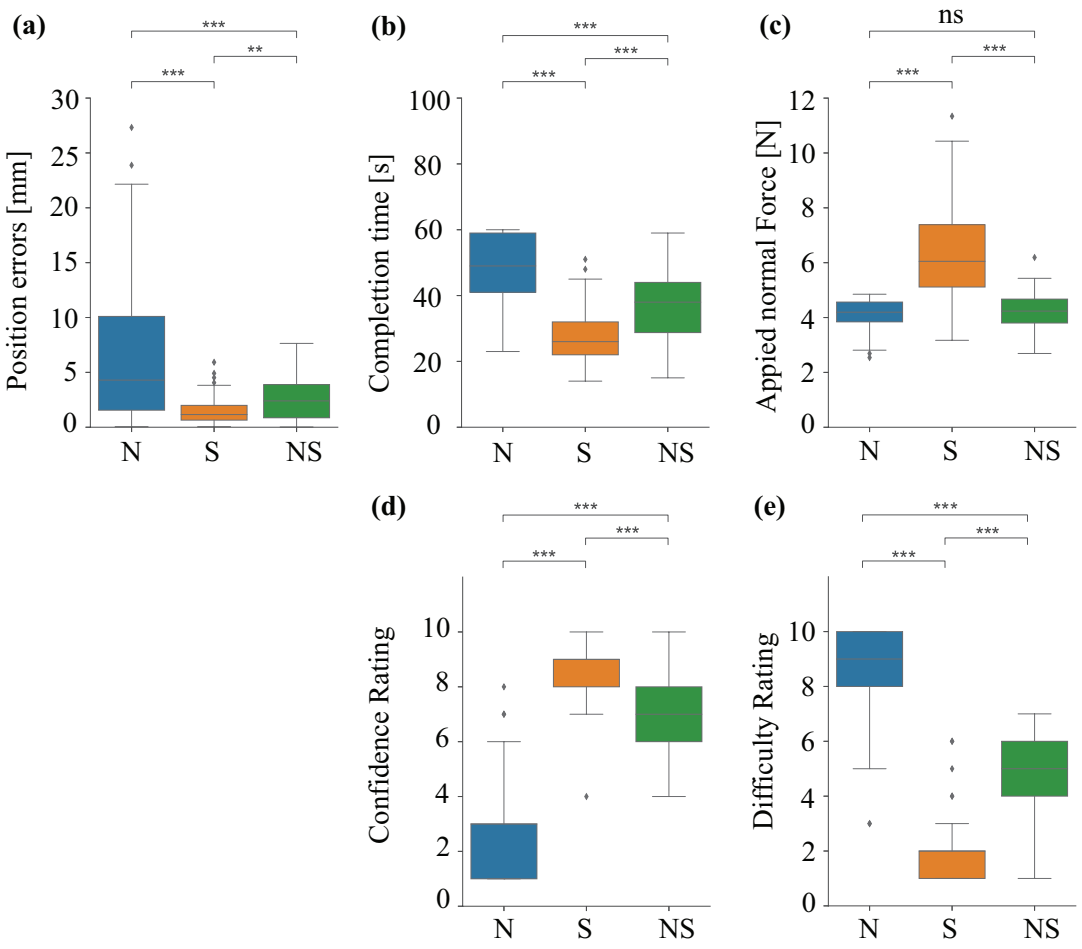

Fig. 4.15: Summary of localization performance for three experimental conditions (N,S, and NS). Boxplot method is used to depict the collected data. Outliers are represented by diamond points. (a) Tumor position errors. (b) Completion time. (c) Average applied normal force. (d) Confidence ratings. (e) Difficulty rating. *** indicates $p < 0.001$, ** indicates $p < 0.01$, and ns indicates $p > 0.05$ with post hoc Wilcoxon signed rank tests with Bonferroni correction.

Fig. 4.15 (e) shows the difficulty ratings for each condition. The Friedman test showed a significant difference between the three feedback conditions ($\chi^2(2) = 133.74$, $p < 0.001$). The Wilcoxon signed rank test showed significant differences between conditions N and S ($W(12) = 0$, $p < 0.001$), between N and NS ($W(12) = 1.5$, $p < 0.001$), and between S and NS ($W(12) = 38.5$, $p < 0.001$). This result shows that the difficulty ratings in condition N were significantly higher than those in the remaining conditions.

4.5 Discussion

First, we discuss the characterization of the SuP–Ring pneumatic control module. Regarding the static response, the input value is linearly related to the generated pressure, and the standard deviations of the collected data were very small. Thus, the inner pressure of the device's tactile elements can be precisely controlled. Regarding the dynamic responses, the rising step response for a low target pressure of 15.38 kPa (input value of 0.164 V) was not really quick. The pressure bandwidth of this target pressure was smaller than that at a higher target pressure (2 Hz compared to 4.5 Hz). We decided to generate the pressure above 15.38 kPa (with the offset values) to achieve better performance of the pneumatic control module. In tissue palpation, the natural tissue probing could involve quasi–static motions, which usually do not exceed frequencies of 1 Hz [85]. In this study, we also focused on representing the tactile feedback for slow exploring motions, which surgeons could control. Thus, we believed that the current pneumatic system's response is sufficient for the MIS task. Moreover, the characterizations of the control module may be affected by various factors, ranging from the air pressure (0.5 MPa) supplied from the air compressor to the mass and elastic properties of the membrane [114]. In future work, an appropriate supplied air pressure value and a better membrane material will be determined to optimize the performance of the control module. The JND test shows the pressure presented by the SuP–Ring that can be perceived by the users. For normal element interaction only, the Weber fraction was at least 0.5. This value is slightly higher than the obtained WF of a similar tactile display that also applies pressure to the user's finger [85]. The WF of the tactile device should be constant for reference pressures, as expected in

Weber's law. However, it decreased as the intensity increased, as shown in Fig. 4.13. This phenomenon was reported in [115]. A modification of Weber's law can be applied to the JND test results as follows:

$$k = \frac{\Delta I}{I + I_0} \tag{4.7}$$

where k is the WF, ΔI is the JND value, I is the reference value, and I_0 is a constant value (or correct value). The addition of the correct values could align Weber's law with the collected data. Eq. 4.7 reveals that if the reference intensity value is higher than the constant value, the JND value is almost proportional to the intensity value. In contrast, I_0 may greatly influence ΔI for a low reference intensity value. This might be caused by the sensory noise that occurs at small values of I [115]. In the tactile display, the contact area between the tactile elements and the user's skin depends on the expansion of the silicone membrane (thin and soft). At a low value of the reference stimulus, the contact area was narrow. The area is significantly changed according to the adjustment of applied pressure leading to sensory noise, which impairs the human perception of the change in pressure. Otherwise, the contact area remained almost unchanged when the reference pressure value was high. Thus, users could better perceive the change in pressure at a high reference intensity. The use of stiffer (or thicker) membranes instead of the silicone membranes, which marginally allows the change in the contact area according to different pressures, may be a possible solution for reducing the effect of sensory noise on the user's perception.

In our proposed tactile device, we aimed to represent the pressure in relation to the contact force. Before conducting the palpation task, the offset pressures of the SuP–Ring's tactile element were delivered to the participants according to the experimental conditions. Because the SuP–Ring's control module does not have a good response for small inner pressures, the offset values were 23.38 kPa and 31.1 kPa (higher than 15.38 kPa) for the normal and shear elements, respectively. The provision of the offset pressure before starting the task is also to notify the participants of the experimental conditions. The offset and gain values of the shear elements were higher than those of the normal elements. This is because the performed shear force range tends to be much smaller than the normal force range performed in MIS. To enable the user to

perceive the change in shear force, the presented pressure of the shear elements should be high according to the JND test results. The optimal offset and gain values of each tactile element were determined to improve the performance of the tactile device in future studies.

Next, we discuss the participant's performance in tumor localization using our developed device. The palpation task showed the effect of the SuP–Ring in the three experimental conditions. The experimental results showed that the participants had the best performance in condition S, followed by condition NS, and then condition N. Under conditions S and NS with shear feedback, the detected tumor positions were more accurate than those in the remaining condition (N) without shear feedback. The participants took less time to perform the palpation task with a higher confidence rating in conditions S and NS. Moreover, the tissue palpation task under these conditions was easier than that under condition N, according to the participant's evaluations. In the conditions with shear feedback, the participants rarely felt any change in the shear element when they scanned the normal tissue area. The strong response of the shear elements appeared when the participant moved the force sensor to the embedded tumor margin. The negative positive shear and tactile elements interacted independently with each side of the tumor's margin. Based on the stimuli, the participant could localize the tumor. In condition N, the participants only received normal feedback that was affected by their applied force. Therefore, the participants experienced difficulty in detecting the embedded tumor with only normal feedback. Thus, it is believed that shear feedback could enhance the performance of the participant and their confidence in localizing the tumor.

Regarding the applied normal force by the participants during the palpation task, as shown in Fig. 4.15 (c), they applied the normal force with a median value of approximately 6 N and sometimes up to approximately 10 N in condition S. Otherwise, in the condition with normal feedback (N and NS), the participants tended to exert less contact force (with median values of approximately 4 N) than the other condition without normal feedback (S) because they could adjust the applied normal force based on the provided auditory and tactile (normal) feedback. In the MIS, the applied normal force should be small. For example, the normal force range of the sensor (0–5 N) is adequate for common laparoscopic tissue manipulation [55]. The experimental results

showed that normal feedback could contribute to ensuring the safety requirements of laparoscopic tissue palpation. Furthermore, it is claimed that the applied normal force might also affect the participant's performance. The larger normal forces exerted under condition S causes a higher shear force to be exerted in the tumor position. This might lead to better performance, as shown in the palpation task results. The decline in their performance in the NS might also result from the smaller applied normal force. The interference effect of dynamic normal (force) feedback was also another possible reason, leading to the worse performance of the participant under condition NS (compared to condition S). The JND test results revealed an insignificant effect of the normal stimuli level on the shear stimuli perception. For the results, there might be no interference between the normal and shear feedbacks if the SuP–Ring represented the quasi–static force information. However, the participants received the dynamic normal stimuli during their palpation with NS condition. The dynamic stimuli might affect the shear stimuli perception and reduce the participant's performance. The interference effect will be investigated in further works. Overall, it is believed that the tactile display with both normal and shear feedback rendered functions could be effective in laparoscopic tumor localization.

Here, the advantages and challenges with the SuP–Ring are discussed. Regarding the feasibility of SuP–Ring in surgical applications, the device could be utilized in a disposable manner because of its low–cost manufacturing. Moreover, the device components were made of biocompatible materials, similar to a tactile ring device [85], which was confirmed to be capable of sterilization. Because the device was lightweight and a strap was used to mount the device on the user's finger, the SuP–Ring has high wearability. The use of normal indentations substituted to provide shear force information (including its intensity and direction) led to shear feedback that could be controlled independently with the normal feedback. The effect of friction between the end effector and human skin as representing shear feedback of the tactile device using lateral skin stretch, could be neglected in our proposed tactile device. In order to utilize the tactile display in an actual MIS palpation, users (or surgeons) will be required to move the probing tool in a single horizontal direction, as the tool's movements in the simulated experiment. In such situation, the applied force could be represented in 2D. Thus, the tactile display's function is sufficient to provide the force feedback for tumor

localization. Although the tactile display with the provision of 2–DoF force feedback has the limitation for the scanning direction, it has an advantage in terms of simplicity. A simple tactile display is required fewer control system components. This leads to a reduction in the system's cost as well as its complexity.

Although the SuP–Ring could be effective in laparoscopic tumor localization, the tactile device still has some limitations. First, because the SuP–Ring could be worn on any position of the user's finger, the position might influence performance. Thus, the effect of the worn position will be evaluated in further studies. Secondly, regarding the current tactile feedback system, the system might be only suitable for experiments because it is still a complicated system with bulk size. In future work, we plan to propose a portable and low–cost tactile feedback system using Raspberry Pi. Thirdly, the movement of the probe is limited. In actual MIS palpation, when the user pushes the surgical tools against the tissue in multiple directions, the applied force will consist of one–dimension (1–D) normal force (along the z–axis) and 2–D shear force (along the x–axis and y–axis) components. In order to use the current tactile display, the superposition of the two shear force components could be employed as the input of the shear feedback instead of using one–axis shear force information. Another method is improving the structure of the tactile display. A tactile display representing multiple DoF force feedbacks might enrich the user's perception during their tissue palpation. Two more tactile elements could be added to the display in the circumferential direction. In such situation, the tactile display could provide 3–DoF force feedback, including 1–DoF normal and 2–DoF shear (along with x–axis and y–axis) feedback. Regarding the participant, twelve novices verified the SuP–Ring to avoid the influence of the variation in surgical skills and experiences in the tissue palpation task. We plan to evaluate the SuP–Ring in actual laparoscopic tissue palpation conducted by professional surgeons in future work. We hope that they will give us valuable feedback to enhance the device's performance.

Finally, using the adjacent tactile elements (normal indentations) might provide a feeling of shear force on the user's skin (pseudo shear feedback). However, we did not consider representing the pseudo shear feedback in this study. An evaluation test will be conducted to justify the capability of tactile display in representing the pseudo shear feedback. If it is possible, the tactile display will be an interesting device in

numerous applications, such as virtual object interaction or telerobotic manipulation.

4.6 Summary

In this chapter, we developed a ring–type tactile display using pneumatic power, called SuP–Ring. The tactile display employed normal indentation substituted for lateral skin stretch to provide both normal and shear feedback. The SuP–Ring comprises three tactile elements in which the central tactile element displays normal feedback, and the other tactile elements display shear feedback. With the proposed method, the shear feedback could be provided independently of normal feedback regardless of friction between the end effectors and human skin as the other tactile display using lateral skin stretch. The tactile device can be easily worn on the user's finger because it is lightweight and is ring–shaped. Owing to the low-cost fabrication of SuP–Ring using biocompatible materials, it has high applicability to surgical situations, such as sterilizability or disposability. Fundamental investigations of the tactile display system showed that the pressure presented by the SuP–Ring could be linearly controlled by the input signal from a sensing device, such as a force sensor. The JND test indicated the pressure that can be distinguished by users. The test results show that the user could perceive the change in the pressure of the shear elements regardless of the difference in the normal element stimulus. An evaluation of tissue palpation was conducted to investigate the effectiveness of SuP–Ring for tumor localization. The experimental results indicated that SuP–Ring, which has the capability of rendering normal and shear feedback is effective for tumor detection. The shear feedback of the tactile device enables users to improve their performance in localizing tumors. Normal feedback could contribute to preserving tissue safety in laparoscopic tissue palpation. However, an improvement of the tactile display needs to be carried out to apply the device in actual surgery. Furthermore, we believe that our proposed tactile display has the potential to be used in a wide range of fields, such as virtual reality or robot teleoperation in addition to MIS.

Chapter 5

Tumor characterization in laparoscopic surgery using the tactile display having multicomponent force feedback function

This chapter describes assessments of multiple contact force components in determining the tumor features such as tumor depth and size. A palpation strategy can achieve the tumor characterization based on tactile feedback obtained during tissue palpation. Several artificial phantom tissue models with embedded tumors of different sizes and depths were prepared for the assessments. A fundamental experiment was conducted to investigate the response of the contact force component obtained by a force sensor for tissue palpation. The experimental results indicated the contact force component's potential use in determining the tumors' depth or size with the proposed palpation strategy. Psychophysical experiments were performed to assess the user's ability to identify the tumor depth and size of the embedded tumors within the prepared phantom models, using the tactile feedback from SuP–Ring, the tactile display proposed in the previous chapter. The effectiveness of tactile display with multicomponent force feedback function for tumor characterization in LS is discussed.

5.1 Introduction

In tumor resection surgery, characteristics such as the location, depth, and size of the tumor are important information. If surgeons know the characteristic information, they can resect the entire tumor with a minimum margin without interfering with the function of surrounding tissue or remaining organs [11, 12]. The tumor characteristic could be determined by preoperative image–based techniques such as CT, MRI. However, due to the tumors and surround tissue are shifted during surgery, the preoperative

information is not completely reliable. Palpation is a promising technique for obtaining tumor characteristics during operation. In MIS, surgeons based on haptic sensation from haptic devices to palpate abnormal tissue [26].

Tactile feedback is a promising method for providing haptic information to surgeons during intraoperative tissue palpation. Tactile feedback not only provides an intuitive understanding of tissue properties, but it is also independent of the visual channel; thus, it rarely impedes the surgeon's operation. Numerous actuation methods have been employed to generate the tactile feedback for tissue palpation, such as tactile displays using shape memory alloy wires [77], multiple servomotors [79], and pneumatic systems [82] to drive pin-array elements to represent the spatially distributed reaction force. Bianchi et al. [116] and Rizzo et al. [117] utilized pneumatic air–jet and magnetorheological–fluid (MRF) devices, respectively, to display lumps (or tumors) of different sizes. Although these tactile displays can provide information about tumor shape, size, or stiffness, the perception of tumor depth is arguable. In addition, these devices are often large and complex. They are expensive to manufacture because they consist of multiple display elements, large drive units, and tactile array sensors to acquire tactile information. Thus, the tactile display may not be used as a disposable device for widespread surgical applications.

In previous chapter, SuP–Ring, a ring–type tactile display that uses pneumatic power to provide instantaneous tactile feedback to assist surgeons in tumor localization. This tactile display with two force–feedback functions has high clinical applicability owing to its simple structure, low cost, disposability, and robustness to sterilization. The tactile display employs normal indentation, a substitutional modality, driven by pneumatic power to produce normal and shear force feedback. In the tactile display, the shear feedback is provided independently of normal feedback regardless of the friction between the tactile elements and human skin as the other tactile display uses lateral skin stretch, a popular feedback modality, in which a shear force is applied to the skin. Although SuP–Ring have been effective in localizing tumors intraoperatively, their ability to characterize tumors has not been considered. Konstantinova et al. reported that the use of a combination of normal (related to normal force) and lateral (related to shear force) motions is more effective in exploring hard nodules (or tumors) [22]. Thus, we assumed that the provision of both normal and shear force feedback, such as

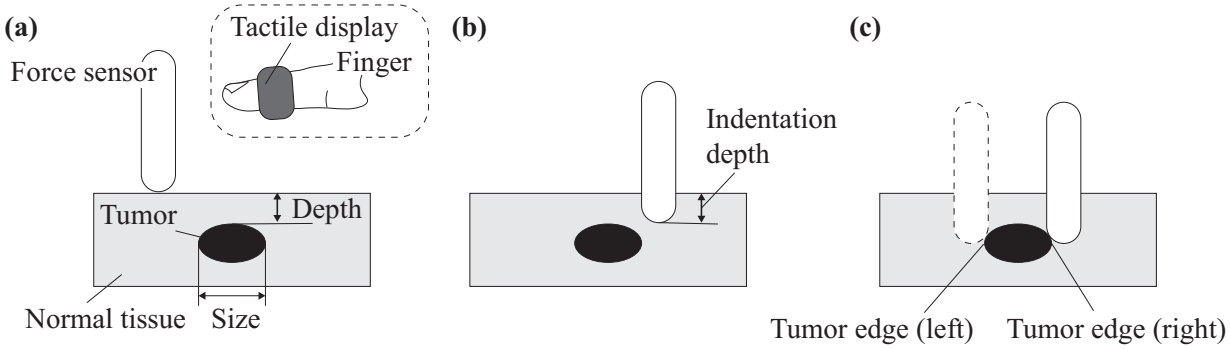

Fig. 5.1: Illustration of the proposed tissue palpation strategy. (a) Tissue model with embedded tumor and haptic devices for the tissue palpation. (b) Tumor depth determination. (c) Tumor size determination.

SuP–Ring, might be effective in assessing characteristics such as tumor depth and size.

We propose a palpation strategy with a force sensor and a tactile display to identify the depth and size of the abnormal tissue (Fig. 5.1). The user palpates the tissue using the force sensor, and the force feedback of the tactile display provides the user with contact force information. First, the user estimates the indentation depth of the force sensor based on the provided force feedback (Fig. 5.1(b)). Subsequently, they attempt to determine the tumor's depth by detecting its presence at the indentation depth of the given sensor. Furthermore, we assume that the size of the tumor can be obtained by localizing the tumor edges using force feedback. As shown in Fig. 5.1(c), if the left and right edges of the tumor are located, the entire tumor area (or the tumor size) can be determined.

In this chapter, we aimed to assess the use of normal and shear feedback to identify tumor depth and size during laparoscopic tissue palpation. First, fundamental experiments were conducted to investigate the response of the contact force components during tissue examination. Several artificial phantom tissue models with embedded tumors of different sizes and depths were prepared for the experiment. The experimental results revealed which contact force components are effective in determining the tumor depth and which components are useful in determining the size of tumors based on the proposed palpation strategy. Next, we conducted psychophysical experiments to investigate the user's ability to determine the tumor's depth and size using

tactile feedback from a tactile display. Participants with no medical background were requested to wear our developed tactile display and perform palpation tasks with artificial phantom tissue models. They were required to respond to the depth and size of the embedded tumor within the examined tissue under three feedback conditions (of the tactile display): only normal force feedback, only shear force feedback, and both normal and shear force feedback. The experimental outcomes were used to evaluate the identification performance.

5.2 Materials and Methods

5.2.1 Fundamental experiments

Fundamental experiments were designed to assess the response of contact force components, including normal and shear forces, for tumor characterization. In the experiments, we established an automated tissue palpation setup that provides accurate and consistent force responses for evaluation.

Phantom tissue with embedded tumor

Nine artificial phantom tissue models with embedded tumors were prepared. The dimensions of each model were 80 mm × 50 mm × 15 mm (Fig. 5.2). The phantom tissue were fabricated from pourable urethane rubber (Young's modulus: 6 kPa) using a 3–D printed mold. Semicylindrical tumors with a height of 5 mm, a square base, and side lengths of 10, 15, and 20 mm (as the size of the tumor) were fabricated from silicone rubber (Young's modulus: 28 kPa), as shown in Fig. 5.2(a). The tumors were embedded at depths of 2, 5, and 8 mm from the surface of the phantom tissue. The depth and size of the embedded tumor in the models were within the depth range (0–30 mm) [12] and size range (6–160 mm) [11] of hepatocellular carcinoma. The identity (ID) of the phantom tissue model and the location, size, and depth of each embedded tumor are shown in Fig. 5.2(b). The stiffness of normal (phantom) tissue is similar to that of the human liver (ranging from 4 to 6.5 kPa) [110]. In comparison, the embedded tumor stiffness matched the hepatocellular carcinoma range (20.4–75 kPa) [111].

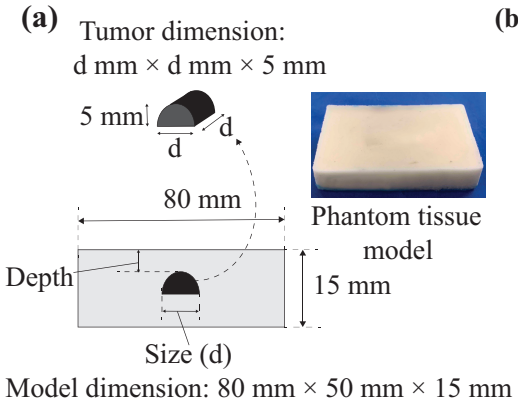

Model ID	Depth (mm)	Size (mm)
A1	2	10
A2	2	15
A3	2	20
B1	5	10
B2	5	15
B3	5	20
C1	8	10
C2	8	15
C3	8	20

Fig. 5.2: Artificial phantom tissue model. (a) Structure of the tissue model (c) The dimension of tissue models and the embedded tumors.

Experimental setup

Fig. 5.3(a) shows the experimental setup using the prepared tissue models. A 6–axis force/torque (F/T) sensor (ATI, Inc. Nano 17) was employed to measure the contact force. A sensing rod with a hemispherical tip (diameter of 8 mm), fabricated from photopolymer resin (clear resin 1 L) using a 3–D printer (Form 3, Formlabs, Inc.), was attached to the sensor. The rod was used as a sensing component that directly contacted the tissue models. The force sensor was mounted on an adjustable stage (vertical stage), which was fixed on another adjustable stage (horizontal stage). The horizontal stage was mounted on a stand established from the aluminum frames. Stepper motors adjusted the movement of the stages. The phantom tissue model was placed on a polyurethane foam plate with dimensions of 80 mm × 50 mm × 20 mm (Fig. 5.3(b)). The foam plate simulated the soft tissue (or organ) beneath the evaluated human tissue (liver tissue). The phantom tissue and foam plate were placed in a plastic case to hold them in position. The case was fixed on a 2–axis manual stage to adjust the position of the phantom tissue model.

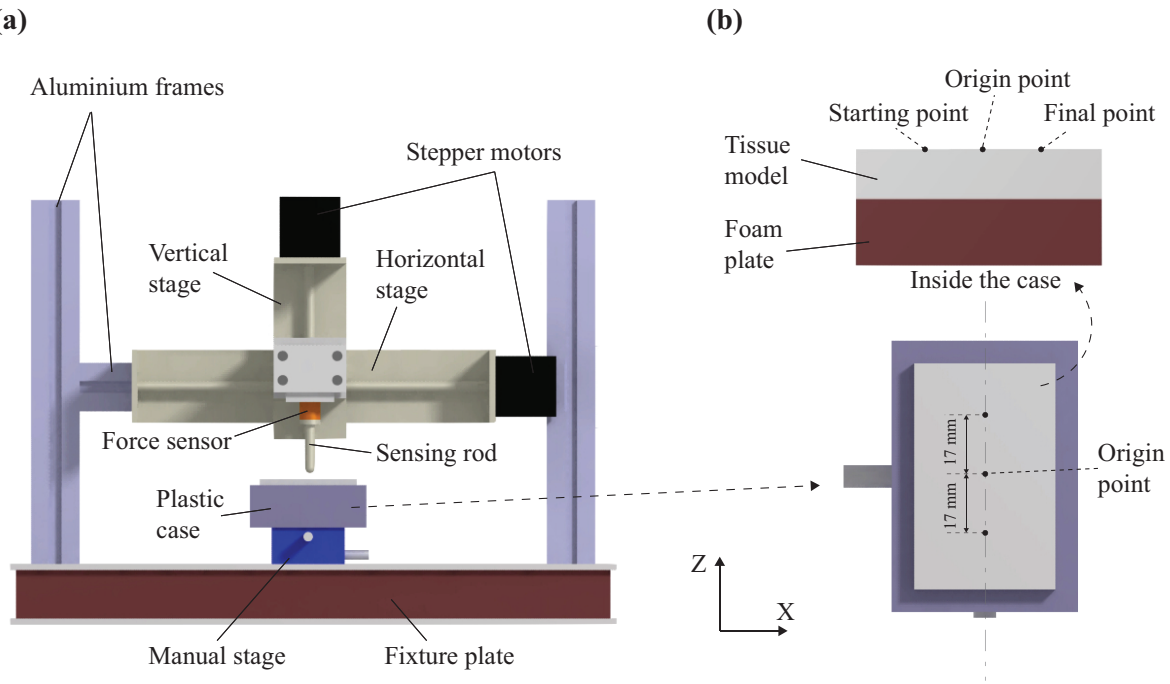

Fig. 5.3: Setup of the fundamental experiment. (a) Front view of the setup. (b) Tissue model setup.

Experimental procedures

Some essential points were defined in the fundamental experiment. The central point on the surface of the phantom tissue was defined as the origin point, with $Z = 0$ mm and $X = 0$ mm (Fig. 5.3(b)). The initial point was 5 mm above the origin. The starting point was a point on the surface of the phantom tissue, which was 17 mm to the left of the origin (with $Z = 0$ mm and $X = –17$ mm). The final point (with $Z = 0$ mm and $X = 17$ mm) was symmetric to the starting point through the origin (Fig. 5.3(b)). The tip of the sensing component (the sensing tip) was adjusted using the vertical and horizontal stages. The collection cycle was conducted as follows:

First, the vertical stage was adjusted to move the sensing tip along the z–axis away from the tissue surface ($Z = 0$ mm). At the surface of the model, the normal and shear force outputs of the sensor were set to 0 N to eliminate the effect of the initial noise. The stage was moved from $Z = 0$ mm to $Z = 14$ mm in 2 mm increments to

increase the applied force. At each increment (collection point), the tip was stopped for 1 s to collect the components of the contact force, including normal and shear forces (z–axis and x–axis forces, respectively). Subsequently, the sensing component was rapidly returned to the tissue surface ($Z = 0$ mm) and the collection cycle was completed.

In the experiment, the sensing tip moved from the initial point to the origin. At the origin, the applied force was zero. Next, the tip was moved to the starting point by adjusting the horizontal stage. A collection cycle was conducted at the starting point. Subsequently, the horizontal stage was used to adjust the position of the tip in the x–axis direction from the starting point to the final point in increments of 2 mm. A collection cycle was applied at each increment. After the data was collected at the final point, the tip was returned to the initial point. Experiments were conducted on the nine prepared models.

Data analysis

Data preparation

In the fundamental experiments, we aimed to evaluate the effectiveness of the force component in identifying the depth and size of the embedded tumor. The raw normal and shear force outputs tended to have different ranges of values. Thus, the raw data were normalized to the range 0–100 to provide the two force components an equal scale [118]. The normalized values (called evaluation values, E) were calculated as follows:

$$\mathrm{E} = \frac{F - F_{\min}}{F_{\max} - F_{\min}} \times 100, \tag{5.1}$$

where F is the absolute value of the measured normal (or shear) force at each collection point in each tissue model. $F_{\min}$ and $F_{\max}$ are the minimum and maximum absolute values of the measured normal (or shear) force within all collection points from the nine tissue models, respectively. In this experiment, the $F_{\min}$ values were 0 N at the tissue surface for both measured force components.

Detection sensitivity

According to the proposed palpation strategy for determining tumor features, the

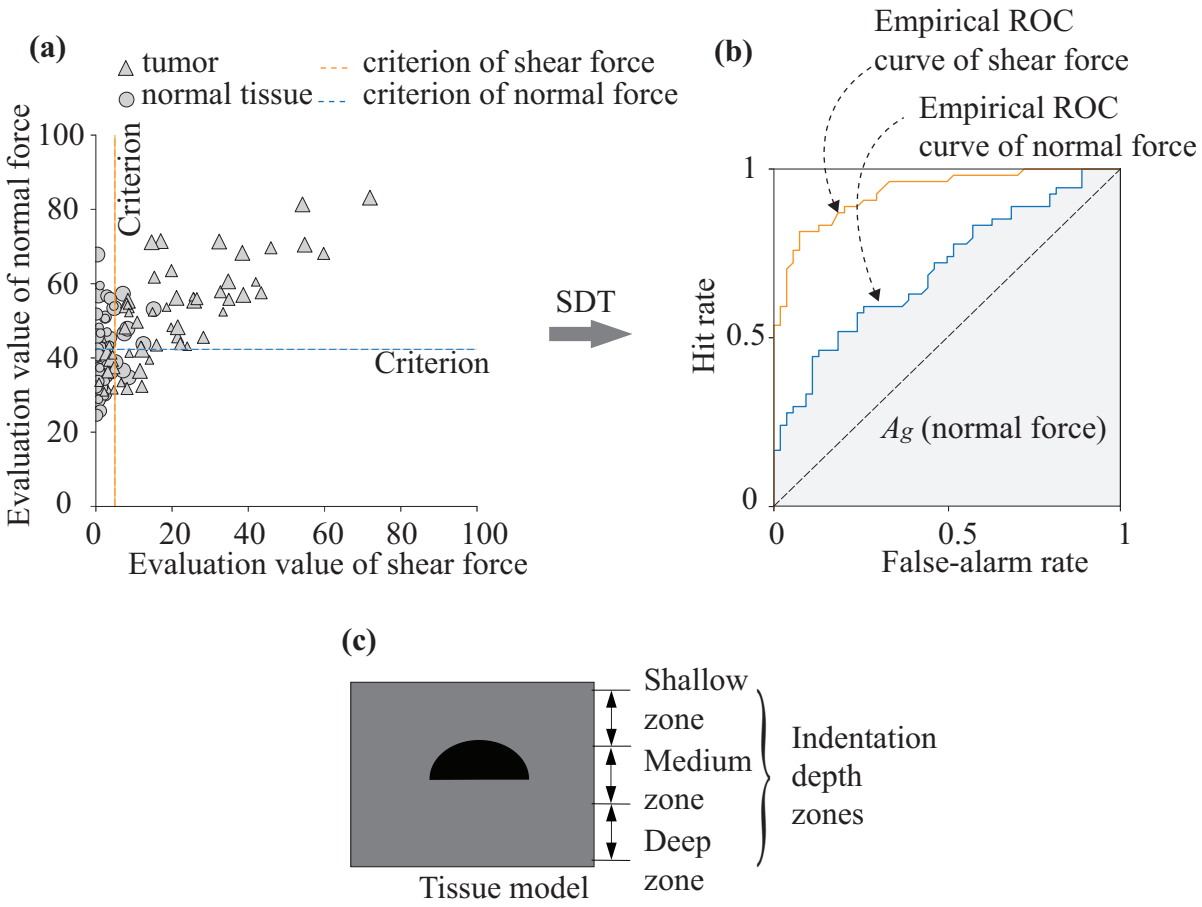

Fig. 5.4: Detection sensitivity of contact force components for tumor detection by signal detection theory. (a) Tumor detection by criterion. (b) ROC curves of normal and shear force for tumor detection. (c) Indentation depth zones of the sensor

indentation depth of the sensor should first be estimated from the contact force information. The indentation depth of the sensor was divided into three depth zones: shallow (2–6 mm), medium (6–10 mm), and deep (10–14 mm) according to the depth of the tumor embedded in the nine tissue models (Fig. 5.4(c)). Assuming that the indentation depth zones were obtained, we had to locate the tumor in each depth zone to determine the tumor depth. Similarly, to determine the size of the tumor, we had to identify the edge of the tumor over the depth zones. Overall, to assess the ability of normal and shear forces to determine tumor features, we investigated the sensitivity

of the force components in distinguishing between the tissue area with and without tumors. For example, when we obtained the contact force data for all tissue models in fundamental experiments, the Cartesian display of the evaluation values of the normal and shear forces in the deep zone could be shown in Fig. 5.4 (a). A simple method of detecting the tumor area is to select an appropriate criterion for each force component. Since the force response of the tissue area with tumor tends to be higher than that of the tissue area without the tumor, if the evaluation value of the force component is greater than the criterion, it is classified as "tumor." Conversely, if the evaluation value is lower than the criterion, it is classified as a "normal tissue" (or "no tumor") (Fig. 5.4 (a)). This classification method is rooted in signal detection theory (SDT) [118]. The tests using this classification method can be evaluated using a hit rate $H \in [0, 1]$ (the ratio of "tumor" class response when a tumor is present) and a false alarm rate $F \in [0, 1]$ (the ratio of "tumor" class response when a tumor is absent). The values of hit and false alarm rates are based on the selected criterion, which is a scale from 0 to 100 (according to the range of the evaluation value). If the sensitivity of the force component is good, the hit rate approaches 1, and the false alarm rate approaches 0. However, there is no way to select a criterion that achieves only hits ($H = 1$) and no false alarms ($F = 0$) for all tissue models. With SDT, we can analyze the empirical receiver operating characteristic (ROC) curve of each force component response to remove the effect of the selected criteria. The ROC curve indicates pairs of (F, H) for the different criteria. To obtain the ROC curves for each normal and shear force response, the criteria vary from low to high levels (from 0 to 100 with an increment of 1). The area under the ROC curve can be used as a sensitivity index to assess the sensitivity of each force component information in detecting the tumor area (Fig. 5.4 (b)). The sensitivity index (A_{g}) was computed as follows [119]:

$$A_{\mathrm{g}} = \frac{1}{2} \sum_{0}^{N-1} (H_{\mathrm{i+1}} + H_{\mathrm{i}}) \times (F_{\mathrm{i+1}} - F_{\mathrm{i}}), \tag{5.2}$$

where $(H_{\mathrm{i}}, F_{\mathrm{i}})$ is the pair of hit and false alarm rates, and N is the number of criteria. A_{g} ranges from 0 to 1, with a chance level of 0.5. If the A_{g} value is less than the chance level, it means that the evaluated force component cannot distinguish between the tissue area with and without the tumor. A higher A_{g} value indicates that the

evaluated force component can be more effective for tumor detection.

5.2.2 Psychophysical experiment

We conducted psychophysical experiments to assess the ability of users to identify abnormal tissue features. The users provided tactile feedback using our developed tactile display and performed simulated tissue palpation tasks. The effectiveness of the tactile feedback conditions in characterizing the tumor was analyzed using experimental results.

Participants

In this chapter, we aimed to examine the effects of tactile feedback on tissue palpation in a fair manner. Since skilled surgeons vary widely in their surgical skills and experience, novices were employed to reduce the influence of variation in the palpation experiments [85]. Ten participants, including seven men and three women (ranging in age from 23 to 28 years), without any medical background, participated in the experiments. All participants were right–handed according to the Coren test [120]. The participants consented to conduct the experiment with an experimental protocol according to the ethical standards of the Helsinki Declaration and approved by the Ethical Committee of the Nagoya Institute of Technology.

Tactile display

Fig. 5.5(a) shows the ring–shaped tactile display (SuP–Ring) using pneumatic power that we developed for laparoscopic tumor localization. The development of SuP–Ring was describe in Chapter 4. The tactile display consists of three tactile elements (silicone membranes): a normal element, positive shear element, and negative shear element. The normal indentations generated from these tactile elements provide tactile feedback to the users. This display method can represent the shear force independently of the normal force without being affected by the friction between the tactile elements and human skin, as in the other tactile display that employs other feedback representation methods such as the lateral skin stretch method. In addition, because the SuP–Ring is lightweight and has a ring shape, it can be easily worn on the user's fingers and rarely

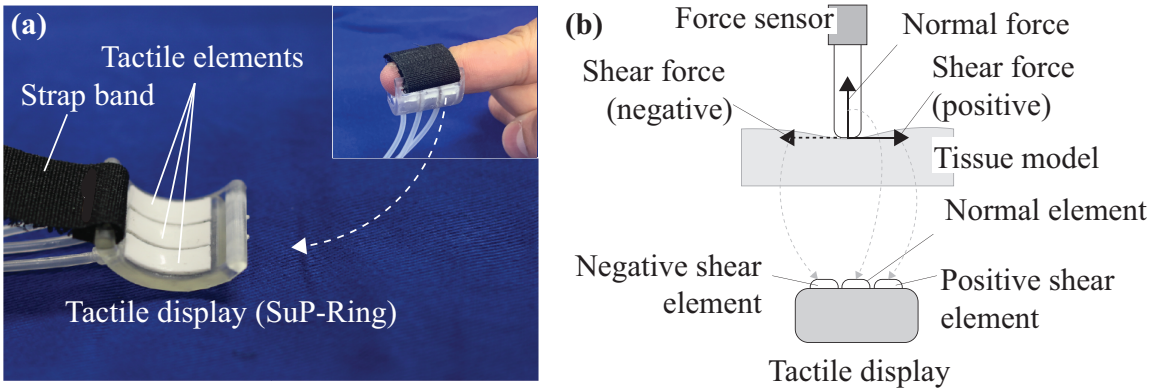

Fig. 5.5: Tactile display. (a) Tactile display's prototype. (b) Operation mechanism of the tactile display.

impedes the surgeon's movement during operation. Furthermore, this tactile device is sterilizable and disposable, making it highly clinically applicable.

The SuP–Ring provides the relative pressure based on the force information from a force sensor according to Equations 4.2, 4.3, 4.4. In this experiment, the maximum pressure value of $P_{\text{threshold}} = 101.89$ kPa for the device's tactile elements was set to prevent these silicone elements from being ruptured. $P_{\text{N0}} = P_{\text{S0}} = 23.3$ kPa are the offset pressure values of the corresponding normal and shear force elements. $G_{\text{N}} = 15.4$ kPa/N and $G_{\text{S}} = 39.02$ kPa/N are the gain values of the normal and shear elements, respectively. The gain values were set such that the range of the air pressure for providing normal and shear feedback was the same, based on the results of the fundamental experiments. The feedback of shear force information from the tactile display enabled surgeons to detect the tumor within the normal tissue area, and the normal force feedback contributed to preserving the safety requirements for laparoscopic tumor localization, as reported in the previous chapter.

Experimental setup

A simulated tissue palpation experiment was designed to assess the user's ability to characterize the tumor using the SuP–Ring (Fig. 5.6). A similar experimental setup was used in our previous chapter to evaluate the effectiveness of the SuP–Ring in tumor

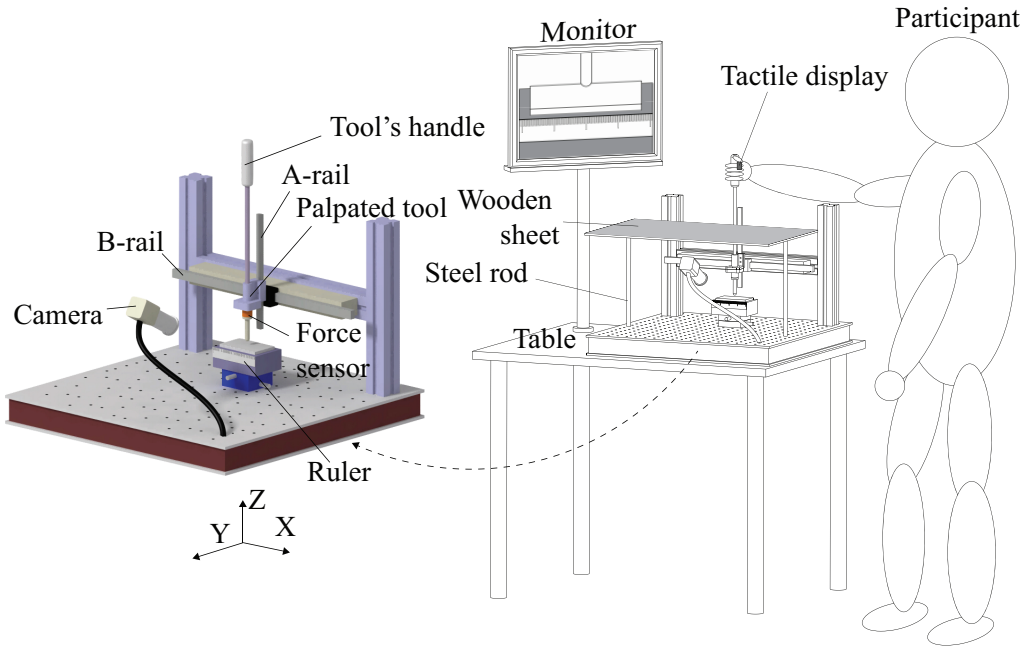

Fig. 5.6: Simulated laparoscopic tissue palpation setup.

localization. A palpated tool with a 6–axis F/T sensor (ATI, Inc. Nano 17) and a sensing rod as the tool's sensing component, similar to the fundamental experimental setup, was used to measure the contact force. The tool can traverse vertically over a linear guide rail (A–rail), which can move horizontally over another linear guide rail (B–rail). The user can control the tool's tip position by moving the handle of the tool. The tactile feedback of the tactile display presented the normal force (z–axis force component) and shear force (x–axis force component) from the force sensor.

The phantom tissue model was the same as that used in the fundamental experiment. A ruler was attached to the case as a reference. The experimental images from the camera were displayed on a monitor mounted on the table. A wooden sheet simulating the abdominal wall was placed above the experimental setup with steel rods. Because of the wooden sheet, the user could obtain only visual information through the monitor.

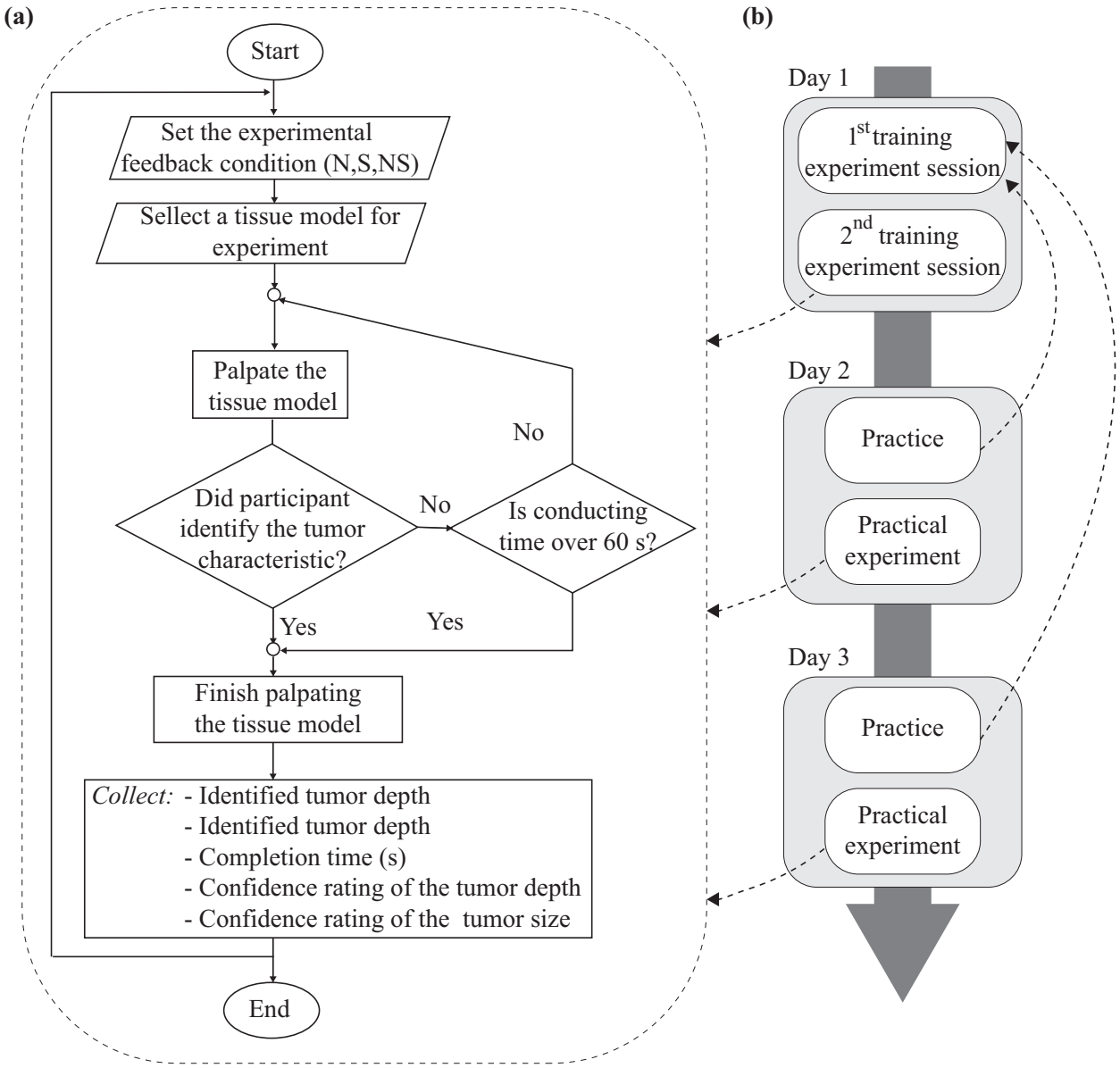

Fig. 5.7: Experimental procedure. (a) Experimental procedure for each palpation task. (b) Experimental procedure for each participant.

Experimental Procedures

The aim of the experiment was explained to the participants before conducting tissue palpation using the tactile display. Not all participants had experience with a tissue

model with embedded tumors because they did not have a medical background. The participants need to know the tissue model they would be testing. Thus, we requested them to touch the tissue model with their index fingers to determine the depth and size of the embedded tumor. The operating mechanism of the tactile display was then demonstrated. The experiments were conducted under three conditions according to the feedback from the tactile display: normal feedback only (condition N), shear feedback only (condition S), and both normal and shear feedback (condition NS). In condition N, only normal feedback was provided to the users through the normal elements of the tactile display. In condition S, the shear elements represent the shear force information, and the normal force information is ignored. In condition NS, three tactile elements of the tactile display were activated to provide both normal and shear force feedback to the user.

The participants wore the tactile display on their right–hand index finger pad and stood in front of the table to perform the tissue palpation experiment. The participants held the tool handle with their right hand. The participants palpated the phantom tissue models by moving the tool. The position of the tool tip was observed via the monitor. The participants were informed that the embedded tumor was always located near the central point of the model. In the palpation experiment, the depth and size of the tumors were categorized into three types. For tumor depth, we defined "shallow," "medium," and "deep" depth corresponding to tumor depths of 2, 5, and 8 mm. For the size, "small," "medium," and "large" size were defined for tumors with sizes of 10, 15, and 20 mm. The participants were required to identify the tumor depth and size categories based on tactile feedback. They conducted training experiments to fully understand the experimental procedure before performing practical experiments to collect the necessary data. Each participant spent three days on the psychophysical experiments, including one day for the training experiments and two days for the practical experiments (Fig. 5.7(b)). Both training and practical experiments were conducted under three feedback conditions.

Training experiment

At the beginning of the training experiments, the participants examined the tissue model in the regions with and without tumors and felt the tactile feedback they

received. They were requested to memorize tactile feedback in each region. After confirming that the participants could distinguish between the tumor and the normal tissue areas based on tactile feedback, they were requested to identify the tumor depth and size. For the tumor depth determination, the participants attempted to detect the embedded tumor based on the tactile feedback provided. The participants were requested to examine the tissue model in all three indentation depth zones (shallow, medium, or deep). They determined the order of palpated depth zones. The depth zone was perceived based on the intensity of tactile feedback. The tumor depth (shallow, medium, or deep) was identified by determining the shallowest depth zone at which the participant detected the tumor. Regarding tumor size determination, the participants were requested to localize the edges of the tumor. Based on the location of the tumor edges and reference dimension with the ruler, the participants could identify the size of the tumors (small, medium, or large). During tissue palpation, because the tumor was semi–cylindrical, the edges of the tumor may have been incorrectly detected when the participant palpated the tissue model in the inappropriate depth zone, for example, if a large tissue model with a medium depth tumor is palpated in the shallow depth zone. Thus, the participant might receive the same tactile feedback if a small tissue model with a shallow depth tumor is palpated in the shallow depth zone, resulting in incorrect detection of tumor size. Moreover, the results of fundamental experiments (to be mentioned in the next section) demonstrated that force feedback is capable of detecting all tumors in the deep depth zone only. Thus, the participants were instructed to examine the tissue model in the deep zones to accurately detect the location of the tumor edge. The training experiment consisted of two training sessions.

In the first training session, the depth and size of the embedded tumors were informed to the participants in advance. The participants palpated the tissue model to confirm the perception of tumor characteristics in each feedback condition. The main objective of the first training session was to aid the participants in identifying the tumor depth and size using tactile feedback from the tactile display. All tissue models were palpated under the three feedback conditions. There was no time limit for palpation during the training session. The participants were permitted to examine any tissue model repeatedly under any feedback condition until they were confident in identifying the tumor characteristics.

In the second training session, several phantom tissue models were randomly selected from the nine models. The participants were requested to determine the depth and size of the tumors embedded in the models. The aim of the training session was to practice palpating the tissue in a practical experimental scenario. One of the three feedback conditions was selected for the experiment. The tissue palpation task was performed within 60 s, and the participants were requested to complete the task as rapidly as possible. Completion time was recorded using a stopwatch. After 60 s, the participant had to immediately stop tissue palpation. After completing the task, the participants indicated their perceived depth (shallow, medium, or deep) and size (small, medium, or large) of the embedded tumor. They were also requested to provide the "confidence rating" for their identification of each tumor's characteristics. The ratings ranged from 1 (not confident at all) to 100 (very confident). At the end of each trial of the training session, the participants were informed of the actual information (the depth and size of the embedded tumor) of the model that they palpated. The participants could check the correctness of their identification. After completing the trial with the selected model, each participant took a break for approximately 30 s and then performed the tissue palpation task with other tissue models. The experimental procedure is shown in Fig. 5.7(a). In the second training session, each participant experimented with all feedback conditions in a random order.

Practical experiment

Before undertaking the practical experiment, the participants were permitted to practice palpating the tissue model several times in the same way as in the first training session. After they were confident about their perceptions, a practical experiment was started. In the practical experiment, all nine tissue models were examined one at a time for each feedback condition on each day. In each trial, the model was selected randomly. Each participant performed 54 trials over two days (27 trials each day), and ten participants conducted 540 trials in the practical experiments. The procedure of each tissue palpation trial in the practical experiments was the same as that in the second training session of the training experiments. After each trial, the participants responded to the identification of the tumor depth and size, as well as the confidence rating of each identification. In the practical experiment, we did not inform the partici-

pants of the correct characteristics of the implanted tumor at the end of each trial, as in the training experiment. During the experiment, participants were requested to wear headphones that produced white noise to eliminate the influence of other cues (such as sound noise from the pneumatic system) on the performance of the experiment. After completing tissue palpation in one condition, the participants took a 5–min break before moving to the next condition. Each participant spent approximately 1 h each day to complete the palpation tasks (27 trials) (about 2 h for two days). The participants conducted the experiment in different orders of feedback conditions on the two days of the experiment. The feedback condition order was also shuffled and partially counterbalanced across the participants.

5.3 Results

5.3.1 Fundamental experiment

Fig. 5.8 shows qualitatively the contact forces measured from the force sensor of the nine tissue models in the experiment ($X \in$ [–17 mm, 17 mm] and $Z \in$ [2 mm, 14 mm]). The model IDs are shown in the corner of each image. Each image indicates the raw data of the normal force (Fig. 5.8(a)) or shear force (Fig. 5.8(b)) applied to each tissue model. The maximum absolute values of normal and shear force in the experiments were $F_{\max} = 4.64$ N and $F_{\max} = 1.53$ N, respectively. The obtained data were depicted and smoothed by contour plotting using Python.

Indentation depth

Fig. 5.9 shows the relationship between the evaluation values of the normal (and shear force) and the indentation depth of the force sensor during the fundamental experiments. The evaluation values were computed from the raw data of all models according to Eq. (1). Pearson's correlation coefficient was used to evaluate the relationships. The results indicated a strong correlation between the evaluation value of the normal force and the indentation depth ($r(1134) = 0.94$, $p < 0.01$), and a moderate correlation between the evaluation values of shear force and indentation depth ($r(1134) = 0.46$,

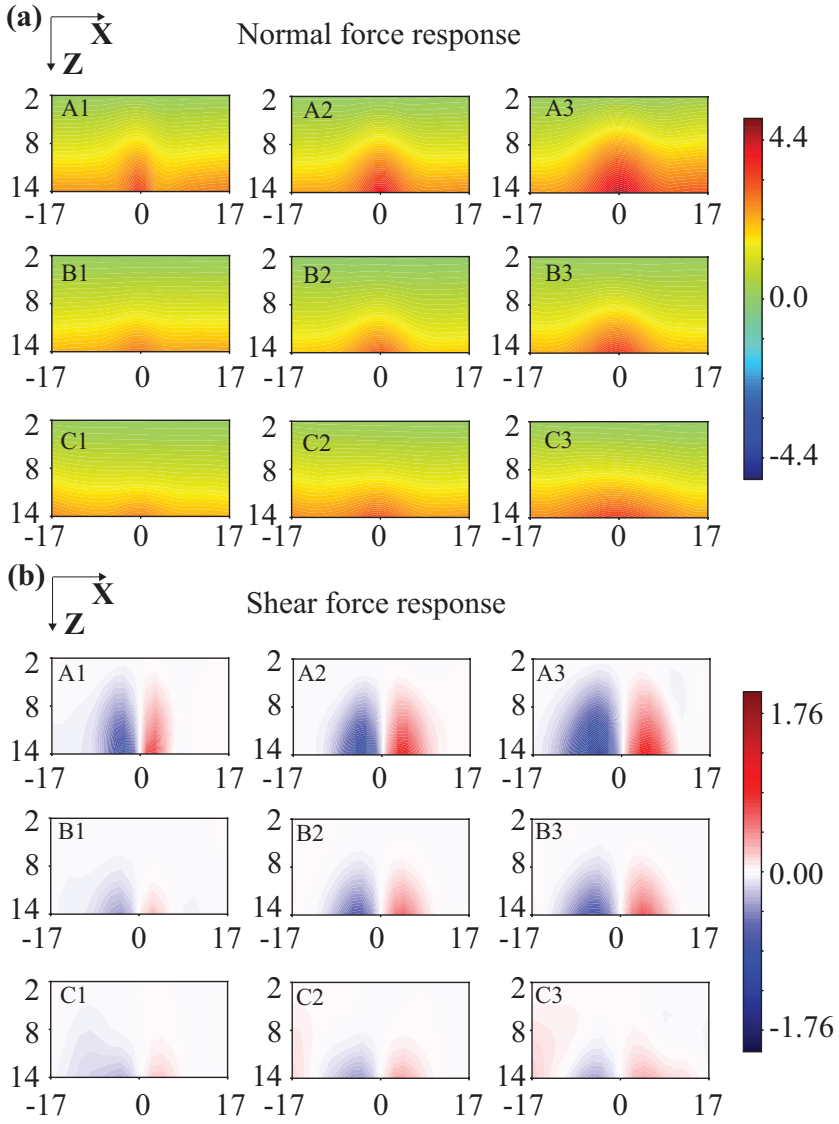

Fig. 5.8: Results of the fundamental experiments. (a) Response of the normal force. (b) Response of the shear force.

$p < 0.01$). This suggested that the use of normal force information is more effective in estimating the indentation depth of the sensor (or indentation depth zone).

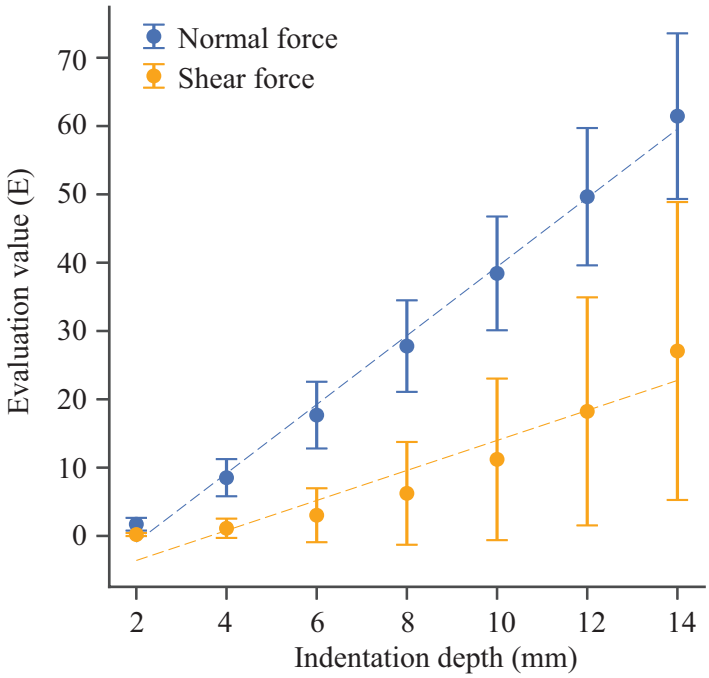

Fig. 5.9: Relationships between the contact force components and the indentation depth of the force sensor.

Tumor depth determination

From the above results, we can determine the indentation depth zone of the sensor using normal force information. Regarding the tumor depth determination, we need to investigate the sensitivity of the force component information for detecting the tumor area in each indentation depth zone.

The tissue model was divided horizontally (along the x–axis) into four evaluation regions: region 0 (X $\in$ [–17 mm, –11 mm]), region 1($X \in$ [–7 mm, –1 mm]), region 2 ($X \in$ [1 mm, 7 mm]), and region 3 ($X \in$ [11 mm, 17 mm]), as shown in Fig. 5.10(a). In all tissue models, the embedded tumors were located in regions 1 and 2 (the "tumor" region), while regions 0 and 3 were the normal tissue without the presence of tumor (the "no tumor" region). The means of the normal and shear force evaluation values in the "tumor" and "no tumor" regions were employed to assess the sensitivity of the force components for tumor detection. Fig. 5.10(b) shows the sensitivity index of the

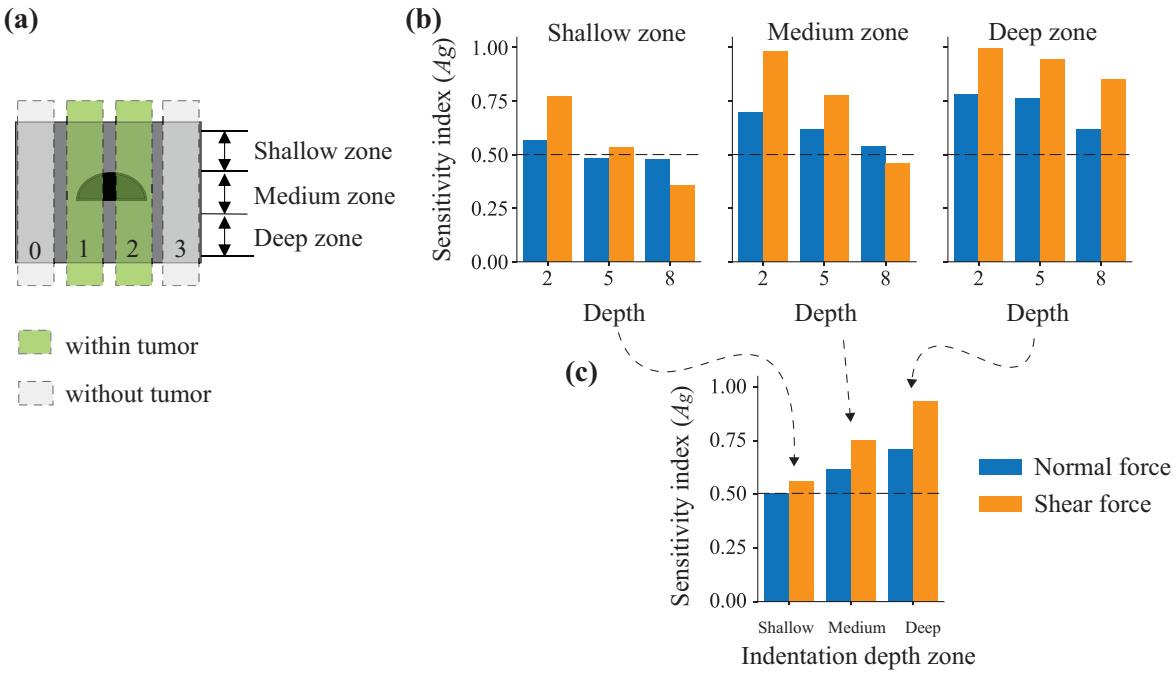

Fig. 5.10: Detection sensitivity in tumor depth determination. (a) Illustration of evaluation regions and indentation depth zones. (b) Detection sensitivity of normal and shear force in determining the embedded tumor in different indentation depth zones, regarding the tumor depth. (c) Detection sensitivity of normal and shear force in determining the embedded tumor in different indentation depth zones for all tissue models.

two force components for three tumor depths in three indentation depth zones of the sensor, regardless of the tumor size. In the shallow zone, the A_g value of the shear force for the shallow embedded tumor (2 mm depth) was approximately 0.75. On the other hand, the A_g values of normal force for the shallow embedded tumor and of normal and shear force for the medium (depth of 5 mm) and deep (depth of 8 mm) embedded tumors were roughly the chance level (0.5). This indicated that the shear force can only be used to distinguish between the areas with and without tumors in the shallow zone. In the medium zone, the results indicated that we can use the normal and shear forces to detect shallow and medium tumors, while deep tumors may be difficult to detect using both normal and shear forces. In the deep zone, normal or shear forces can be

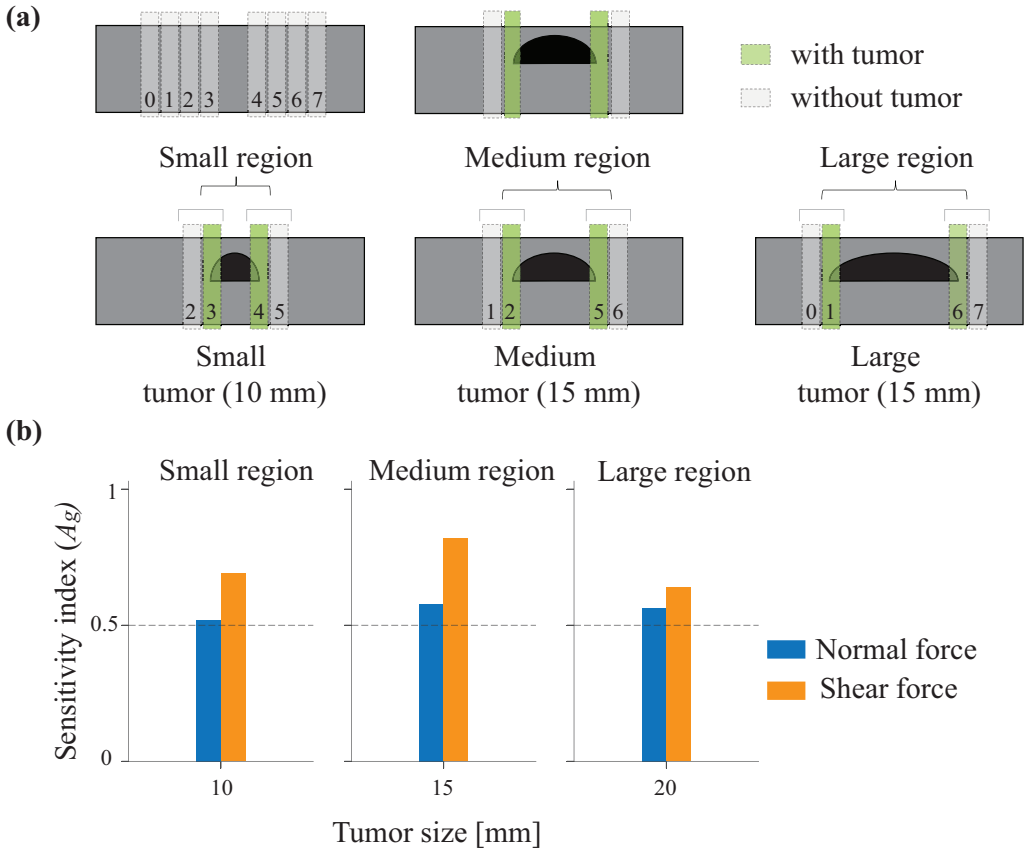

Fig. 5.11: Detection sensitivity in tumor size determination. (a) Illustration of evaluation regions. (b) Detection sensitivity of normal and shear force in determining the edge of embedded tumors in the evaluation regions, regardless of the tumor depth.

used to localize the tumor at different depths. Fig. 5.10(c) shows the sensitivity index of the force components of all tissue models in the three indentation depth zones of the sensor. Generally, the shear force revealed a better sensitivity in detecting tumors in each depression depth zone.

Tumor size determination

For tumor size determination, we investigated the capability of the force components in detecting tumor edges. Eight evaluation regions were set horizontally in the tissue

model (Fig. 5.11(a)). To detect the tumor edges, we distinguished tissue regions with and without tumors in the tumor edge region. In the models with small tumors (10 mm), the tumors were present in regions 3 ($X \in$ [–7 mm, –5 mm]) and 4 ($X \in$ [5 mm, 7 mm]), whereas the tumor was absent in regions 2 ($X \in$ [–9 mm, –7 mm]) and 5 ($X \in$ [7 mm, 9 mm]). Here, we defined the small region as regions 3 and 4 and regions 2 and 5. With this detection method, we observed that the edges of small tumors were located in the small region. Similarly, the medium region consists of evaluation regions 1 ($X \in$ [–11 mm, –9 mm]),6 ($X \in$ [9 mm, 11 mm]), 2, and 5. The large region consisted of the evaluation regions 0 ($X \in$ [–13 mm, –11 mm]), 7 ($X \in$ [11 mm, 13 mm]), 1, and 6. The edges of the medium (15 mm) and large (20 mm) tumors were located in the medium and large regions, respectively. The A_{g} value was also used to evaluate the normal and shear force sensitivities for tumor edge detection. Furthermore, the results of the tumor depth determination indicated that the contact force information was not effective in detecting several tumors of medium or deep depth in the shallow and medium depth zones. The sensitivity of the force components for tumor depth detection had the best performance in the deep indentation depth zone. Thus, we decided to evaluate their sensitivity to tumor size determination in the deep zone only.

Fig. 5.11(b) shows the sensitivity index of the two force components for detecting the tumor edge in the deep zone. The results indicated that the edge of small embedded tumors can be detected in the small region, the medium tumor in the medium region, and the large tumor in the large region. Generally, the shear force also exhibited better sensitivity in detecting tumor edges (or tumor size determination) compared with the normal force.

5.3.2 Psychophysical experiment

Fig. 5.12 shows the confusion matrices of the participants' responses in the three feedback conditions provided by the tactile display for the three tumor depths and three tumor sizes of the nine tissue models. The average accuracy for each feedback condition is also listed below each confusion matrix. The results indicated that condition NS had the best matching performance, followed by conditions S and N.

Statistical tests with a significance level of 0.05 were used to investigate the effect of the feedback conditions on the participant's performance in determining the tumor

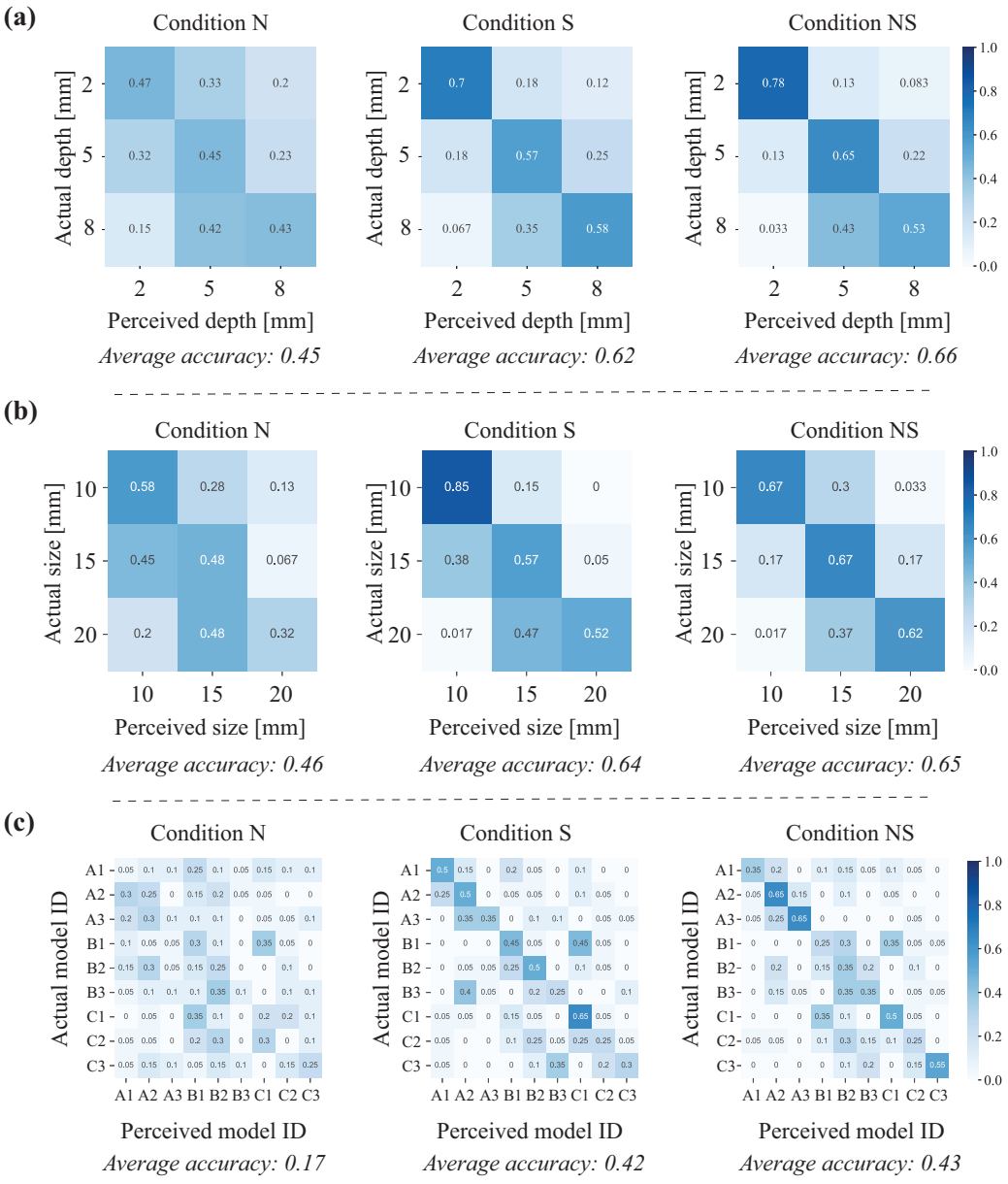

Fig. 5.12: Confusion matrices of the participant's performance on tumor characterization under three feedback conditions. (a) Results of tumor depth identification. (b) Results of tumor size identification (c) Results of both tumor depth and size identification.

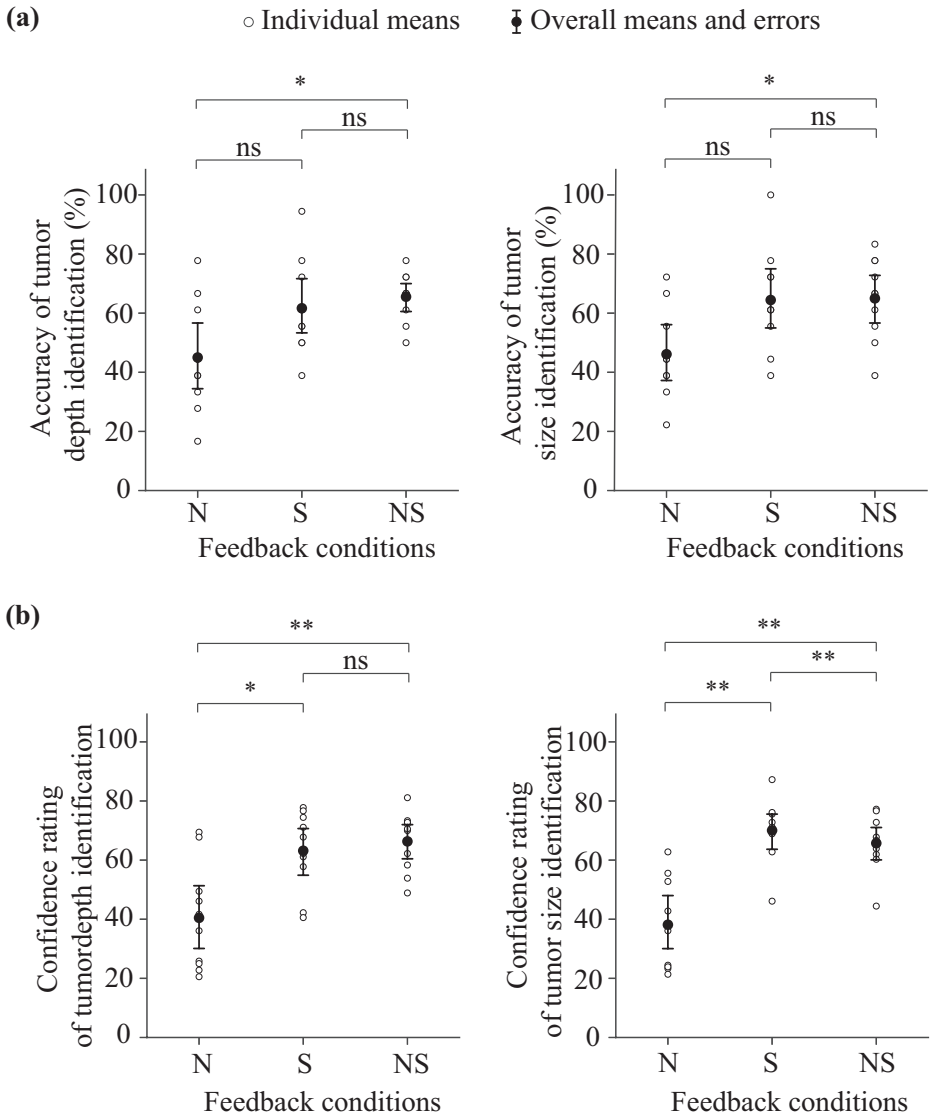

Fig. 5.13: Summary of identification performance for three experimental conditions (N,S, and NS). (a) Accuracy of tumor depth and tumor size identification. (b) The confidence ratings of tumor depth and tumor size identification. ** indicates $p < 0.01$, * indicates $p < 0.05$, and ns indicates $p > 0.05$.

depth and tumor size independently. Fig. 5.13(a) shows the accuracy of all participants' identification of the tumor depth and size in the three conditions. The accuracy is

expressed as the ratio of correct identification responses (N_{correct}) to the number of identification targets (N_{target}) (multiplied by 100 to turn it into a percentage) using the following equation:

$$\text{Accuracy} = \frac{N_{\text{correct}}}{N_{\text{target}}}. \tag{5.3}$$

The accuracy data were normally distributed using the Shapiro–Wilk test. The data also passed Mauchly's test of sphericity. Thus, a repeated–measures analysis of variance (ANOVA) was conducted to evaluate the effect of the feedback conditions on the identification accuracy. The ANOVA test results indicated that the feedback condition significantly affected the identification accuracy of tumor depth ($p = 0.013$) and tumor size ($p = 0.03$). Multiple comparisons using paired t–tests with Bonferroni correction indicated that a significant difference in determining tumor depth ($p = 0.012$) and tumor size ($p = 0.024$) between conditions N and NS, whereas no significant difference was observed in the identification accuracy between condition S and the other feedback conditions.

The average confidence ratings of the participants for their identification of each tumor depth and tumor size under the three feedback conditions are shown in Fig. 5.13(b). The rating data were normally distributed based on the Shapiro–Wilk test. Mauchly's test of sphericity revealed that the sphericity assumption was violated ($p < 0.01$). A repeated–measures ANOVA with a Greenhouse–Geisser correction indicated a statistically significant difference between the means of the three feedback conditions for both the depth ($p < 0.01$) and the size ($p < 0.01$) determination of the embedded tumors. Paired t–tests revealed that there were significant differences in confidence ratings between conditions N and NS ($p < 0.01$ for both depth and size identifications) and between conditions N and S ($p = 0.02$ for depth identification, and $p < 0.01$ for size identification). Furthermore, a statistically significant difference was observed between conditions S and NS in tumor size identification ($p < 0.01$), but there was no significant difference between the two conditions for tumor depth determination ($p = 0.23$).

We also investigated the effect of the feedback conditions on the participants' time to complete the palpation task. The completion time data (Fig. 5.14) passed the Shapiro–Wilk normality test and Mauchly's sphericity test. The results of the

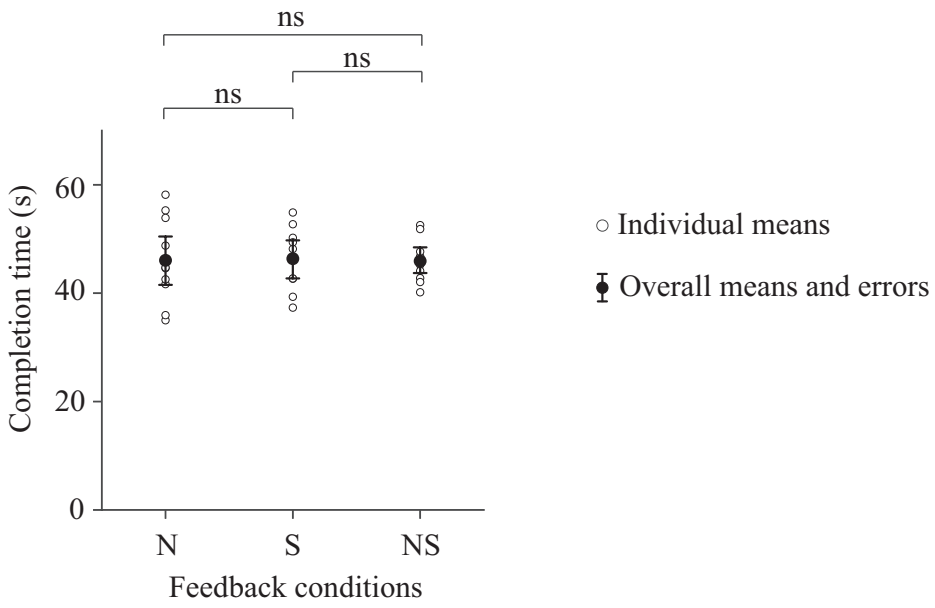

Fig. 5.14: Completion time of participants in their tumor characterization. * indicates $p < 0.05$, and ns indicates $p > 0.05$.

repeated–measures ANOVA indicated that the feedback conditions had no significant effect on the participants' completion time ($p = 0.96$). The average completion time of the participants in the three feedback conditions was approximately 46 s.

5.4 Discussion

5.4.1 Fundamental experiments

The results of the fundamental experiments indicated the response of normal and shear forces during tissue palpation in nine tissue models. The tumor depth information was obtained by estimating the indentation depth of the force sensor at which the tumor was present. According to the Pearson correlation tests, the normal force indicated a high linear correlation with the indentation depth of the sensor, whereas the shear force was slightly correlated with the indentation depth over the entire tissue area that was examined. Thus, it is better to use normal force information to estimate the

indentation depth of the sensor.

SDT was used to evaluate the capability of the force components to distinguish between the tissue areas with and without tumors. SDT is a better method for evaluating the results of fundamental experiments than machine learning–based methods, which tends to cause overfitting on a small dataset [26]. In manual tissue palpation, although surgeons might perceive the indentation depth of the sensor based on force feedback information, achieving the same indentation every time as in robot–assisted tissue palpation is challenging. However, surgeons may have the ability to reach the relative indentation of the sensor during palpation. Thus, in the fundamental experiment, we investigated the capability of the contact force components to determine the tumor in three indentation depth zones, which might be achieved by manual tissue palpation. Fig. 5.10(b) and Fig. 5.10(c) show the sensitivity indices of the two force components in tumor detection for the three tumor depths in the three indentation depth zones. The shear force indicated a higher sensitivity at each indentation depth zone compared with the normal force. The small effect of normal force on tumor detection might stem from the boundary conditions of the examined tissue. In actual scenarios, human tissue is located on top of other organs or soft tissue. Thus, the human tissue might be deformed during palpation with probes or sensors, causing a decrease in the normal force response. In this chapter, we used a polyurethane foam plate to simulate the underlying soft tissue. Here, the shear force exhibited better sensitivity in tumor localization, as reported in Chapter 3. Other studies achieved better tumor characterization results with the normal force because the experimental tissue were placed on rigid bases [7,86]. According to the fundamental results, both the normal and shear forces should be used to identify the depth of the embedded tumor.

The tumor size information can be obtained by localizing the two edges of the embedded tumor. The sensitivity indices of the contact force responses in the deep zones for detecting tumor edges were evaluated. Based on the results of the fundamental experiments, we could detect the tumor edge of the small embedded tumor in the small region, the medium tumor in the medium region, and the large tumor in the large region. Generally, the shear force also exhibited higher sensitivity for tumor edge detection compared with the normal force component. Thus, the use of shear force information is considered an effective method of determining tumor size.

Fundamental experiments demonstrated the possibility of using the contact force components (normal and shear forces) information to characterize the tumor. The experimental results support the hypothesis of the proposed palpation method. Normal force information can be used to estimate the indentation depth of the sensor. The tumor depth can be obtained by localizing the tumor using shear force information at a given indentation depth. The tumor size can be determined in the deep zone by relying only on shear force information. From the results, a tactile display with normal and shear force feedback functions, such as our developed tactile display (Sup–Ring), can be a good candidate for identifying tumor characteristics.

5.4.2 Psychophysical experiments

The psychophysical experiments indicated the effect of tactile feedback conditions produced by the SuP–Ring on the participant's performance in tumor characteristics identification. For tumor depth identification, higher determination accuracy and higher confidence were obtained in condition NS than in condition N. The results revealed that additional shear feedback was necessary to detect the tumor at a given depth. In addition, the mean accuracy of identifying the tumor depth under condition S was up to 62 %, which was slightly lower than that under condition NS. However, there was no statistically significant difference in accuracy and participant confidence under the two conditions. A possible reason is that the participant received kinesthetic feedback on their palms in addition to the tactile feedback in the simulated tissue palpation tasks. This might enable the participants to estimate the indention depth of the sensor using kinesthetic feedback under condition S. However, in actual surgery, the perception of kinesthetic feedback tends to be impaired owing to the friction between the surgical tool shaft and trocar [121]. Meanwhile, the normal tactile feedback, which represented the normal contact force at the tip of the palpated tool, was not affected by trocar friction. Thus, we consider that normal feedback is necessary to determine the depth of the tumor during actual surgery.

For tumor size identification, the participants responded more accurately and confidently to tumor size when both normal and shear feedback were provided (condition NS), compared with when only normal feedback was provided (condition N). The average accuracy of tumor size identification in condition NS was 65 %. The ac-

curacy value was slightly lower than the accuracy of participants' performance (73 %) in the task of identifying the size of 10 rectangles generated using the MRF haptic display [117]. However, the MRF display in this study was a large device (with a base of 200 mm × 200 mm), and it presented rectangles of large size (ranging from 20 mm × 20 mm to 155 mm × 155 mm). Thus, MRF displays are not suitable for surgical applications. Meanwhile, our tactile display has significant clinical advantages, such as simple structure, small size, low cost, disposability, and sterilizability. In the other feedback conditions, there was no difference in the participants' performance in identifying tumor size between conditions S and NS. However, the participants responded more confidently when only the shear feedback (condition S) was represented. In condition NS, dynamic normal feedback of the SuP–Ring could have interfered with the participant's perception of shear feedback, causing them to lose confidence in identifying the tumor size. Furthermore, in the determination of tumor depth under condition NS, the dynamic effect between the two feedback components may have caused the participant to lose confidence in determining the tumor location. However, providing normal feedback might have caused them to be more confident in estimating the indentation depth of the sensor. Thus, there was no significant difference between conditions S and NS in participants' confidence in identifying the tumor depth. In the future, we plan to investigate the dynamic effects between the two tactile feedback components of tactile displays.

The participants' completion time was not significantly affected by the tactile feedback conditions in the palpation tasks. These results indicate that participants may need a certain period, called the standard period, to determine the tumor features. In this experiment, the average completion time was approximately 46 s, which was considered a standard period. In some conditions, participants could rapidly identify the tumor features but needed the standard time to confirm this information. However, in other feedback conditions, if the tactile feedback did not provide much useful information, the participant could assume that increasing the time spent on tissue palpation would not provide any further useful information. Therefore, the standard time may be sufficient for the participants to complete the tissue palpation task, regardless of feedback conditions.

5.4.3 Limitations and future works

Generally, the experiments indicated that the users had a high potential in identifying the depth and size of embedded tumors when they were provided with both normal and shear feedback using a tactile display. However, some problems should be addressed to enhance tissue characterization performance. First, although our developed tactile display has significant clinical advantages, it does not provide high–resolution tactile feedback. This may cause a reduction in the user's ability to determine tumor features. We plan to improve our tactile display in further studies to obtain a better identification performance, as mentioned in Chapter 4. Second, in the tissue palpation task, the participants conducted the training experiments and practiced again before conducting the practical task. However, the training time might have been insufficient for them to remember the feedback perception properly and provide consistent estimations. If the participants were trained for a longer time, they would determine the tumor characteristics more accurately. Finally, all participants in this study were novices, which enabled us to fairly evaluate the effectiveness of tactile feedback for tissue characterization. In future research, we plan to perform experiments with skilled surgeons. We consider that experts will perform better in tumor characterization because they have higher surgical skills and more experience in tissue palpation. The effect of participants' skills and experience will be investigated in future studies.

5.5 Summary

In this chapter, we investigated the capability of tactile feedback in characterizing tumors during laparoscopic tissue palpation. We proposed a palpation strategy to identify tumor features, such as depth and size. Contact force components (normal and shear force) were used to determine the indentation depth of the palpated sensor and to detect the tumor area and the edges of the tumor. The tumor depth was determined by detecting the presence of the tumor at a given indentation depth of the sensor. The size of the tumor can be derived by localizing the tumor edges. The responses of the contact force components when palpating the tissue were indicated through fundamental experiments with nine artificial phantom tissue models. The experimental

results indicated that both normal and shear force information should be used to determine tumor depth. Additionally, the shear force provides a higher sensitivity for determining tumor size. Twelve participants without a medical background performed simulated tissue palpation tasks to identify the depth and size of the embedded tumor within the tissue model. The normal and shear force feedback during tissue palpation was provided to the participants using our developed pneumatic tactile display. The tactile display has high clinical applicability owing to its simple structure, light weight, and sterilizability. In the experiment, we evaluated the effectiveness of tactile feedback on the participants' identification performance. The experimental results indicated that the participants identified the tumor characteristics more correctly when provided with both normal and shear feedback. However, the tactile display requires further improvements to enhance the user's identification performance.

Chapter 6

Conclusion

In tumor resection surgery, the tumor characteristics such as location, size, and depth are essential information for surgeons. By understanding these characteristics, the surgeon can maximize and accurately remove the tumor, to preserve the functions of the surrounding tissue and remaining organ of the patent. Preoperative imaging techniques such as CT and MRI could be utilized to determine the abnormal tissue. However, accurate registration of the tumor characteristics, such as its location, using the obtained information from these techniques is difficult due to the movement of the soft tissue and the shifting of the tumor position during surgery. In open surgery, surgeons can identify the tumor in soft tissue through a palpation procedure using tactile sensation on their fingers. However, this procedure is more challenging when the surgeon's fingers do not directly contact the tissue, as in LS or RMIS. Computer technologies can compensate for the lack of surgeons' tactile sensation in laparoscopic tumor determination.

The main focus of this thesis is to propose intraoperative tissue palpation systems using haptic technology to assist surgeons in MIS, especially in LS. A palpation system consists of a sensing device to acquire tissue data during laparoscopic palpation and a display device to convey the data to the surgeon. The haptic devices in laparoscopic surgery are often force–based devices. Since the sensation of lumps or tumors through palpation is a complex process (even for human sensation), devices for tissue palpation are required to have multiple sensing or display functions to enrich the surgeon's perception of tumors. However, too many elements may complicate the structure of the palpation device or increase its size, which may be disadvantageous for MIS applications. For example, a large sensing device cannot be inserted into the patient's body, and a complex display device interferes with surgeons' movement during surgery. Thus, the balance between the devices' functions and the simplicity of their structure is im-

portant. Furthermore, in the manual palpation technique, the combination of normal and lateral motions (related to normal and shear forces, respectively) is necessary to explore the target tissue. Thus, a 2–DoF force–sensing device (having normal and shear force–sensing functions) and a 2–DoF force–displaying device (providing normal and shear force feedback) were developed to achieve the balancing purpose in laparoscopic tissue palpation. In addition, to apply the system to MIS, we focused on developing devices that could meet the requirements of the clinical environment, such as sterilizability and electrical safety. Thus, two technologies, acoustic reflection principle and pneumatics, were used to design the sensing and display devices, respectively, because of their advantages in medical device development. Moreover, tissue deformation, surgeon's motions, and the data display modalities often cause the surgeon's difficulties in identifying the tumor. For example, surgeons might miss tumor position due to unclear obtained tissue data, or visual sensory overload might occur since the surgeons are required to focus on laparoscopic images during surgery. The proposed devices aimed to reduce these difficulties and improve the surgeon's performance and confidence in tumor detection. Furthermore, this thesis also focused on introducing a palpation method using the proposed devices that could enable the surgeons to determine the tumor characteristics, such as its depth and size.

The first contribution of this thesis is to introduce a forceps–type tactile sensor, a sensing device using the acoustic reflection principle, which would be helpful for decision–making of surgeons in intraoperative tumor detection in laparoscopic gastric tumor resection surgery. We proposed a novel acoustic sensing design consisting of two acoustic cavities to acquire two contact force components information, including normal and shear force. Since the tactile sensor has no electrical components inserted into the patient's body, it offers great advantages in MIS regarding sterilizability and electrical safety. In addition, the sensor also has a simple structure with a small size that is suitable for use in MIS. Since the developed tactile sensor has low manufacturing and computational costs, it could be used as a disposable device, compared to the other expensive sensing devices such as ultrasonic sensors. The tissue palpation experiment's results with an artificial gastric tissue having an embedded tumor showed that the normal force information from the tactile sensor significantly fluctuated during the tissue palpation, causing difficulties in localizing the tumor position. The bending of

the gastric tissue due to applied force by surgeons and their sensor's movements are often the reasons for the reducing effect of the normal force in intraoperative tumor localization. On the other hand, the shear force information was relatively stable and greatly changed at the tumor position, regardless of the tissue bending or the sensor's movements. The surgeon could more easily detect the tumor position based on the shear force information than the normal force. In summary, this finding showed that the shear force information would be useful for the decision–making of the surgeons in their intraoperative tumor localization.

Owing to the use of visual feedback for displaying the contact information might cause a potential overloading visual channel, another feedback modality, such as tactile feedback, that is independent of visual channel should be used to transmit contact information to surgeons during surgery. The second contribution of this thesis is to propose a pneumatic ring–type tactile display (SuP–Ring) having two force feedback functions to assist surgeons in laparoscopic tissue palpation. The tactile display employed normal indentation, a substitutional sensory modality, which was largely unaffected by skin friction (as skin stretch modality), to provide force feedback to the surgeon. The SuP–Ring comprises three tactile elements to display normal feedback, shear feedback of the contact force in tissue palpation procedures. Due to the tactile display's elements are controlled by pneumatic power, it has high clinical applicability, such as simple structure, low–cost, disposability, and strong robustness to sterilization. The results of a psychophysical experiment show that the user could perceive the change in the pressure of the shear elements regardless of the difference in the normal element stimulus. The effectiveness of SuP–Ring on tumor localization was investigated through a palpation experiment with an artificial phantom tissue. The experimental results showed that the shear feedback of the tactile device could enable surgeons to improve their confidence and performance in localizing tumors, while normal feedback could contribute to the avoidance of tissue damage in intraoperative tissue palpation.

The above findings showed that tactile devices have normal and shear force sensing or feedback capabilities is useful for tumor localization. The next contribution of this thesis is to introduce a palpation strategy using multiple contact force component sensory devices to determine tumor characteristics, such as depth and size. In the strategy, the tumor depth is determined by detecting the presence of the tumor at a

given depth position of the sensor. The size of the tumor can be derived by localizing the tumor edges. Fundamental experiments using nine phantom tissue models with embedded tumors of different sizes and depths were conducted to investigate the use of contact force components in determining tumor features using the proposed strategy. The experimental results indicated that both normal and shear force information should be used to determine tumor depth, while the shear force provides high sensitivity for determining tumor size. The effectiveness of tactile feedback on tumor characterization using the prosed palpation strategy was investigated via tissue palpation experiments. Participants without any medical background wore the SuP–Ring on their fingers and tried to identify the depth and size of the embedded tumor within the phantom tissue models using the proposed palpation strategy. The experimental results showed that participants could identify tumor features more correctly and confidently when given normal and shear force feedback.

Although the proposed tactile devices and palpation method proved to be useful for laparoscopic tumor characterization, they still have several limitations that should be addressed in future studies. Firstly, since the developed tactile sensor is designed for sliding palpation, it is not yet suitable for use with the proposed tactile display, which is designed for tapping palpation. We plan to improve the structure and function of the tactile sensor to integrate with the SuP–Ring, to achieve a complete haptic system for laparoscopic tissue palpation. Developing a 3–axis force sensor similar to commercially available force sensors could be a possible approach. Secondly, the tissue palpation with the SuP–Ring was limited direction movement and relatively time-consuming. Thus, the SuP–Ring's structure could be improved to achieve a 3–DoF tactile display. In that case, the surgeon could flexibly palpate target tissue from multiple directions to obtain more tissue information, enabling more accurate tumor characterization. Thirdly, in this thesis, the effectiveness of the proposed devices for tumor characterization was verified by novices in experimental environments. In future work, we plan to investigate the effectiveness of the devices and the palpation method in actual tissue palpation with experts. Their performance and advice would be helpful for us to improve the current systems.

Finally, we are considering various applications of the developed tactile devices and the sensing (and feedback) principle, in addition to medical applications. For

example, since acoustic-based sensing devices have no electrical elements at the sensing (or contact) section, it is possible to propose a sensor using the acoustic principle for systems that need to work in wet environments, such as underwater robots. For the substitutional feedback modality, normal indentation, it is possible to consistently provide normal and shear force feedback to the user with high fidelity regardless of the user's skin friction, wet or dry conditions, compared to other tactile feedback modalities such as skin stretch. Thus, we believe that virtual reality devices developed based on the substitutional feedback modality will be a potential reliable devices that allow users to feel digital objects in a virtual environment.

References

[1] W. A. Woodward et al.: "Changes in the 2003 American Joint Committee on Cancer staging for breast cancer dramatically affect stage-specific survival", *J. Clin. Oncol.*, vol. 21, no. 17, pp. 3244–3248, 2003.

[2] "Surgery for cancer", *National Cancer Institute*, 29-Apr-2015. Accessed on : Dec 21, 2021. [Online]. Available: https://www.cancer.gov/about-cancer/treatment/types/surgery.

[3] L. W. T. Alkureishi et al.: "Does tumor depth affect nodal upstaging in squamous cell carcinoma of the head and neck?", *Laryngoscope*, vol. 118, no. 4, pp. 629–634, 2008.

[4] J. K. Williams, G. W. Carlson, C. Cohen, P. B. Derose, S. Hunter, and M. J. Jurkiewicz: "Tumor angiogenesis as a prognostic factor in oral cavity tumors", *Am. J. Surg.*, vol. 168, no. 5, pp. 373–380, 1994.

[5] M. Li et al.: "Intra-operative tumour localisation in robot–assisted minimally invasive surgery: A review", In: *Proc. Inst. Mech. Eng. H*, vol. 228, no. 5, pp. 509–522, 2014.

[6] I. B. Wanninayake, P. Dasgupta, L. D. Seneviratne, and K. Althoefer: "Air-float palpation probe for tissue abnormality identification during minimally invasive surgery", *IEEE Trans. Biomed. Eng.*, vol. 60, no. 10, pp. 2735–2744, 2013.

[7] M. Sadeghi-Goughari, A. Mojra, and S. Sadeghi: "Parameter estimation of brain tumors using intraoperative thermal imaging based on artificial tactile sensing in conjunction with artificial neural network", *J. Phys. D Appl. Phys.*, vol. 49, no. 7, p. 075404, 2016.

[8] S. J. Lederman and R. L. Klatzky: "Sensing and displaying spatially distributed fingertip forces in haptic interfaces for teleoperator and virtual environment systems", *Presence (Camb.)*, vol. 8, no. 1, pp. 86–103, 1999.

[9] K. Hoyt et al.: "Tissue elasticity properties as biomarkers for prostate cancer", *Cancer Biomark.*, vol. 4, no. 4–5, pp. 213–225, 2008.

[10] T. A. Krouskop, T. M. Wheeler, F. Kallel, B. S. Garra, and T. Hall: "Elastic moduli of breast and prostate tissues under compression", *Ultrason. Imaging*, vol. 20, no. 4, pp. 260–274, 1998.

[11] K. Sasaki et al.: "Minimum resection margin should be based on tumor size in hepatectomy for hepatocellular carcinoma in hepatoviral infection patients: Base resection margin on tumor size", *Hepatol. Res.*, vol. 43, no. 12, pp. 1295–1303, 2013.

[12] B. Liu et al.: "Improving the surgical effect for primary liver cancer with intraoperative Trejos–Force fluorescence navigation compared with intraoperative ultrasound", *Med. Sci. Monit.*, vol. 25, pp. 3406–3416, 2019.

[13] T. N. Robinson and G. V. Stiegmann: "Minimally invasive surgery", *Endoscopy*, vol. 36, no. 1, pp. 48–51, 2004.

[14] H. Xina, J. S. Zeleka, and H. Carnahanb: "Laparoscopic surgery, perceptual limitations and force: A review", In: *Proceedings First Canadian Student Conference on Biomedical Computing*, 2006.

[15] A. Hamed et al., "Advances in haptics, tactile sensing, and manipulation for robot–assisted minimally invasive surgery, noninvasive surgery, and diagnosis", *J. robot.*, vol. 2012, pp. 1–14, 2012.

[16] P. Basford, G. Longcroft-Wheaton, and P. Bhandari: "ASGE Technology Committee reviews on real-time endoscopic assessment of the histology of diminutive colorectal polyps, and high–definition and high–magnification endoscopes", *Gastrointest. Endosc.*, vol. 82, no. 6, pp. 1139–1140, 2015.

[17] R. Bogdanova, P. Boulanger, and B. Zheng: "Depth perception of surgeons in minimally invasive surgery", *Surg. Innov.*, vol. 23, no. 5, pp. 515–524, 2016.

[18] S. Masroor, C. Plambeck, and M. Dahnert: "Complex repair of a Barlow"s valve using the Da Vinci robotic surgical system", *J. Heart Valve Dis.*, vol. 19, no. 5, pp. 593–595, 2010.

[19] M. E. Currie et al.: "Long–term angiographic follow–up of robotic–assisted coronary artery revascularization", *Ann. Thorac. Surg.*, vol. 93, no. 5, pp. 1426-1431, 2012.

[20] A. M. Okamura: "Haptic feedback in robot–assisted minimally invasive surgery", *Curr. Opin. Urol.*, vol. 19, no. 1, pp. 102–107, 2009.

[21] N. Wang, G. J. Gerling, R. M. Childress, and M. L. Martin: "Quantifying palpation techniques in relation to performance in a clinical prostate exam", *IEEE Trans. Inf. Technol. Biomed.*, vol. 14, no. 4, pp. 1088–1097, 2010.

[22] J. Konstantinova, G. Cotugno, P. Dasgupta, K. Althoefer, and T. Nanayakkara: "Palpation force modulation strategies to identify hard regions in soft tissue organs", *PLoS One*, vol. 12, no. 2, p. e0171706, 2017.

[23] C. R. Wagner, N. Stylopoulos, and R. D. Howe: "The role of force feedback in surgery: analysis of blunt dissection", In: *Proceedings 10th Symposium on Haptic Interfaces for Virtual Environment and Teleoperator Systems*, pp. 68–74, 2002.

[24] W. Semere, M. Kitagawa, and A. M. Okamura: "Teleoperation with sensor/actuator asymmetry: task performance with partial force feedback", In: *Proceedings 12th International Symposium on Haptic Interfaces for Virtual Environment and Teleoperator Systems*, pp. 121–127, 2004.

[25] A. L. Trejos, R. V. Patel, and M. D. Naish: "Force sensing and its application in minimally invasive surgery and therapy: A survey", *Proc. Inst. Mech. Eng. Part C*, vol. 224, no. 7, pp. 1435–1454, 2010.

[26] J. C. Gwilliam, Z. Pezzementi, E. Jantho, A. M. Okamura, and S. Hsiao: "Human vs. robotic tactile sensing: Detecting lumps in soft tissue", In: *Proceedings 2010 IEEE Haptics Symposium*, pp. 21–28, 2010.

[27] C. Huang, Q. Wang, M. Zhao, C. Chen, S. Pan, and M. Yuan: "Tactile perception technologies and their applications in minimally invasive surgery: A review", *Front. Physiol.*, vol. 11, p. 611596, 2020.

[28] J.-H. Hwang, J. H. Kwon, T.-K. Kim, and D. Hong:

"Design of simple structured tactile sensor for the minimally invasive robotic palpation", In: *Proceedings of the 2013 IEEE/ASME International Conference on Advanced Intelligent Mechatronics*, pp. 1296–1299, 2013.

[29] J. Dargahi, S. Najarian, and R. Ramezanifard: "Graphical display of tactile sensing data with application in minimally invasive surgery", *Can. J. Electr. Comput. Eng.*, vol. 32, no. 3, pp. 151–155, 2007.

[30] W. Lin, B. Wang, G. Peng, Y. Shan, H. Hu, and Z. Yang: "Skin–inspired piezoelectric tactile sensor array with crosstalk–free row+column electrodes for spatiotemporally distinguishing diverse stimuli", *Adv. Sci. (Weinh.)*, vol. 8, no. 3, p. 2002817, 2021.

[31] M. V. Ottermo, ⊘. Stavdahl, and T. A. Johansen: "A remote palpation instrument for laparoscopic surgery: design and performance", *Minim. Invasive Ther. Allied Technol.*, vol. 18, no. 5, pp. 259–272, 2009.

[32] J. Dargahi, S. Payandeh, and M. Parameswaran: "A micromachined piezoelectric teeth–like laparoscopic tactile sensor: Theory, fabrication and experiments", In: *Proceeding of the 1999 IEEE International Conference on Robotics and Automation*, pp. 299–304, 1999.

[33] S. Sokhanvar, M. Packirisamy, and J. Dargahi: "A multifunctional PVDF–based tactile sensor for minimally invasive surgery", *Smart Materials and Structures*, Vol. 16, No. 4, pp. 989–998, 2007.

[34] L. Weng, G. Xie, B. Zhang, W. Huang, B. Wang, and Z. Deng: "Magnetostrictive tactile sensor array for force and stiffness detection", *J. Magn. Magn. Mater.*, vol. 513, no. 167068, p. 167068, 2020.

[35] O. H. Paydar, C. R. Wottawa, R. E. Fan, E. P. Dutson, W. S. Grundfest, and M. O. Culjat: "Fabrication of Thin–film capacitive force sensor array for tactile feedback in robotic surgery", In : *Proceedings 2012 Annual International Conference of the IEEE Engineering in Medicine and Biology Society*, pp. 2355–2358, 2012.

[36] A. P. Miller, W. J. Peine, J. S. Son, and M. D. Z. T. Hammoud: "Tactile imaging system for localizing lung nodules during video assisted thoracoscopic surgery", In: *Proceedings 2007 IEEE International Conference on Robotics and Automation*, pp. 2996–3001, 2007.

[37] A. Talasaz and R. V. Patel: "Telerobotic palpation for tumor localization with depth estimation", In: *Proceedings 2013 IEEE/RSJ International Conference on Intelligent Robots and Systems*, pp. 463–468, 2013.

[38] A. S. Naidu, R. V. Patel, and M. D. Naish: "Low–cost disposable tactile sensors for palpation in minimally invasive surgery", *IEEE ASME Trans. Mechatron.*, vol. 22, no. 1, pp. 127–137, 2017.

[39] "Pressure Profile Systems" *PPS*, Accessed on : Dec 21, 2021. [Online]. Available: http://www.pressureprofile.com.

[40] J. Back, P. Dasgupta, L. Seneviratne, K. Althoefer, and H. Liu: "Feasibility study– novel optical soft tactile array sensing for minimally invasive surgery", In: *Proceedings 2015 IEEE/RSJ International Conference on Intelligent Robots and Systems*, pp. 1528–1533, 2015.

[41] H. Xie, H. Liu, L. D. Seneviratne, and K. Althoefer: "An optical tactile array probe head for tissue palpation during minimally invasive surgery", *IEEE Sens. J.*, vol. 14, no. 9, pp. 3283–3291, 2014.

[42] C. Chi, X. Sun, N. Xue, T. Li, and C. Liu: "Recent progress in technologies for tactile sensors", *Sensors (Basel)*, vol. 18, no. 4, 2018.

[43] J. B. Gafford, S. B. Kesner, A. Degirmenci, R. J. Wood, R. D. Howe, and C. J. Walsh: "A monolithic approach to fabricating low–cost, millimeter–scale

multi-axis force sensors for minimally invasive surgery", In: *Proceeding of the 2014 IEEE International Conference on Robotics and Automation*, pp. 1419–1425, 2014.

[44] R. Sedaghati, J. Dargahi, and H. Singh: "Design and modeling of an endoscopic piezoelectric tactile sensor", *International Journal of Solids and Structures*, Vol. 42, Issues 21–22, pp. 5872–5886, 2005.

[45] A. M. Hamed, Z. T. H. Tse, I. Young, B. L. Davies, and M. Lampérth: "Applying tactile sensing with piezoelectric materials for minimally invasive surgery and magnetic–resonance–guided interventions", In: *Proceedings of the Institution of Mechanical Engineers, Part H: Journal of Engineering in Medicine*, Vol. 223, Issue 1, pp. 99–110, 2009.

[46] F. Ju et al.: "A miniature piezoelectric spiral tactile sensor for tissue hardness palpation with catheter robot in minimally invasive surgery", *Smart Mater. Struct.*, vol. 28, no. 2, p. 025033, 2019.

[47] C. H. Chuang, T. H. Li, I. C. Chou, and Y. J. Teng: "Piezoelectric tactile sensor for submucosal tumor hardness detection in endoscopy", In *Proceedings 18th International Conference on Solid-State Sensors, Actuators and Microsystems* pp. 871–875, 2015.

[48] M. Beccani, C. Di Natali, L. J. Sliker, J. A. Schoen, M. E. Rentschler, and P. Valdastri: "Wireless tissue palpation for intraoperative detection of lumps in the soft tissue", *IEEE Trans. Biomed. Eng.*, vol. 61, no. 2, pp. 353–361, 2014.

[49] U. Kim, Y. B. Kim, D.-Y. Seok, J. So, and H. R. Choi: "A surgical palpation probe with 6–axis force/torque sensing capability for minimally invasive surgery", *IEEE Trans. Ind. Electron.*, vol. 65, no. 3, pp. 2755–2765, 2018.

[50] T. Yamamoto, B. Vagvolgyi, K. Balaji, L. L. Whitcomb, and A. M. Okamura: "Tissue property estimation and graphical display for teleoperated robot–assisted surgery", In: *Proceedings 2009 IEEE International Conference on Robotics and Automation*, pp. 4239–4245, 2009.

[51] C. Lv, S. Wang, and C. Shi: "A high–precision and miniature Fiber Bragg Grating–based force sensor for tissue palpation during minimally invasive surgery", *Ann. Biomed. Eng.*, vol. 48, no. 2, pp. 669-681, 2020.

[52] H. Liu, D. P. Noonan, B. J. Challacombe, P. Dasgupta, L. D. Seneviratne, and K. Althoefer: "Rolling mechanical imaging for tissue abnormality localization during minimally invasive surgery", *IEEE Trans. Biomed. Eng.*, vol. 57, no. 2, pp. 404–414, 2010.

[53] P. Puangmali, H. Liu, L. D. Seneviratne, P. Dasgupta, and K. Althoefer: "Miniature 3–axis distal force sensor for minimally invasive surgical palpation", *IEEE ASME Trans. Mechatron.*, vol. 17, no. 4, pp. 646–656, 2012.

[54] S. J. Hammer et al.: "Quantitative mechanical assessment of the whole prostate gland ex vivo using dynamic instrumented palpation", *Proc. Inst. Mech. Eng. H*, vol. 231, no. 12, pp. 1081–1100, 2017.

[55] M. Lazeroms, G. Villavicencio, W. Jongkind, and G. Honderd: "Optical fibre force sensor for minimal-invasive–surgery grasping instruments", In: *Proceedings of 18th Annual International Conference of the IEEE Engineering in Medicine and Biology Society*, Vol. 1, pp. 234–235, 2002.

[56] H. Kim, S. Choi, and W. K. Chung: "Feasibility of a novel indicator for lump detection using contact pressure distribution", In: *Proceedings 2015 IEEE/RSJ International Conference on Intelligent Robots and Systems*, pp. 2111–2117, 2015.

[57] S. McKinley et al.: "A single–use haptic palpation probe for locating subcutaneous blood vessels in robot–assisted minimally invasive surgery", In: *Proceedings 2015 IEEE International Conference on Automation Science and Engineering*, pp. 1151–1158, 2015.

[58] Y. Tanaka, T. Fukuda, M. Fujiwara, and A. Sano: "Tactile sensor using acoustic reflection for lump detection in laparoscopic surgery", *Int. J. Comput. Assist. Radiol. Surg.*, vol. 10, no. 2, pp. 183–193, 2015.

[59] T. Fukuda, Y. Tanaka, A. M. L. Kappers, M. Fujiwara, and A. Sano: "Visual and tactile feedback for a direct-manipulating tactile sensor in laparoscopic palpation", *Int. J. Med. Robot.*, vol. 14, no. 2, 2018.

[60] V. Egorov, S. Ayrapetyan, and A. P. Sarvazyan: "Prostate mechanical imaging: 3–D image composition and feature calculations", *IEEE Trans. Med. Imaging*, vol. 25, no. 10, pp. 1329–1340, 2006.

[61] A. L. Trejos, J. Jayender, M. T. Perri, M. D. Naish, R. V. Patel, and R. A. Malthaner: "Experimental evaluation of robot–assisted tactile sensing for minimally invasive surgery", In: *Proceedings 2nd IEEE RAS & EMBS International Conference on Biomedical Robotics and Biomechatronics*, pp. 971–976, 2008.

[62] M. T. Perri, A. L. Trejos, M. D. Naish, R. V. Patel, and R. A. Malthaner: "New tactile sensing system for minimally invasive surgical tumour localization", *Int. J. Med. Robot.*, vol. 6, no. 2, pp. 211–220, 2010.

[63] M. T. Perri, A. L. Trejos, M. D. Naish, R. V. Patel, and R. A. Malthaner: "Initial evaluation of a tactile/kinesthetic force feedback system for minimally invasive tumor localization", *IEEE ASME Trans. Mechatron.*, vol. 15, no. 6, pp. 925–931, 2010.

[64] P. Richard and P. Coiffet: "Human perceptual issues in virtual environments: sensory substitution and information redundancy", In: *Proceedings 4th IEEE International Workshop on Robot and Human Communication*, pp. 301–306, 1995.

[65] N. Cutler et al.: "Auditory force feedback substitution improves surgical precision during simulated ophthalmic surgery", *Invest. Ophthalmol. Vis. Sci.*, vol. 54, no. 2, pp. 1316–1324, 2013.

[66] M. J. Massimino and T. B. Sheridan: "Sensory substitution for force feedback in teleoperation", *Presence (Camb.)*, vol. 2, no. 4, pp. 344–352, 1993.

[67] O. A. J. van der Meijden and M. P. Schijven: "The value of haptic feedback in conventional and robot-assisted minimal invasive surgery and virtual reality training: a current review", *Surg. Endosc.*, vol. 23, no. 6, pp. 1180–1190, 2009.

[68] A. I. Aviles–Rivero et al.: "Sensory substitution for force feedback recovery: A perception experimental study", *ACM Trans. Appl. Percept.*, vol. 15, no. 3, pp. 1–19, 2018.

[69] J. Rosen, B. Hannaford, M. P. MacFarlane, and M. N. Sinanan: "Force controlled and teleoperated endoscopic grasper for minimally invasive surgery–experimental performance evaluation", *IEEE Transactions on Biomedical Engineering*, Vol. 46, Issue 10, pp. 1212–1221, 1999.

[70] G. L. McCreery, A. L. Trejos, M. D. Naish, R. V. Patel, and R. A. Malthaner: "Feasibility of locating tumours in lung via kinaesthetic feedback", *The International Journal of Medical Robotics and Computer Assisted Surgery*, Vol. 4, Issue 1, pp. 58–68, 2008.

[71] E. P. W. Putten, J. J. Dobbelsteen, R. H. M. Goossens, J. J. Jakimowicz, and J. Dankelman: "Force feedback requirements for efficient laparoscopic grasp control", *Ergonomics*, Vol. 52, Issue 9, pp. 1055–1066, 2009.

[72] H. Li, K. Tadano, and K. Kawashima: "Achieving force perception in master-slave manipulators using pneumatic artificial muscles", In: *Proceedings SICE Annual Conference 2012*, pp. 1342–1345, 2012.

[73] T. L. Gibo, D. R. Deo, Z. F. Quek, and A. M. Okamura: "Effect of load force feedback on grip force control during teleoperation: A preliminary study", In: *Proceedings 2014 IEEE Haptics Symposium*, pp. 379–383, 2014.

[74] F. Bechet, K. Ogawa, E. Sariyildiz, and K. Ohnishi: "Electro-hydraulic transmission system for minimally invasive robotics", *IEEE Transactions on Industrial Electronics*, Vol. 62, Issue 12, pp. 7643–7654, 2015.

[75] E. Beretta, F. Nessi, G. Ferrigno, and E. D. Momi: "Force feedback enhancement for soft tissue interaction tasks in cooperative robotic surgery", In: *Proceeding 2015 IEEE/RSJ International Conference on Intelligent Robots and Systems*, pp. 209–215, 2015.

[76] C. Pacchierotti, L. Meli, F. Chinello, M. Malvezzi, and D. Prattichizzo: "Cutaneous haptic feedback to ensure the stability of robotic teleoperation systems", *The International Journal of Robotics Research*, Vol. 34, Issue 14, pp. 1773–1787, 2015.

[77] R. D. Howe, W. J. Peine, D. A. Kantarinis, and J. S. Son: "Remote palpation technology", *IEEE Eng. Med. Biol. Mag.*, vol. 14, no. 3, pp. 318–323, 1995.

[78] N. A. Mansour, A. M. R. F. El-Bab and M. Abdellatif: "Design of a novel multi-modal tactile display device for biomedical applications," In: *Proceedings 4th IEEE RAS & EMBS International Conference on Biomedical Robotics and Biomechatronics (BioRob)*, pp. 183–188, 2012.

[79] R. L. Feller, C. K. L. Lau, C. R. Wagner, D. P. Perrin, and R. D. Howe: "The effect of force feedback on remote palpation", In: *Proceedings IEEE International Conference on Robotics and Automation* Vol. 1, pp. 782–788, 2004.

[80] C.-H. King et al.: "Tactile feedback induces reduced grasping force in robot-assisted surgery", *IEEE Trans. Haptics*, vol. 2, no. 2, pp. 103–110, 2009.

[81] C.-H. King, M. O. Culjat, M. L. Franco, J. W. Bisley, E. Dutson, and W. S. Grundfest: "Optimization of a pneumatic balloon tactile display for robot-assisted surgery based on human perception", *IEEE Trans. Biomed. Eng.*, vol. 55, no. 11, pp. 2593–2600, 2008.

[82] M. Li, S. Luo, T. Nanayakkara, L. D. Seneviratne, P. Dasgupta, and K. Althoefer: "Multi-fingered haptic palpation using pneumatic feedback actuators", *Sens. Actuators A Phys.*, vol. 218, pp. 132–141, 2014.

[83] C. Pacchierotti, S. Sinclair, M. Solazzi, A. Frisoli, V. Hayward, and D. Prattichizzo: "Wearable haptic systems for the fingertip and the Hand: Taxonomy, review, and perspectives", *IEEE Trans. Haptics*, vol. 10, no. 4, pp. 580–600, 2017.

[84] H.-Y. Yao, V. Hayward, and R. E. Ellis: "A tactile enhancement instrument for minimally invasive surgery", *Comput. Aided Surg.*, vol. 10, no. 4, pp. 233–239, 2005.

[85] T. Fukuda, Y. Tanaka, A. M. L. Kappers, M. Fujiwara, and A. Sano: "A pneumatic tactile ring for instantaneous sensory feedback in laparoscopic tumor localization", *IEEE Trans. Haptics*, vol. 11, no. 4, pp. 485–497, 2018.

[86] S. M. Hosseini, M. Amiri, S. Najarian, and J. Dargahi: "Application of artificial neural networks for the estimation of tumour characteristics in biological tissues", *Int. J. Med. Robot.*, vol. 3, no. 3, pp. 235–244, 2007.

[87] B. Xiao et al.: "Depth estimation of hard inclusions in soft tissue by autonomous robotic palpation using deep recurrent neural network", *IEEE Trans. Autom. Sci. Eng.*, vol. 17, no. 4, pp. 1791–1799, 2020.

[88] J. Palacio-Torralba, R. L. Reuben, and Y. Chen: "A novel palpation-based method for tumor nodule quantification in soft tissue-computational framework and experimental validation", *Med. Biol. Eng. Comput.*, vol. 58, no. 6, pp. 1369–1381, 2020.

[89] F. Saleheen and C.-H. Won: "Dynamic positioning sensing system for estimating size and depth of embedded object", In: *Proceedings 2015 IEEE SENSORS*, pp. 1–4, 2015.

[90] W. J. Hyung, J. S. Lim, J. H. Cheong, J. Kim, S. H. Choi, S. Y. Song, and S. H. Noh: "Intraoperative tumor localization using laparoscopic ultrasonography in laparoscopic-assisted gastrectomy", *Surgical Endoscopy*, Vol. 19, Issue 10, pp. 1353–1357, 2005.

[91] J. Ophir et al.: "Elastography: Imaging the elastic properties of soft tissues with ultrasound", *J. Med. Ultrason.*, Vol. 29, Issue 4, pp. 155, 2002.

[92] R. A. Lathrop, D. M. Hackworth, and R. J. Webster: "Minimally invasive holographic surface scanning for soft-tissue image registration", *IEEE Trans. Biomed. Eng.*, Vol. 57, Issue 6, pp. 1497–1506, 2010.

[93] J. A. Knol, C. S. Marn, I. R. Francis, J. M. Rubin, J. Bromberg, and A. E. Chang: "Comparisons of dynamic infusion and delayed computed tomography, intraoperative ultrasound, and palpation in the diagnosis of liver metastases", *Am. J. Surg.*, Vol. 165, Issue 1, pp. 81–87, 1993.

[94] C. Lv, S. Wang, and C. Shi: "A high-precision and miniature Fiber Bragg Grating-based force sensor for tissue palpation during minimally invasive surgery", *Ann. Biomed. Eng.*, vol. 48, no. 2, pp. 669–681, 2020.

[95] S. Omata, Y. Murayama, and C. E. Constantinou: "Real time robotic tactile sensor system for the determination of the physical properties of biomaterials", *Sens. Actuators A Phys.*, vol. 112, no. 2–3, pp. 278–285, 2004.

[96] U. Kim, Y. B. Kim, D.-Y. Seok, J. So, and H. R. Choi: "A surgical palpation probe with 6–axis force/torque sensing capability for minimally invasive surgery", *IEEE Trans. Ind. Electron.*, vol. 65, no. 3, pp. 2755–2765, 2018.

[97] W. Y. Du: "Resistive, Capacitive, Inductive, and Magnetic Sensor Technologies". *London: CRC Press*, 2019.

[98] Japanese Gastric Cancer Association: "Japanese classification of gastric carcinoma: 3rd English edition", *Gastric Cancer*, vol. 14, no. 2, pp. 101–112, 2011.

[99] G. L. McCreery, A. L. Trejos, M. D. Naish, R. V. Patel, and R. A. Malthaner: "Feasibility of locating tumours in lung via kinaesthetic feedback", *Int. J. Med. Robot.*, vol. 4, no. 1, pp. 58–68, 2008.

[100] S. Akita, T. Fukuda, Y. Tanaka, M. Fujiwara, and A. Sano: "Frequency-based temperature compensation for a tactile sensor using acoustic reflection", *IEEE Robot. Autom. Lett.*, vol. 3, no. 4, pp. 3529–3536, 2018.

[101] H. Culbertson, S. B. Schorr, and A. M. Okamura: "Haptics: The present and future of artificial touch sensation", *Annu. Rev. Control Robot. Auton. Syst.*, vol. 1, no. 1, pp. 385–409, 2018.

[102] D. Tsetserukou, S. Hosokawa, and K. Terashima: "LinkTouch: A wearable haptic device with five–bar linkage mechanism for presentation of two–DOF force

feedback at the fingerpad", In: *Proceedings 2014 IEEE Haptics Symposium*, pp. 307–312, 2014.

[103] D. Leonardis, M. Solazzi, I. Bortone, and A. Frisoli: "A wearable fingertip haptic device with 3 DoF asymmetric 3–RSR kinematics", In: *Proceedings 2015 IEEE World Haptics Conference*, pp. 388–393, 2015.

[104] D. Leonardis, M. Solazzi, I. Bortone, and A. Frisoli: "A 3–RSR haptic wearable device for rendering fingertip contact forces", *IEEE Trans. Haptics*, vol. 10, no. 3, pp. 305–316, 2017.

[105] S.-C. Lim, H.-K. Lee, and J. Park: "Role of combined tactile and kinesthetic feedback in minimally invasive surgery", *Int. J. Med. Robot.*, vol. 11, no. 3, pp. 360–374, 2014.

[106] K. Minamizawa, S. Fukamachi , H. Kajimoto, N. Kawakami , and S. Tachi: "Gravity grabber: wearable haptic display to present virtual mass sensation" In: *Proceedings of ACM SIGGRAPH emerging technologies*, pp. 8-es, 2007.

[107] J. Biggs and M. A. Srinivasan: "Tangential versus normal displacements of skin: relative effectiveness for producing tactile sensations", In: *Proceedings 10th Symposium on Haptic Interfaces for Virtual Environment and Teleoperator Systems*, pp. 121–128, 2002.

[108] M. J. Adams et al.: "Finger pad friction and its role in grip and touch", *J. R. Soc. Interface*, vol. 10, no. 80, p. 20120467, 2013.

[109] R. E. Schoonmaker and C. G. L. Cao: "Vibrotactile feedback enhances force perception in minimally invasive surgery", *Proc. Hum. Factors Ergon. Soc. Annu. Meet.*, vol. 50, no. 10, pp. 1029–1033, 2006.

[110] C. F. Guimaraes, L. Gasperini, A. P. Marques, and R. L. Reis: "The stiffness of living tissues and its implications for tissue engineering", *Nat. Rev. Mater.*, vol. 5, no. 5, pp. 351–370, 2020.

[111] R. Masuzaki et al.: "Assessing liver tumor stiffness by transient elastography", *Hepatol. Int.*, vol. 1, no. 3, pp. 394–397, 2007.

[112] J. Rosen, J. D. Brown, S. De, M. Sinanan, and B. Hannaford: "Biomechanical properties of abdominal organs in vivo and postmortem under compression loads", *J. Biomech. Eng.*, vol. 130, no. 2, p. 021020, 2008.

[113] E. H. Weber: "E. H. Weber on the Tactile Senses". *Psychology Press*, 2018.

[114] G. Frediani and F. Carpi: "Tactile display of softness on fingertip", *Sci. Rep.*, vol. 10, no. 1, p. 20491, 2020.

[115] G. A. Gescheider: "Psychophysics: The Fundamentals", 3rd ed. *London: Psychology Press*, 2015.

[116] M. Bianchi, J. C. Gwilliam, A. Degirmenci, and A. M. Okamura: "Characterization of an air jet haptic lump display", *Annu. Int. Conf. IEEE Eng. Med. Biol. Soc.*, vol. 2011, pp. 3467–3470, 2011.

[117] R. Rizzo, A. Musolino, and L. A. Jones: "Shape localization and recognition using a magnetorheological-fluid haptic display", *IEEE Trans. Haptics*, vol. 11, no. 2, pp. 317–321, 2018.

[118] J. Han, M. Kamber, and J. Pei: "Data Mining: Concepts and Techniques", *Oxford, England: Morgan Kaufmann*, 2012.

[119] N. A. Macmillan and C. D. Creelman: "Detection Theory: A User's Guide", 2nd ed. *Philadelphia, PA: Psychology Press*, 2005.

[120] S. Coren: "The left–hander syndrome: The causes and consequences of left-handedness", *London, England: John Murray*, 1992.

[121] E. P. Westebring-van der Putten, R. H. M. Goossens, J. J. Jakimowicz, and J. Dankelman: "Haptics in minimally invasive surgery–a review", *Minim. Invasive Ther. Allied Technol.*, vol. 17, no. 1, pp. 3–16, 2008.

Publications

Journals

1. H. H. Ly, Y. Tanaka, and M. Fujiwara: "A tactile sensor using the acoustic reflection principle for assessing the contact force component in laparoscopic tumor localization", *The International Journal of Computer Assisted Radiology and Surgery*, Vol. 16, Issue 2, pp. 289–299, 2021, DOI: 10.1007/s11548-020-02294-w.

2. H. H. Ly, Y. Tanaka, and M. Fujiwara: "SuP–Ring: A pneumatic tactile display with substitutional representation of contact force components using normal indentation", *The International Journal of Medical Robotics and Computer Assisted Surgery*, Vol. 17, Article no. e2325, 2021, DOI: 10.1002/rcs.2325.

3. H. H. Ly, Y. Tanaka, and M. Fujiwara: "Tumor depth and size perception using a pneumatic tactile display in laparoscopic surgery", *IEEE Access*, Vol. 9, pp. 167795–167811, 2021, DOI: 10.1109/ACCESS.2021.3135698.

Proceedings of International Conferences

1. H. H. Ly, and Y. Tanaka: "Development of a 2–axis tactile sensor using acoustic reflection principle for tumor detection in laparoscopic surgery", In: *IEEE Haptic Symposium 2020 (Work in Progress)*, Washington, D.C., VA, USA, March 2020.

Proceedings of Domestic Conferences

1. H. H. Ly, and Y. Tanaka: "A basic study on reflection type tactile sensor with multiple detection functions", In: *Proceedings of the 37th Annual Conference of the Robotics Society of Japan*, Article no. 2K1-02, Tokyo, Japan, 2019. (In Japanese)

2. H. H. Ly, and Y. Tanaka: "An assessment of the contact force component in laparoscopic tissue palpation", In: *Proceedings of the 39th Annual Conference of the Robotics Society of Japan*, Article no. 2A1-06, Tokyo, Japan, 2021. (In English)